Collective cell migration: a physics perspective

Vincent Hakim, Pascal Silberzan

Collective cell migration : a physics perspective

Vincent Hakim[1,a] **& Pascal Silberzan**[2,b]

[1] Laboratoire de Physique Statistique, Ecole Normale Supérieure, CNRS, PSL Research University, UPMC, Paris, France.
[2] Laboratoire Physico-Chimie Curie, Institut Curie, PSL Research University - Sorbonne Université- UPMC- CNRS- Equipe labellisée Ligue Contre le Cancer; 75005 Paris, France .

E-mail: [a]vincent.hakim@ens.fr

E-mail: [b]pascal.silberzan@curie.fr

8 February 2017

Abstract. Cells have traditionally been viewed either as independently moving entities or as somewhat static parts of tissues. However, it is now clear that in many cases, multiple cells coordinate their motions and move as collective entities. Well-studied examples comprise development events, as well as physiological and pathological situations. Different *ex vivo* model systems have also been investigated. Several recent advances have taken place at the interface between biology and physics, and have benefitted from progress in imaging and microscopy, from the use of microfabrication techniques, as well as from the introduction of quantitative tools and models. We review these interesting developments in quantitative cell biology that also provide rich examples of collective out-of-equilibrium motion.

Keywords: collective motion, cell migration, epithelium, cell, wound, active matter, out-of-equilibrium, microfabrication.

1. Introduction

Cells are the buildings blocks of biological organisms [1] and their motion is playing a crucial role in many processes. Starting from a single cell, cell division and differentiation give rise to the numerous cells and multiple cell types of the adult during the development of multicellular organisms. The motion of cells with respect to each other is key to shape the organization of different cells in space, the formation of well-formed organs and the body as a whole. It is also central in physiological processes, such as wound healing, and in pathological processes such as cancer development and metastasis formation.

The motion of a single cell is already a complex integrated process [2] which has been the focus of a large number of biological studies. Cells have also attracted the attention of physicists since the invention of the microscope by Hooke and van Leuwenhoek. In recent years, progress in microscopy and visualization techniques, has provided new impulses to these studies. On the experimental side, new physical techniques have been developed to measure for instance the motility forces exerted by cells. On the theoretical side, the cell is a prime example of structured "active matter" [3], one of the main subjects of modern out-of-equilibrium statistical mechanics. Basic mechanisms of cell locomotion and determinants of cell shape have been modeled but a comprehensive picture of cell locomotion is still to be worked out.

In many biological settings, cells do not move as single entities but coordinate their motion. Collective cell migration is essential for several *in vivo* biological processes [4, 5, 6]. Collective cell migration is also worth of special scrutiny by condensed matter and statistical physicists since it both bears resemblance to gas, liquid and glass dynamics, while the self-propelled 'active' character of cells and their complex modes of interactions makes their collective motion depart in rich ways from the behavior of inanimate matter. Measures of "physical parameters", like the cell velocity field and maps of the forces they exert, in space and time, bring information that crucially complements the one gathered by more usual biological techniques. As in more classical physics investigations, modeling and simulations play a crucial role to synthesize elementary mechanisms in a coherent whole, and test their explanatory power. Our aim in the present review is to introduce the reader to this fascinating field and to emphasize its interest from a physical and integrated perspective. While we recall below some well-studied biological examples, we refer the reader to numerous recent reviews [7, 8, 9] for a more detailed description of the underlying biology. We aim at highlighting here links with flocking [10], jamming [11] and glassy dynamics [12]. There are also several recent reviews on the general topic of "active matter" [3, 13] that consider these topics. Our focus on cells makes the present review complementary to these, due to the peculiar and complex character of cells and of their modes of interactions, but also due to the questions themselves that seem interesting to address in this context. Our focus is, for instance, less on the order of a phase transition in the thermodynamical limit or on critical exponents, than on noise, forces, structures and oscillations in medium-size cell assemblies.

The present review is organized as follows. After describing some motivating and fascinating examples of cell motion *in vivo*, we recall some basic facts about cell motion as well as different theoretical frameworks that are used to describe collective cell motion and interpret experimental results. We then describe recent experimental advances which give access to detailed and previously unavailable information. We emphasize the measure of physical quantities such as forces exerted by cells or the full velocity field in space and time for a collection of moving cells but also recall allied biological progress in visualization due to the development of optical sensors or in cell manipulation. Then we describe recent investigations and particular results that have been obtained using these techniques as well as parallel theoretical investigations that have been performed in several cases. These comprise, flow and jamming-like behavior in confluent epithelia, the healing of wounds, the behavior of cell assemblies in confined geometries or the peculiar dynamics of epithelium interfaces in different conditions. We finally consider the different collective taxis modes of cell assemblies that have been recently put to light. We conclude by describing some avenues of research that appear interesting to pursue in the forthcoming years.

2. Some examples of collective cell motion *in vivo*.

The simultaneous migration of many cells is a common physiological event (Figure 1). In some cases, different

cells appear to migrate independently of each other. A notable case is the migration of Cajal-Retzius cells which are among the first-born neurons [14, 15]. These cells migrate tangentially in a random fashion from the borders of pre-patterned domains and transiently cover the entire cortical surface. Cajal-Retzius cells play an important role in cortical development by secreting *Reelin*, an extra-cellular protein crucial for radial migration of subsequently born neurons and for cortical laminar organization. Depending on their origin, they express different molecular markers and invade different territories of the developing cerebral cortex. It has been suggested that Cajal-Retzius cells influence the destiny of cortical progenitor cells and cortical areas specification by secreting different morphogens [16] and acting as "mobile signaling units". Interaction between Cajal-Retzius cells appear to mostly consist of repulsion when two cells touch [17] which speeds up their spreading and reduces density fluctuation. This phenomenon, generally described as Contact Inhibition of Locomotion (CIL) has been found to play an important role in coordinating the motion of different cells [18, 19] in other settings. The term was coined by Abercrombie and Heaysman [20] to describe their observation that, similarly to Cajal-Retzius cells, colliding fibroblasts redirected their motion away from each other upon contact (see Figure 2A-B and section 5.1 below).

"Streaming" of neural crest cells [21] (Figure 1A) provides an important and well-studied example of the migration of loose clusters of cells coordinating their motions by constant interactions between each other via repeated CIL [18, 19]. The neural crest cells are multipotent stem cells that migrate ventrally from the neural plate border during neurulation and differentiate into many different cell types (most of the neurons and glial cells of the peripheral nervous system, smooth muscle, cartilage and bone, pigment cells of the skin, ...) [21, 22]. CIL has been shown to allow the efficient directed migration of neural crest cells (Figure 2C and section 8.1) in a chemoattractant gradient of stromal-derived-factor 1 (Sdf1) which is very inefficient for the chemotaxis of single cells [23]. Interestingly, CIL between neural crest cells and placode cells also induces the directed migration of placode cells, cells which do not show migration directionality on their own [24]. In addition to exerting CIL, neural crest cells have been found to secrete chemoattractant, the complement fragment C3a, to maintain the loose cohesion of the migrating cell group [25].

In many other contexts, cells coordinate their migration, what Abercrombie and Heaysman referred to as the "social behavior" of cells [20]. This coordination can result from signaling or during contact interactions of loosely attached cells but it also happens in dense clusters of cells. The behavior of *Dictyostelium discoideum* ('*Dicty*') amoeba has long been studied both experimentally and theoretically in this context (see e.g. [26, 27] for reviews). When starved, *Dicty* cells aggregate by collectively producing cAMP waves and moving chemotactically in response to them. Moreover, after aggregation they form moving 'slugs' , before sporulating under appropriate environmental conditions. Two other prototypical examples are provided by the migration of border cells in the egg chambers of the *Drosophila melanogaster* ovaries [8] and lateral line migration during the formation of the zebrafish peripheral nervous system. The border cell cluster is a group of follicle cells in which 4 to 8 motile cells collectively carry 2 non-motile polar cells from the anterior border of the fly egg chamber in a posterior direction to their destination, the anterior border of the oocyte (Figure 1B). Migration appears directed by chemoattractants secreted by germline cells and specially the oocyte. These ligands bind two types of receptor tyrosine kinases on border cells and their ectopic expression redirect border cells [28].

The zebrafish lateral line organ primordium provides a well-studied example of a larger cluster of about 100 cells that migrate collectively (Figure 1C). This cell cluster advances along the flank of the fish embryo on a track of Sdf1 chemoattractant. Notably, Sdf1 concentration is not deposited in a graded way, the gradient is self-generated by the moving cluster of cells upon chemoattractant internalization by the trailing cells in the cluster [29]. The dynamics in this group of cells is quite rich and interesting with the periodic deposition of group of cells, "rosettes", that subsequently give rise to mechano-sensory organs, as shown in Figure 1C.

Collective migration is also observed in cases where cells adhere to each other and form a continuous two-dimensional monolayer i.e. in epithelial tissues. This comprises developmental events like dorsal closure in drosophila (Figure 1D), as well as tissue repair after a wound (section 6). In spite of many differences, these processes present similarities and common basic mechanisms [30]. In both, epithelial edges join to close a hole in an epithelium, using a combination of coordinated cell crawling and mechanical tension stored in a multicellular actin cable at the interface edge. Dorsal closure in the fly takes place at the end of gastrulation when a large hole remains in the ectodermal epithelial outer layer of the embryo, covered by a membrane formed of extra-embryonic cells, the amnioserosa. Both contraction and apoptosis of amnioserosa cells, contraction of the actin cable at the edge of ectodermal layer and crawling of

ectodermal cells play a role in dorsal closure. Assessing the respective contributions of these different processes has been the aim of several works in recent years [31, 32].

Wound closure *in vivo* is a complicated event which involves re-epithelization with the proliferation and collective migration of fibroblasts, but also a fast immune response and migration of immune cells to the wound site as well as differentiation of fibroblasts into myofibroblasts and angiogenesis [33]. The desire to analyze it in a simpler setting where only fibroblasts are present has led to the use of *in vitro* migration assays which we will return to below (section 6).

Cancer metastasis has been classically conceived as initiated by the migration of separate malignant cells away from a primary tumor. In the most frequent case when the tumor originates from an epithelium, this cell evasion has been thought to involve an epithelial-mesenchymal transition (EMT), a complex cell change from an epithelial phenotype to a mesenchymal one [34]. Tumor dissemination is now believed to involve a spectrum of cell states (see e.g. [35, 36] for reviews and the recent works [37, 38]). EMT also occurs during normal development, and allows for instance the neural crest cells to escape from the ectoderm at the neural plate border. Similarly to these developmental cases, it has been realized that cancer cells often migrate collectively [39, 4]. Cohort of invading malignant cells are seen in histo-pathological sections [39], which bear a striking resemblance to developmental cohorts, such as the lateral line primordium [4]. Malignant cohorts also display pioneer or leader cells, sometimes of different types like cancer-associated fibroblasts [40] (CAF), that remodel the extracellular matrix and facilitate invasion of normal tissue. Finally, several signaling pathways used in development are important for cancer cells. The importance of collective motion in pathology certainly provides a further incentive to better understand its mechanical basis and its different possible modes.

While much progress has been made in studying collective cell migration *in vivo*, it is still very challenging to obtain quantitative measures of the cell dynamics, such as the cell velocity field at different times or the forces exerted by cells on their neighbors or on the extracellular matrix. This has been a strong incentive to develop controlled *ex-vivo* experiments with the help of modern micro-fabrication techniques that we describe below (section 4). This has also promoted the development of theoretical models to analyze these data and help to identify the mechanisms underlying the coordinated migration of a cell assembly. We describe the two facets of this current endeavor in this review.

3. Mechanisms and models

Before describing models of collective cell migration, it is useful to recall a few facts about single cell motion.

3.1. Single cell motion

There appears to be different modes of locomotion for cells on a rigid surface. Some cells like keratinocytes or neutrophils advance with a stable leading edge and an extended lamellipodium that appears to propulse them like a rolling treadmill. Others, like *Dicty* or macrophages, crawl, in an "amoeboid" way, by extending pseudopodia. In spite of these differences, there are common mechanisms for pushing the membrane forward at the cell front and retracting it at the cell back. Before looking at some of the underlying mechanisms, we consider global phenomenological descriptions of cell motion.

3.1.1. Phenomenological descriptions. Cell motion has been described as persistent random motion since the pioneering description of amoeba motion by Fürth in 1920 [41]. This was shown to apply to fibroblast crawling by Gail and Boone [42] in the 70s and studied by many others since.

When the motion of a single cell is recorded, its velocity appears to change randomly but slowly from one moment to the next. The model for the velocity dynamics proposed by Fürth [41], and independently studied by Ornstein [43], reads

$$\tau \frac{d\mathbf{v}}{dt} = -\mathbf{v} + \sigma\, \xi(t) \tag{1}$$

with $\xi(t)$ a (vectorial) white noise process,

$$< \xi_a(t)\xi_b(t') >= \delta_{a,b}\delta(t-t') \tag{2}$$

The constant σ quantifies the random force magnitude. The indices $\{a, b = x, y\}$ denote space coordinates. For $\tau = 0$, the model reduces to the usual Brownian motion. It should be noted that although (1) formally looks like a description of inertial motion with friction, its interpretation is different. Inertia is entirely negligible at the cell scale and the time τ describes in a phenomenological way the finite duration it takes for a cell to reorient its motion. This could be made explicit by introducing, as frequently done, the pulling force $(-\mathbf{f})$ exerted by the cell on the substrate, with the rewriting of (1) as

$$\mathbf{v} \quad = \mu\, \mathbf{f} \tag{3}$$

$$\tau \frac{d\mathbf{f}}{dt} = -\mathbf{f} + \frac{\sigma}{\mu}\, \xi(t). \tag{4}$$

We have introduced a mobility coefficient μ relating the velocity to the force from which it originates. This second description is entirely equivalent to (1) and it does not bring much at this stage. However, it makes

clear that interactions (with other cells or external obstacles) can modify (3) or (4) depending on their nature. For instance, an external force exerted on the cell will naturally be added to (3) while signaling may change the motility force itself and may more naturally affect (4). A second point that should be noted is the separation in (3) between a motility force on the right-hand-side (r.h.s.) and a friction force on the left-hand-side (l.h.s.). As measured on the substrate both are of equal magnitude and opposite. The cell being an extended object, this is reflected by the dipolar character of its force field. However, decomposing it explicitly between motility and friction forces requires further consideration, as does the role of the force field higher moments.

The analysis of (1) is straightforward since it is linear. It follows from it that the velocity $\mathbf{v}(t)$ is a linear combination of Gaussian variables and is itself a Gaussian variable. This Gaussian velocity field is entirely specified by the velocity autocorrelation $\langle \mathbf{v}(t)\mathbf{v}(t')\rangle$,

$$\langle \mathbf{v}(t)\cdot\mathbf{v}(t')\rangle = \frac{\sigma^2 d}{2\tau}\exp[-|t-t'|/\tau] \quad (5)$$

where $d = 2$ or 3, denotes the space dimension. One also sees from (5) that the velocity has a 'memory' time of order τ. The cell displacement $\mathrm{x}(T) - \mathrm{x}(0)$ can be expressed as an integral of the velocity,

$$\mathrm{x}(T) - \mathrm{x}(0) = \int_0^T dt\ \mathbf{v}(t) \quad (6)$$

When combined with the velocity auto-correlation (5), this provides after averaging, the expression of the cell mean square displacement during a time T,

$$< [\mathrm{x}(T) - \mathrm{x}(0)]^2 >= \sigma^2 d\,\{T - \tau[1-\exp(-T/\tau)]\} \quad (7)$$

The model of Fürth has been used as a phenomenological description of cell motion in a number of studies. Selmeczi et al [44] directly examined its accuracy. They recorded the motion of human keratocytes *in vitro* and assessed the validity of equation (1). Namely, they analyzed the observed distribution of accelerations $d\mathbf{v}/dt$ conditionned on the instantaneous cell velocity $\mathbf{v}$. They found that, for a given speed $|\mathbf{v}|$, in agreement with (1), the mean acceleration was opposite to the velocity $\mathbf{v}$ with the acceleration component orthogonal to $\mathbf{v}$ symmetrically distributed around zero and the acceleration component parallel to $\mathbf{v}$ distributed around a linearly decreasing mean (i.e. proportional to $-|\mathbf{v}|$) . However in contrast to the prediction of (1), these distributions were found to be non-gaussian and with a width increasing with the velocity modulus. Additionally, the cell velocity autocorrelation was found to be described by a sum of two exponentials rather than by a single exponential as in (5). Remarkably, the data was found to be well-accounted for by the addition of a simple supplementary memory kernel to (1), as well as a velocity dependent noise-amplitude,

$$\frac{d\mathbf{v}}{dt} = -\beta\mathbf{v} + \alpha^2\int_{-\infty}^{t} dt'\exp[-\gamma(t-t')]\mathbf{v}(t') + \sigma(|\mathbf{v}|)\,\xi(t) \quad (8)$$

with

$$\sigma(|\mathbf{v}|) = \sigma_0 + \sigma_1 v \quad (9)$$

and $\xi(t)$ a white noise as in (1). The velocity dynamics (8) appears to accurately describe the motion of human keratocytes. Other types of cells may require further refinements. For instance, Selmeczi et al [44] have shown that to precisely account for human fibroblasts motion, one should replace the constant β in (8) by a linear function of v, as well as choosing different noise amplitude for the two components of the acceleration (parallel and perpendicular to $\mathbf{v}$). This refined model was found adequate for the description of *Dicty* cells in [45] although it needs even further refinements to account for the observed oscillations of the cell velocity on the time-scale of minutes [46]. It is nonetheless remarkable that an extended dynamical system like a cell can be accurately described by a few coupled (stochastic) ordinary differential equations. In this respect, ref. [47] provides an interesting attempt to write the motion of a self-propelled deformable body as coupled dynamics between its center of mass and shape degrees of freedom.

3.1.2. Basic mechanisms. The phenomenological equations (1) or (8) usefully describe the motion of a cell with a few effective parameters. A deeper mechanistic understanding requires an analysis of the different cellular processes that underlie the motion of a cell. Different cell types move in different ways. Isolated keratocytes appear to glide over a two-dimensional substrate, propulsed by a well developed lamellipodium at their fronts, while neutrophils extend pseudopods in various directions. Nonetheless, the basic mechanisms underlying propulsion in these different cases are similar. Key processes involve determination of the cell front and back (i.e. cell polarization), actin assembly and treadmilling at the cell front together with the formation of new adhesion sites, coordinated with actin contraction with membrane retraction and de-adhesion at the cell back. These different processes have been the subject of intensive research which has uncovered their molecular complexity and the large number of involved proteins. A detailed description lies much beyond the scope of the present article. For a summary of the current knowledge, we refer the readers to the reviews [48, 49] and content ourselves with noting several points of prime physical interest.

The basic cell propulsion mechanism relies on actin treadmilling. Actin filaments are formed by two parallel polar polymers of (globular) actin units and are thus oriented. They can polymerize at their "plus" end and depolymerize at the other "minus" end under suitable non-equilibrium conditions. The process requires energy consumption under the form of ATP hydrolysis when bound to filamentous actin subunits. This polymerization/depolymerization has been particularly well studied *in vitro* with the measure of the different kinetic constants of globular actin at the two ends of actin filament (F-actin). As measured *in vitro*, treadmilling is slow. *In vivo* various enzymes modify and speed up the process, enabling in particular the formation of branched actin filaments off the sides of other filaments. The classic view (e.g. [1]; but see [50]) is that the growing filament plus ends abut the front cell membrane and push it forward. Whether the front membrane actually protrudes or the branched actin network flows backward depends on the coupling between adhesion on the substrate and the branched actin network: the retrograde flow of the whole actin meshwork can be observed [51] in immobile cells and this backward motion relative to the substrate is also observed to different extents in forward moving cells. This possible adjustment of cell speed by regulating the coupling of actin treadmilling to adhesion has famously been compared to a clutch mechanism [52] and some of its molecular bases have since been identified [53]. How the traction force itself depends on the speed of retrograde flow has also been investigated experimentally by measuring both quantities simultaneously [54]. The found increase of traction stress at low speed and decrease at high speed can be explained with the help of Bell's classic model [55] in which adhesive molecules bind and unbind stochastically with a stress-dependent unbinding rate (see [56, 57] for reviews).

De-adhesion of the cell membrane at the cell back is thought to involve contraction of the cell acto-myosin cortex. In striated muscle sarcomeres, the ordered arrangement of actin and myosin filaments [1] makes clear how contraction is achieved through the motion of myosin II heads toward the plus end of actin filaments. However, the actomyosin cortex of cells does not seem to possess such an ordered microstructure and understanding how contraction is achieved is much less obvious. Different mechanisms have been considered [58]. It has been proposed that the main motor of contraction is actin depolymerization at its minus end in the presence of actin cross-linkers that would not detach from the depolymerizing end [59]. Support for this mechanism has been obtained in actomyosin ring contraction in budding yeast cytokinesis [60] . Alternatively, it has been shown that buckling of actin filaments under compression introduces an intrinsic asymmetry between expansion and contraction that can lead a disordered actomyosin network to preferentially contract [61, 62, 63].

As seen from the above description, polarization of cells between front and back is crucial as well as specific spatial regulation. Some key molecules in this respect are three Rho-family GTPases, Rho itself, Rac and Cdc42. They are active in the GTP bound form and become inactive upon GTP hydrolysis. The simple classic picture is that Rho and Rac are antagonistic. Rac and Cdc42 are active at the cell front where they stimulate actin polymerization and the formation of membrane protrusions. Rho is active at the cell back where it promotes acto-myosin contraction. Recent works and visualization have however shown that the reality is more complex, specially in cohesive cell groups, as further discussed below (section 6.3.3).

Finally, it is worth mentioning that contraction oscillations in acto-myosin networks on the time scale of minutes have been observed in different contexts, for instance in the fly, during gastrulation [64] or in amnioserosa cells during dorsal closure [65]. A simple model of these pulsatile contractions has been proposed in [65], based on the idea that contraction kinematically increases Myosin density which itself increases contraction. Supplementing this positive feedback loop, by a negative one coming from relaxation of Myosin to a preferred homeostatic concentration, naturally leads to oscillation in a suitable parameter regime [65].

Integration of the different basic steps in a full description of single cell motion has been the aim of numerous mathematical models (reviewed in [2]). Further recent developments of interest include the universal relation between cell speed and velocity persistence (the time τ in (1)), recently studied and modeled in [66], as well as the elucidation of some of the molecular underpinning of steering and cell directional persistence (reviewed in [67]).

3.2. Collective cell motion.

As recalled above, cells have been observed to coordinate their motion in different situations. A basic distinction between these different cases is whether cells move autonomously on a substrate or whether their motion within a tissue is dominated by adhesion between cells and happens mostly by cell rearrangements. The motions of neural crest cell *in vivo* [18, 25] or of MDCK cells *ex vivo* [68] provide examples of the first type of dynamics where autonomous cell motion is the main motor of the collective dynamics. On the contrary, tissue dynamics is mainly powered in some cases, by cortical cytoskeleton contraction and adhesion between cells

with no significant contribution of autonomous cell crawling. Tissue convergence and extension during fly gastrulation provides a well-studied example of this last situation [69]. Both types of dynamics have given rise to modeling efforts. We will primarily focus in the following on the first type of motion when cell autonomous motion plays a central role while acknowledging that there certainly are mixed situations. For instance, dorsal closure in fly development or healing of small wounds [70]) both exhibit tissue healing via cell crawling and cellular rearrangements driven by actin cable contraction and cell apoptosis [71, 31]. Healing of model wounds *in vitro* allow one to assess the respective contributions of the different processes, as discussed in section 7.2.

3.2.1. Vicsek Model and velocity alignment Besides cells, it is a widespread observation that different elementary "entities" have correlated motion over scales that are large compared to their own size, from molecules in flowing liquids to large organisms such as birds [72], sheep or fish [73, 74]. Vicsek et al [75], building on earlier works [76], proposed a minimal model to try and capture the essence of this phenomenon. The elementary entities or particles are simply points which move at constant speed v and which can thus be characterized by their position $\mathbf{x}_i$ and in two dimensions, their angular direction of motion θ_i. In the initial proposal, time is discretized and the evolution from one time step to the next given by

$$\theta_i(t+\Delta t) = \langle \theta_j(t) \rangle_{j\in\mathcal{N}_i} + \sigma\xi(t) \tag{10}$$

$$\mathbf{x}_i(t+\Delta t) = \mathbf{x}_i(t) + \mathbf{v}_i(t+\Delta t)\Delta t \tag{11}$$

where the velocity $\mathbf{v}_i(t+\Delta t)$ has constant modulus v and points in the direction $\theta_i(t)$. The average in (10) is performed over all the points contained in the neighborhood $\mathcal{N}_i$ of particle i, taken to be simply a disk of radius a. It embodies the 'elementary' velocity alignment mechanism in the model, which acts somehow like a discrete description of viscosity. (10) contains also a noise term of magnitude σ with $\xi(t)$ a random number uniformly drawn in $[-\pi, \pi]$. The model properties depend on 3 parameters, the noise amplitude σ and 2 dimensionless ratio between the 3 lengths, a, $v\Delta t$, and the inverse square (in two dimensions) root of the density $1/\sqrt{\rho}$,

The main qualitative observation [75] is that the model has two phases. There is a disordered one for low density or strong noise in which the velocities of sufficiently distant particles have negligible correlations. More strikingly, at low noise amplitude or high density, velocity alignment extends to large distances, and distant particles move on average in the same direction. This spontaneous appearance of orientational order in two dimensions, besides being reminiscent of flocking behavior, stirred a large interest in the physics community, since it contradicted the classical Hohenberg-Mermin-Wagner theorem [77, 78] which holds for equilibrium systems. The emergence of this order has been theoretically rationalized using a continuum formulation (see section 3.2.4) and renormalization-group techniques [79, 80] and examined in a multitude of variants of the original Vicsek model. These include modifying (10) by including noise in a different way [81] or by taking a topological neighborhood for the velocity averaging instead of the above-described metric one (for a recent review of these variant models, see [82]). One main point of focus has been the nature of the flocking phase transition, namely whether orientational order continuously grows about a threshold parameter value like in a 2nd order phase transition as initially described [75] , or whether it jumps to a finite value in a 1st-order phase transition manner as subsequently found [83]. Band-like traveling structures of higher densities have been observed in the transition region. Much progress has recently been made towards an analytic understanding by formulating mean-field equations that appear able to properly describe these structures ([84] and references therein).

The ordered flock-like phase of the Vicsek model has been found to be subject to giant density fluctuations [85]. In a subregion with a mean number of particles N, the fluctuations ΔN in the number of particles obey,

$$\sqrt{\langle \Delta N^2 \rangle} = N^a,\ \alpha \simeq 0.8 \tag{12}$$

The fact that the exponent a takes a larger value than $1/2$, its value for an equilibrium media with a finite compressibility, appears to be a widely shared characteristic of active media. This presence of large density fluctuations first emphasized in the context of active nematics [86], and found in diverse experiments with synthetic walkers (e.g. [87] but note their absence in the experiments of ref. [88] presumably due to long-range hydrodynamic interactions).

The model described by (10,11) interestingly demonstrates that a mean flow velocity and motion can arise from local velocity alignment interactions between neighboring particles in an active system that is analog to an ideal gas. It appears interesting to investigate the effect of other interactions between the moving particles, so that the model is able to describe analogs of other usual phases of matter and also finite-size droplet-like multiparticle objects. The model was therefore generalized [89] to include short range repulsion as well as longer range attraction between

neighbor particles, with (10) replaced by

$$\theta_i(t+\Delta t) = \arg\left[\alpha \sum_{j\in\mathcal{N}_i} \mathbf{v}_j(t) + \beta \sum_{j\in\mathcal{N}_i} \mathbf{f}_{ij}\right] + \sigma\,\xi(t) \quad (13)$$

where arg[**u**] gives the angular direction of the vector **u**. The interparticle force $\mathbf{f}_{ij}$ was taken to be of Lennard-Jones type and restricted, as the alignment force, to nearest neighbors which were defined by a Voronoi construction at each time step, as well as by the previous metric constraint (i.e. nearest neighbors are defined as Voronoi neighbors at a maximal distance a of each other) ‡. This augmented model displays gas, liquid and solid phases as the strength β of the interparticle force is increased. These phases come themselves in 'immobile' or 'mobile' types depending on the strength of the velocity alignment interaction α. In the "mobile' parameter regime, the model supports moving droplets or moving finite crystalline pieces.

3.2.2. Particle-based model of cell motion Vicsek model and its variants show that correlated motion over large scales can arise from local interactions. The moving patches of particles and transient vortices seen in simulations, are also reminiscent of patterns seen in cell assemblies (see section 6.2). These observations, added to the attractive simplicity of particle-based models, have motivated the formulation of particle-based descriptions of cell collective motion (see [90] for another very recent review). These also constitute natural developments of the classic descriptions of single cell motion, recalled in section 3.1. Time discretization is usually required for simulations, but the models themselves are best described in continuous time as cell motion itself.

Szabó et al [91] directly built on [75]. They measured the velocity directional order for keratocytes *in vitro* and concluded to the existence of a flocking transition from its observed sharp increase with density. In the model formulated to account for their observations, they opted for a two variable description of the single cell, and avoided introducing an explicit velocity alignment term as in [75]. Each cell is characterized by its velocity $\mathbf{v}_i = d\mathbf{x}_i/dt$ and by a motility force $v_0\mathbf{n}_i = v_0(\cos(\psi_i), \sin(\psi_i))$, with a tendency for the motility force to align with the velocity on the time scale τ,

$$\frac{d\mathbf{x}_i}{dt} = v_0\mathbf{n}_i + \sum_{j\in\mathcal{N}_i} f_{ij} \quad (14)$$

‡ In the simulations reported in [89], the noise term is actually included in the argument of the arg function and is therefore multiplied by the number of neighbors of the considered particle. This modification does not change the existence of the model different phases [89] but it could modify the location of the phase boundaries. See [82] for a discussion of this point in the context of the original Vicsek model.

$$\frac{d\psi_i}{dt} = \frac{1}{\tau}(\theta_i - \psi_i) + \sigma\,\xi_i \quad (15)$$

where θ_i denotes the angular direction of the velocity of the i-th particle. The time τ in (15) accounts for the directional persistence of the mobility force as in (4). Similarly to (13), the two-body force $\mathbf{f}_{ij}$ is taken to be repulsive at short distance, attractive at longer distances, and oriented along the vector that join the position of particle i and j. It acts between neighbors, defined in a purely metric way in [91]. For a single particle or for many particles without the interparticle forces, the cell motion takes place at constant speed v_0 with rotational diffusion. This model is a special instance of what is sometimes called an "active brownian particle" (see [92] and references therein), a particle that is ruled by Langevin-dynamics with a nonlinear "friction" term $\gamma(v)$ that vanishes at a preferred speed v_0 (with $\gamma(v) < 0$, $v < v_0$ and $\gamma(v) > 0$, $v > v_0$). This privileged intrinsic speed makes it qualitatively different from Fürth's description and subsequent refinements [44]. Nonetheless, as for an Ornstein-Uhlenbeck process, the velocity decorrelates exponentially in time,

$$< \mathbf{v}(t)\cdot\mathbf{v}(t') >= v_0^2 \exp[-\sigma^2|t-t'|/2] \quad (16)$$

The many-particle model is found in [91] to have a flocking transition as density is increased, similarly to the simple Vicsek model. It is also found to produce an increase of directional order with density similar to the experimentally observed one, with a suitable choice of the (adimensionned) noise amplitude. Visual motion of cells in the experiments and model particles also looked similar near boundaries (Figure 3A). More quantitative comparisons between the dynamics of the model described by (14,15) are however not pursued in [91]. The idea that the cell motile force tends to align with the cell velocity is pursued and modeled in a different way in [93]. The motility force **f** is taken to have a fixed direction during successive intervals of random duration. Alignement of the motility force with the cell velocity **v** is implemented by taking different rates for the Poisson-distributed interval depending whether the motility force is in the direction of the cell velocity ($\mathbf{f}\cdot\mathbf{v} > 0$) or opposite to it ($\mathbf{f}\cdot\mathbf{v} < 0$). As in [91], the alignment of motility forces with cell velocity (i.e. tissue flow) is able to produce, in a suitable parameter regime, velocity fields with large correlation lengths similar to those seen in experiments.

The behavior of the model described by (14,15) was subsequently considered [94] for different numbers of particles confined in a large disk (ie at different particle densities). An alignment transition was observed together with the appearance of large density fluctuations at an intermediate density. At a larger density, a jamming transition was observed with each

particle remaining caged around a mean position and performing a small circular oscillatory motion around it. This latter regime may apply to the dynamics of some active particles. For cells, CIL is expected to be dominant at high cell densities and the potential relation to jamming is discussed in section 5.2. Oscillatory motion of cell polarization has however not been reported in this context.

The wish to have a simple particle model that could be fitted in a simple and quantitative way to experimental observations has motivated the formulation of the interacting particle dynamics proposed in ref. [95]. It reads

$$\frac{d\mathbf{v}_i}{dt} = -\alpha \mathbf{v}_i + \beta(\langle \mathbf{v}_j \rangle_{j\in\mathcal{N}_i} - \mathbf{v}_i) + \sum_{j\in\mathcal{N}_i} \mathbf{f}_{ij} + \sigma\,\eta_i \quad (17)$$

The particle dynamics combine several pieces proposed in previous works. The α term describes the cell velocity persistence as in the Fürth description while η_i is an independent noise term for each particle which accounts for the active and intrinsically stochastic motion of cells. In addition, each particle i interacts with its nearest neighbors in the neighborhood $\mathcal{N}_i$, defined here in a topological way with an upper bound on distance (each particle interacts with its nearest neighbors as long as they are not farther than a distance comparable to maximal cell extension). The interaction with neighbors has two components. The β term drives velocity alignment between neighbors with the velocity of particle i tending to align with the mean velocity of its nearest neighbors. This term acts as a discrete viscosity and is directly inspired by Vicsek et al's proposal [75]. Another type of interaction between nearest neighbor i, j, is mediated by the two-body force $\mathbf{f}_{ij}$ which , as in previous descriptions (13, 14), is repulsive at short distances and attractive at longer ones. In the context of the previous distinction (3,4) between motility and friction forces, one can note that in (17) interactions have implicitly been taken to affect the motility force and thus considered as originating more from signaling than from pure mechanical interactions in contrast to (14).

The model was found to reproduce well the motions of cells as quantified by their velocity probability distribution function (p.d.f.), velocity temporal autocorrelation and velocity-velocity cross-correlation as further described in section 6.1. This quantitative analysis obviously required a suitable choice of parameters but also that the noise η_i was not white but itself an Ornstein-Uhlenbeck process

$$\tau \frac{d\eta_i}{dt} = -\eta_i + \xi_i(t), \quad \langle \eta_{a,i}(t)\,\eta_{b,i}(t')\rangle = \delta_{a,b}\delta(t-t') \quad (18)$$

where the indices $\{a, b = x, y\}$ denote space coordinates. Whereas for a white noise, (17) would be associated with a stationary equilibrium measure of a Boltzmann form with an effective temperature, the colored noise (18) makes the model depart more fully from an equilibrium description. With these choices, the model was also found useful to interpret the motion of MDCK cells in confined environments (section 7.2) as well collective migration on free surfaces (section 6) and the allied interface dynamics (section 6.2 and 7.3). It should be remarked that (17,18) are phenomenological. The velocity alignment term produces, with a suitable choice of the parameter β, a velocity correlation length which is large as compared to the cell size. It remains however to explain how such a term emerges from more elementary processes, for instance via mechanical processes such as repeated encounters between neighbors as observed for synthetic walkers [87], via alignment of motility force and cell velocity [91, 93], or as it is probable, whether it also involves signaling processes through adhesion between cells [96, 97, 98] or CIL as recently proposed [99]. For a system in close vicinity of the jamming transition (section 5.2), the collective dynamics can also exhibit a large velocity correlation length without the need for an explicit velocity alignment mechanism (Figure 3B). It should be further noted that the model of (17,18) is qualitatively different from the previously described (14) or from more general active brownian particle model. As the single cell Fürth's model on which it is based, or more recent refinements [44], it does not assume a preferred nonlinearly selected cell velocity. As such, it does not exhibit a true flocking transition. This was found [95] to match the experimental results of [100] but it cannot be excluded that the model should be modified for different substrates, different conditions or different cells. In this respect the recent single cell model of [66] which presents different cell dynamical regimes appears of interest.

3.2.3. More extended cell description Cells mechanically interact with each other by contact. Cell-cell adhesion, cell-substrate adhesion and cell contractility are central in the control of their shape and motility. It is therefore desirable to develop models that explicitly incorporate these elements.

The need to include a description of cell shape and of a cell interface with its neighbors is most clearly apparent when cell dynamics are primarily controlled by interactions between neighbors rather than by locomotion on a substrate. Representative processes include cell segregation and developmental processes such as gastrulation in which exchanges of neighbors appear to be the primary dynamical drive. It has been observed that in a mixture of cells of different types, cells rearrange and sort out. The process is reminiscent of domain growth after a quench in a two-phase equilibrium region and demixing of

two immiscible liquids. These dynamics are driven by minimization of interface energy. Similarly, it was suggested long ago in the seminal work of [101], that cell sorting is a consequence of differential adhesion. Inspired by the physics analogy, Glazier and Graner [102, 103] proposed to model this process by simulating a q-state Potts model, where each cell is represented in an extended way by a domain of sites in a given Potts state.

The Cellular Potts model (CPM) is formulated on a lattice of N sites. Each site i can be in one of Q states, i.e. $\sigma(i)$ can take one of the values $1, \cdots, Q$ as in the Potts model. In a configuration of lattice state, each cell corresponds to the (possibly disconnected) ensemble of sites in a given lattice state, so that a model with Q states represents $Q-1$ cells and the intercellular medium (m). One can also represent cells of different types, by choosing states to come in different "colors". To investigate cell sorting, "light" and "dark" colors can be chosen to distinguish two different cell types, such that e.g. states/cells $1, \cdots, q_1 - 1$ are light (l) and states/cells $q_1, \cdots, Q-1$ are dark (d) [102, 103]. An energy is assigned to each configuration of lattice sites as a sum of the energies assigned to lattice bonds. The energy is the lowest possible, taken to be 0, when two neighboring sites are in the same state i.e. belong to the same cell. When the two sites are in different states the energy is higher and depends only on their respective colors, i.e on the cell type, with the 5 possibilities $J(d,d), J(l,l), J(d,l), J(d,m)$ or $J(l,m)$. The relative values of these energies control the model favored states. Finally, an energy term enforces the area of each cell, i.e. the number of sites in a given state. The energy $E(\mathcal{C})$ of a given site configuration $\mathcal{C}$ thus reads,

$$E((C)) = \sum_{\mathcal{N}(i,j)} J\left(c[\sigma(i)], c[\sigma(j)]\right) \left\{1 - \delta[\sigma(i), \sigma(j)]\right\} + \lambda \sum_{i=1,\cdots,q} [A_i - n(i)]^2 \quad (19)$$

where the first sum is over the pairs of neighbors in the lattice, chosen as nearest as well as next-nearest neighbors on a square lattice to minimize the unphysical anisotropy arising for discretization. In the first sum, $c[\sigma(i)]$ and $c[\sigma(j)]$ denote the colors of the two neighbors of the pair $\mathcal{N}(i,j)$ in configuration (C) and the discrete δ-function ($\delta[i,j] = 1$ if $i = j$, and 0 otherwise) enforces that there no energy cost to have neighboring states in the same state, i.e. belonging to the same cell. The second sum constrains the area of each cell to be close to a desired area with A_i is the desired number of sites (area) of cell i, and $n(i)$ the number of sites in state i in configuration (C).

The model is simulated by Monte-Carlo (Metropolis) dynamics at a temperature low enough so that energy minimization is the dominant factor driving the dynamics. This is required to have a single connected domain containing (almost) all sites in the same state (i.e. cells in one piece). A modified Metropolis algorithm has also been introduced to strictly preserve cell connectedness at the expense of maintaining detailed balance and a strict connection to equilibrium statistical mechanics (see Glazier et al in [104] for a review). In this low temperature regime, the dynamics follows a decreasing energy path. One can, for instance, easily determine the conditions for cell sorting [103].

The popularity of the CPM is due in part to the fact that it can describe adhesion without the need to explicitly track cell interface. This makes the model easy to program and to simulate. The CPM has been extended to include cell growth, cell division, external fields to model chemotaxis, and the original Metropolis algorithm has been modified to avoid disconnected cells (for a review of these model refinements and some simulation packages [104]).

This has also motivated several groups to try and generalize it to motile cells [105, 106, 107] (Figure 3B). The general idea is to add forces that tend to move cell q (i.e. the ensemble of spin values in the state q) in the motile force direction $\mathbf{n}_q$. This can be done by adding to the energy (19) the "motility" term

$$E_{motility} = - \sum_{q=1,\cdots,Q-1} \mu_q \mathbf{n}_q \cdot \mathbf{X}_q \quad (20)$$

where $\mathbf{X}_q$ is the "center of mass" of cell q, namely the average position of the sites in state q. Motility is driven by the changes of the cell interface which preferentially take place in the direction $\mathbf{n}_q$. The dynamics of the vector $\mathbf{n}_q$ is taken to align with the cell center of mass velocity on a time scale τ, similarly to the single particle (15).

The appealing features of the CPM come, however, with less attractive ones that originate from the biologically unrealistic microscopic dynamics of the CPM. In the model, cell motion is driven by membrane fluctuations. However, these fluctuations are somewhat artificial since they are quite different from the actual cell membrane dynamics. The allied necessary fine discretization of the cell and its interface makes model simulations time-consuming without bringing realism at the scale that is simulated. It also comes with undesirable features, like surface tension anisotropy, detachment of cell pieces that have to be corrected in a somewhat ad-hoc fashion. This has motivated the search for alternative more-controlled descriptions of cell adhesion and contractibility.

One such description [108] of epithelial tissues that is enjoying renewed interest [109, 110, 69] is provided by the so-called *vertex* models. In a two-dimensional setting, the vertex model takes interfaces between cells as straight segments and cells assume a polygonal shape. As for the CPM, this type of

models has first been applied to tissue dynamics driven by cell rearrangement. It is assumed to be well described by motion of the polygon vertices driven by energy minimization, with the energy of a cell configuration depending on the cell areas A_i, the cell perimeter P_i and the length L_{ij} of the interfaces between neighboring cell pairs $< ij >$. A popular choice [110] reads,

$$E_v = \sum_{<ij>} G_{ij} L_{ij} + \sum_i \frac{H_i}{2} P_i^2 + \sum_i \frac{K_i}{2}(A_i - A_i^0)^2 \quad (21)$$

$$= \sum_i \left[\frac{H_i}{2}(P_i - P_i^0)^2 + \frac{K_i}{2}(A_i - A_i^0)^2 \right] + cst. \quad (22)$$

In (21), the first term with $G_{ij} < 0$ favors the growth of L_{ij} and represents adhesion between cell i and j. The second term is meant to represent the elasticity of the cell cortex with P_i the cell perimeter. As written in (22), both terms combine to set a preferred cell perimeter P_i^0 for cell i ($P_i^0 = -\sum_j G_{ij}/(4H_i)$). The last term in (21) prescribes a preferred area A_i^0 for cell i. In the simplest case [110], these parameters take the same values G, H, K and A_0, for all cells and cell interfaces. The minimum energy configurations depend on the parameter choice. They include a stable honeycomb lattice when the preferred perimeter P_0 arising from the first two terms in (21) is smaller than the perimeter of the hexagon of area A^0 and "soft" lattices in the opposite case. Germ-band extension in Drosophila has interestingly been shown to be well-described by a vertex model with an orientation-dependent tension [69]. Algorithms have also been devised to compute the relative energy constants associated to different cells and interfaces from the morphology of an actual epithelium [111, 112, 113]. Finally, the model has been extended to describe non-planar configurations and tissue buckling with an added bending energy term [114].

As the CPM, vertex models can also be generalized to motile cells. The "center of mass" $\mathbf{X_i^{cm}}$ of cell i can be defined as the average of the coordinate of its vertices. In order to generate a cell motility force, [115] introduces the average location $\mathbf{R_i}$ at which cell i adheres and pulls itself on the substrate and add to the energy (21) the elastic term E_{mot} with

$$E_{mot} = \frac{\kappa}{2} \sum_i ||\mathbf{R_i} - \mathbf{X_i^{cm}}||^2 \quad (23)$$

The dynamics of the pulling location is taken in [115] to be relaxational with a random pulling component

$$\sigma \frac{d\mathbf{R_i}}{dt} = \kappa(\mathbf{X_i^{cm}} - \mathbf{R_i}) + \gamma \xi_i(t) \quad (24)$$

where $\xi(t)$ is a vectorial white noise as in (2). Motility could alternatively be created by an energy term like (20) and a persistent dynamics for the motility force like (15).

Finally, there also exists attempts to include adhesion and contractibility in particle models when the cell descriptions are reduced to single points. In this case, a Voronoi construction does not only determine neighbors. It is also used to define cell interfaces which are approximated by the edge of the Voronoi lattice. The dynamics of the cell center can then be driven both by motility and from the variation of a vertex-model-like energy [116, 117].

Both in the CPM and in the vertex model description or its variants, it is assumed that forces in epithelial tissue can be fairly described as the gradient of an energy. This certainly needs to be scrutinized in future works. We have discussed in 3.1.2 the recently described pulsatile character of actomyosin dynamics. It has also been described recently how an actomyosin driven retrograde flow of cell adherens junctions allows dynamic rearrangement of intercellular contact and makes strong adherence between epithelial cell compatible with their collective motion [118]. Clearly, these features of contractility and adhesion lie beyond the simple assumed description. It remains to see what the implication of these results is for tissue level dynamics and generally what a more accurate description of contractility and adhesion dynamics brings.

3.2.4. Continuous media approaches Cell-based approaches offer the advantage that the biology of cells and their interactions can be described in a transparent way and can be easily refined if useful. With present computers, the corresponding models are also easy to program and simulate. However, mathematical analysis and conceptual understanding are often simpler to develop when continuous descriptions are used, as experience with fluid mechanics and solid mechanics clearly shows, as well as sophisticated analyses of statistical mechanics problems (e.g. the renormalization group approach to phase transitions). In general, continuous descriptions require that the spatial variations take place at scales that are large compared to the size of the individual agents (although structural small-scale variations, as in the case of deformations of non-Bravais lattices, can be taken into account by introducing supplementary fields (see e.g. [114] for an example in the context of tissues). In the simplest cases, the specificities of the elementary interacting agents are simply condensed at large scale in the symmetry invariance of the continuous equations (e.g. translation invariance, isotropy or rotational invariance under a restricted rotation group for crystals) and a few parameters (viscosity, elasticity moduli,...). Continuous descriptions often also render easier the numerical description of large scale movements or large scale structures since the relevant scale for the needed resolution

is more tied to the movement correlation length rather to the scale of the elementary moving agent. These different reasons have provided a strong incentive for different groups to develop continuous approaches for collective motion in general and for cells in particular.

Continuous descriptions are classically obtained by focusing on "slow modes" with vanishing restoring drive at long wavelength. Slow modes can arise in different ways. A first common one is that spatially homogeneous steady states form a continuous attractor rather than discrete states. This can be due to the existence of symmetries or to conservation laws (which can be unrelated to symmetries, like particle number). There clearly is no restoring drive when one spatially homogeneous state is changed for another one. For a spatially-varying solution on the continuous attractor, one then can assume that the restoring drive vanishes as the length-scale of the spatial variation grows. This allows one to use a gradient expansion and write "hydrodynamic" equations valid for slow spatial and temporal variations.

A second usual way to obtain a continuous description consists in focusing on the neighborhood of a supercritical bifurcation (e.g. a 2nd order phase transition in equilibrium statistical mechanics). Associated to the bifurcation, there is a zero-mode, that is a perturbation of the homogeneous critical state with a vanishing linear restoring drive. Again in the vicinity of the critical point, long-wavelength perturbations in the direction of the zero-mode produce weak restoring drive and give rise to a slow mode. Gradient expansions can be used to obtain continuous descriptions à la Landau-Ginzburg, eventually also taking into account hydrodynamic modes associated to symmetries or conserved quantities [119]. In this second approach, one also takes advantage that the bifurcation amplitude (a.k.a the order parameter) is small, close to the critical point. This allows one to only keep the first few algebraic powers of the order parameter as nonlinear terms in the continuous equations (the so-called bifurcation normal form).

For "active" particles, both approaches have been employed. For cells moving on a substrate (the so-called "dry-friction" case), cell number is an (approximately) conserved quantity when cell division and apoptosis do not play an important role. Additional slow modes come from deformation associated to translation invariance i.e. compression modes. They can also arise from rotational invariance in the presence of cell velocity and polarization ordering with also an additional slow mode in the vicinity of this flocking transition. One difficulty is that the general approaches outlined above generally produce a multiplicity of possible terms and unknown parameters in the equations. It is then tempting to derive the continuous media parameters from microscopic ones [120] but this requires to consider limiting cases (e.g. dilute media) that are generally far from those of interest. Another less-principled approach is to simply consider the terms that are thought to reflect the dominant mechanisms of interest. We discuss a few examples of these general strategies below.

One of the early continuous description was developed for the Vicsek model by Toner and Tu [79, 80]. It illustrates the hydrodynamic approach as well as some the encountered difficulties. In the original approach [79, 80], it was proposed that the large scale dynamics of the Vicsek model is equivalent to that of a density field $\rho(\mathbf{x},t)$ advected by a velocity field $\mathbf{v}(\mathbf{x},t)$, as for a fluid. Since in the model, there is no division nor death of particles, the density should obey a conservation equation written under the usual form for a compressible fluid,

$$\partial_t \rho + \nabla(\rho \mathbf{v}) = 0 \tag{25}$$

Note that even this usual equation requires further justification: one could have written a more general density current and for instance have added a diffusive term for the density on the r.h.s. of (25).

Toner and Tu focus on the flocking phase for which the local average velocity $\mathbf{v}(\mathbf{x},t)$ serves as an order parameter. The robustness of the postulated flocking phase to intrinsic fluctuations, is investigated by using a a gradient expansion with all the relevant terms compatible with rotational and translational symmetries,

$$\begin{aligned}\partial_t \mathbf{v} + \lambda_1(\mathbf{v}\cdot\nabla)\mathbf{v} + \lambda_2(\nabla\cdot\mathbf{v})\mathbf{v} + \lambda_3(\nabla|\mathbf{v}|^2) = \mathbf{v}F(|\mathbf{v}|) \\ -\nabla P + D_B\nabla(\nabla\cdot\mathbf{v}) + D_T\nabla^2\mathbf{v} + D_2(\mathbf{v}.\nabla)\mathbf{v} + \xi\end{aligned} \tag{26}$$

with the constants λs and Ds respectively controlling the magnitude of advection-like terms and viscosity-like terms. The pressure term $P(\rho)$ is taken to be an arbitrary function of the density and, although not indicated explicitly, all coefficients are supposed to be function of the velocity modulus. The function F is as well an arbitrary function of the velocity with an assumed zero at $|\mathbf{v}| = v_0$, so that the homogeneous steady flocking states stand on a circle of radius v_0 in the velocity plane. The last ξ term in (26) is a white noise field, kept to study the effect of remaining averaged microscopic fluctuations. After linearization of (26) around one of the homogeneous bifurcated steady states, a straightforward calculation shows that at lowest order, noise gives rise to divergent fluctuations of the macroscopic average velocity $\mathbf{v}$. For the equilibrium XY model, the analogous divergence points out the inconsistency of assuming long range order [78, 77]. Toner and Tu however argued in [79, 80] that the non-galilean invariance of (26) introduces a drastic change. Using renormalization

group calculation, they conclude that allowed relevant nonlinear terms in the nonequilibrium (26) modify the critical exponents and allow the existence of the flocking phase. The calculation also explains the occurrence of giant density fluctuations.

In spite of this success, several facts make the problem worth of further theoretical scrutiny in two dimensions. First, the calculations are done near 4 dimensions so the extrapolation to 2D is not obvious. Initially, this was elegantly surmounted by obtaining the values of the 2D exponents from scaling relations between them. Unfortunately, more recent work has shown that the neglect of a possible anisotropic pressure term $Q(\rho)$ (i.e. $[\mathbf{v}\cdot\nabla Q(\rho)\,]\,\mathbf{v}$) invalidates this analysis [121]. Second, the flocking transition itself was not considered in [79, 80] and remained to be described. Third, there has not been much theoretical analysis of the other phases numerically identified in the generalized Vicsek model of [89]. Particle interchange is thought to be at the root the Vicsek phase stabilization. One can thus wonder whether the "moving crystal" of [89] truly exists and how it is stabilized.

Several works have tackled some of these questions. Kinetic theory has been used to derive (25, 26) from a Vicsek-like model, relating the different coefficients in (25, 26) to the parameters of the particle model in the dilute limit [120]. A simple heuristic modification of (26) has been recently elaborated [84] to describe the 1st order flocking transition. It also seems to account for the allied travelling bands of flocking states that are seen in the vicinity of the transition.

Some authors have also proposed continuous descriptions for a cell monolayer moving on a substrate which include both cell velocity $\mathbf{v}$ and cell polarization $\mathbf{p}$ [122, 123, 124]. It is generally supposed that cells exert a pulling force $-f\mathbf{p}$ on the substrate opposite to their polarization, as well as a friction force $\zeta\mathbf{v}$ in agreement with the simple single cell description (3). Force balance reads

$$\nabla.\sigma + f\mathbf{p} - \zeta\mathbf{v} = 0 \tag{27}$$

where σ is the stress tensor in the monolayer. The stress tensor itself is decomposed in an intercellular stress tensor σ_c and an active intracellular stress tensor σ_a. One can remark that this continuum description features two sources of active forces, $f\mathbf{p}$ (cell motility) and σ_a (cell contractility), whereas most particle cell models include only an active cell motility.

It appears reasonable to assume [122] that the intercellular stresses obey Maxwell visco-elastic description,

$$\tau\frac{\partial\sigma_c}{\partial t} + \sigma_c = \frac{\eta}{2}[\nabla\mathbf{v} + (\nabla\mathbf{v})^T - \nabla\cdot\mathbf{v}\,\mathbf{I}_d] + \lambda\cdot\mathbf{v}\,\mathbf{I}_d \tag{28}$$

with $\mathbf{I}_d$ denoting the identity matrix.

Cell division and apoptosis have been shown to contribute to tissue fluidization [125] but even in their absence, it is estimated that $\tau = 15$ mn in [122] based on cadherin turnover rate. Note also that a total derivative including advection terms could be appropriate on the l.h.s. of (28). The active intracellular stress tensor is supposed to be along the cell polarization $\sigma_a \propto \mathbf{pp}$ in [122] whereas an isotropic tensor is taken in [124]. Finally, one needs to describe the dynamics of the cell polarization. This has been modeled [122, 126, 124] similarly to a nematic director [127, 128],

$$\frac{\partial\mathbf{p}}{\partial t} + \mathbf{v}\cdot\nabla\mathbf{v} - \frac{1}{2}(\nabla\times\mathbf{v})\times\mathbf{v} = \kappa\nabla^2\mathbf{p} \tag{29}$$

where the elastic Franck moduli have been supposed to be equal. The advection terms are borrowed from the liquid crystal literature [127, 128] by identifying cell polarization and nematic director, an assumption that would deserve further scrutiny. These advective terms are estimated to be small and are neglected in other works [124]. It should be noted that the innocuous-looking elastic coupling term for cell polarization is important since it takes the role of the Vicsek alignment term in this description. Its biological origin remains however to be determined. As we discuss below, this type of continuous model has been used to describe epithelium dynamics in wound assay experiments either in the free interface geometry [126, 124] (section 6.2) or the closed contour one [122] (section 7.2).

We have shortly surveyed here, different types of modeling that have been developed to describe collective cell motion. The present models account for the underlying biology in a very simplified way, certainly oversimplified in many respects. Basic assumed features and interactions are somewhat uncertain, in several instances. It appears that more firmly grounded theoretical descriptions can only be gained from well-controlled experimental investigations and detailed tests. We proceed and describe where we presently stand in this quest.

4. Experimental approaches-Experimental models

Studying *in vitro* situations of collective cell migration relies on specific techniques and analyses. Although this review does not specifically deal with experimental details, it seems useful to go rapidly over the major techniques used in this context and to insist on the most recent developments. The mechanical characterization of assemblies of cells in motion encompasses in particular dynamically mapping the displacements of the cells, the forces they exert on the substrate (traction forces), and the intercellular

forces. A full characterization, however, is not limited to these physical descriptors. To fully understand the phenomena at play, it is also necessary to probe in parallel the signalization pathways. Importantly, to address the emergence of collective phenomena, it is crucial to characterize the system both at the population scale and at the scale of the individuals within these populations. This is the equivalent of macroscopic vs. microscopic scales in many classical statistical physics problems.

4.1. Experimental in vitro *systems*

In vitro, a vast majority of the collective migration experiments deals with epithelial cells plated on a surface. Among the model experimental cell systems, the Madin-Darby Canine Kidney (MDCK) cells are probably the most popular. They represent a prototype of epithelial cells in culture with well-marked apico-basal polarity and strong cadherin-mediated cell-cell adhesions. To study human cell lines, other cell types have been investigated and in particular the MCF-10A epithelial cell line derived from the breast as well as various derived tumorigenic cell lines.

Most of the experiments deal with cells plated on planar rigid surfaces (glass or plastic). These substrates may be coated with extra-cellular matrix proteins such as fibronectin, laminin or collagen. They can also be used directly, in which case, the cells produce their own matrix on which they migrate. Soft polyacrylamide or silicone gels have also been used as substrates because of their compatibility with Traction Force Microscopy (TFM, see section 4.4) and in this case, a coating is mandatory.

Some experiments have dealt with 3D situations by growing cells in collagen or matrigel gels. Intermediate situations where cells migrate in topologically complex environments (pillars, wires, ..) or sandwiched between two gel slabs, have also been investigated.

4.2. Observing cells in a monolayer

As already mentioned, collective migration requires analyses at different scales. Optical microscopy is particularly well suited to the study of cells, allowing to go from monolayer imaging at low magnification to subcellular details. Beyond cell observation, optical microscopy is also the right tool to access the flows and forces in the monolayer as described below. Of note, the dynamics of these systems is slow and goes with long acquisition times (days or weeks).

Phase contrast microscopy that allows detecting thickness gradients such as cell contours is well-suited to the observation of cells in a monolayer. Specific cell components can be imaged by fluorescence microscopy at high magnification after fixation and labeling (in particular by immunofluorescence techniques).

Live cells can be observed by fluorescence microscopy at the extra cost of a transfection of the cells with a fluorescent construct. In this way, specific components of the cells can be dynamically monitored. In particular, targeting the nucleus allows the measurement of cell density and the tracking of cell trajectories. Nuclei can be labeled with a chemical dye for a limited time because of toxicity or, via the labeling of histones with a fluorescent construct.

4.2.1. Wound healing To offer free surface to a bidimensionnal cell confluent layer, the wound healing assay appears to be the technique of choice. It has been used for decades and consists in making a physical scratch in a confluent monolayer [129]. One then observes how the monolayer responds to this stimulus by migrating collectively on the cell-free surface to restore its integrity. Very small (typically one cell size) wounds can also be created in a cell monolayer by laser ablation [130].

Although this technique is widely used and provides an easy-to-implement tool to study cell migration, several practical caveats should be noted. First, the scratch creates a physical wound in the monolayer and therefore, damages or permeabilizes the cells of the newly created border. Second, the initial free edge of the monolayer is not well defined, debris are left in the scratched gap and the cellular content of the mechanically destroyed cells goes in the culture medium. Third, and perhaps more importantly, prior to the wound, cells modify the surface they adhere to, in particular by secreting extra cellular matrix; therefore, the cells set to migrate by a scratch-wound actually move over a conditioned, largely uncontrolled, substrate. Finally, besides the trauma caused to the cells by the ripping off of cell-cell adhesions needed to create the free edge, it may take some time for cells to switch from their phenotype in the bulk of the initial monolayer to the one they may eventually acquire at the edge.

To alleviate some of these drawbacks, alternative techniques have been proposed. For example, microfluidic assays have used the laminar flow characteristic of low Reynolds number microfluidic flows to remove human vein endothelial cells (HUVECs) from a confluent monolayer with high precision along a well-defined stripe [131]. However, the most commonly used alternative to the scratch wound assay remains the barrier assay that consists in culturing a monolayer limited by a physical barrier until it reaches confluence. The barrier is then removed and cells are left to migrate [132, 100, 133]. By not physically injuring the cells, this approach solves some of the ambiguities of the scratch

wound assays.

The recent and massive development of microtechnology in biology has allowed the design of barriers of various shapes and sizes (squares, disks, ellipses etc...) and the testing of relevant features such as wound size or curvature. A related technique consists in micropatterning the surface with a cell-repellent coating separating areas where cells are grown to confluence. The chemistry of the coating is tailored so that it can be desorbed by an external signal such as light or an electrical field, which then triggers cell migration [134, 135]. These barrier or barrier-like assays can be used to produce long wounds with basically infinite edges or smaller closed-contour wounds with a continuous edge. Upon migration, these two geometries correspond to expanding or converging flows [136].

Of note, several works have combined surface patterning with cell migration by coating the substrate with robust adherent/non-adherent domains. Adherent domains are classically glass or plastic possibly coated with an extracellular matrix component like Fibronectin or Collagen. The non-adherent coating is generally based on polyethyleneglycol (PEG) chemistry [137, 138]; it has to be very robust to allow for long observation times.

4.3. Displacement field

In the particular situation of wound healing, the progression of the front edge of the monolayer can be monitored with time. This provides a first global indication on the cell dynamics. A more detailed interpretation requires the simultaneous characterization of individual cell trajectories within this population. However, monitoring the trajectories of cells which collectively migrate within a monolayer proves to be a difficult task. The high cell density makes it difficult to follow cells from one frame to the next and to extract individual trajectories, when they are not labeled with a fluorescent dye. Tracking individual cells is however possible at the free edge where the cell density is smaller. Therefore, the common strategy of analysis of wound assays is to track several edge cells (most of the time, manually) and extract an average speed and persistence [139].

The difficulty of accessing information on the cell displacements within the monolayer can however be overcome in different ways. The first approach is to label cells in the monolayer. Sparse cells transfected with a cytoplasmic fluorescent protein [68] or even densely packed cells whose nuclei or membranes have been fluorescently labeled [140] can be tracked and their trajectories reconstituted. This strategy can be automated up to a certain point; however it necessitates the extra cell labelling step, notwithstanding the potentially deleterious effects of this treatment on cell viability or motility. Moreover, some degree of manual supervision is often necessary for the analysis, which can dramatically increase the analysis time.

Another strategy (Particle Image Velocimetry - PIV) has recently proved to be very well suited to the mapping of local displacements in cell monolayers. In contrast with the Lagrangian approach of cell tracking, PIV takes an Eulerian approach by mapping the velocity field in the monolayer at each timepoint, without relying on the actual trajectories of the individual cells. PIV is widely used in hydrodynamics to measure local flows in liquids where small beads have been dispersed. Briefly, subwindows are defined in each image of a movie and a cross-correlation is performed between subwindows identically positioned in successive frames (Figure 4A). The correlation peak then corresponds to the average displacement [141]. One of the major advantages of the technique is that it does not require cells to be modified, with a fluorescent dye for example. The texture of images acquired in phase contrast is sufficient to allow the computation of the correlation plane [142, 143].

From the velocity fields, it is then easy to quantitatively measure and map various descriptors such as the divergence of the velocity field or its vorticity[12, 142]. For example, it is straightforward to measure the velocity spatial correlation function and extract a correlation length that describes the range over which movements in the monolayer are correlated. Time correlations can be similarly assessed.

Therefore, PIV provides a fully automated, objective way to quantify collective migration for cells positioned not only at the front edge but also in the monolayer. For instance, the distribution of the cell speeds can be measured as well as the orientational order of the cell velocities. The allied order parameter is a good descriptor of the coordination of the displacements in the monolayer; it conveys an information equivalent to the persistence computed on individual trajectories [142]. Moreover, mapping the velocity field is fully automated and fast once the parameters of the analysis have been set. PIV makes it possible to analyze many movies and therefore to integrate this analysis in high throughput migration assays to classify genes or drugs [144].

4.4. Stress field

Mechanical traction forces exerted by cells on their substrate are classically measured by plating cells on soft gels (Polyacrylamide or PDMS) in which small fluorescent beads have been dispersed [145]. The displacement field measured on the position of the beads can be inverted to access the force field [146, 147] (Figure 4B). This approach has been recently

extended to multicellular assemblies [148]. Of note, this inversion is a complex mathematical problem that necessitates a fine tuning of the parameters used to perform it. Thanks to the constant increase in computational power, this technique is now very widely used under the name of Traction Force Microscopy (TFM). Importantly, using soft continuous gels as a substrate allows stress to be transmitted via this substrate which in return can modify the behavior of the cells [149].

Another technique has been proposed to get around some of these limitations. In the micro-pillar assay, cells migrate on top of an array of flexible PDMS micron-size pillars (Figure 4C). The deflection of each pillar whose geometry and elasticity are known, gives directly the local force exerted on the surface [150, 151].

The forces at cell-cell junctions are a very important piece of information that can be extracted from the strain field caused by the cell traction forces at the surface of the gel [152] or from the map of the traction forces exerted on the surface using force balance (Monolayer Stress Microscopy (MSM); Figure 4D) [153]. In one dimension, the calculation is exact [148]. However, in 2 dimensions, it requires knowledge of the monolayer rheological properties [154]. It is typically assumed that the monolayer behaves elastically [154]. This assumption has been supported by independent numerical simulations [155] and by recent inference Bayesian inversion techniques [113]. In any case (soft pillars or soft gels), forces are measured via displacements at the surface. This means that the substrate must have some flexibility that can itself affect the result [156] and, more generally, the behavior of the cells, including the characteristics of their collective migration [157]. Therefore, the choice of the "right" stiffness results from a trade-off (the gel has to be soft enough to be able to measure the forces, yet stiff enough not to perturb too much the migratory phenotype).

4.5. Signaling

A full description of the various techniques used to identify the proteins at play and measure their concentration and activity is beyond the scope of the present review. We merely mention here a few recent developments. To identify in an unbiased way the genes regulating collective migration, several studies have performed high-throughput wound-healing assays [129]. These screens, that can use different read-outs, have identified several protein families with an emphasis on cytoskeleton or cytoskeleton-associated proteins [139], growth factors [140] or adhesion proteins [139, 140, 158]. Once a protein of interest has been identified, its function can be targeted using specific inhibitors or with mutants lacking this specific protein. The proteins that participate to cell-cell epithelial or endothelial junctions are among the favorite targets of these experiments. They include cadherins, myosins that ensure contractility, and the previously mentioned Rho-GTPases, Rho itself which acts upstream of myosins, and Rac, that is involved in actin polymerization and is antagonistic with Rho [159]. Concentrations of these proteins can be locally estimated by fluorescence. In many situations, the activity of the protein is a more relevant measurement. The active form of the protein goes with a change of conformation that can be measured locally by using cells transfected with biosensors that emit a specific FRET signal when the protein is active [160, 161].

5. Flows and forces in confluent monolayers

5.1. Contact inhibition of locomotion

As described in section 2 (see Figure 2),"Contact inhibition of locomotion" (CIL) describes the arrest of two migrating cells when they touch and the subsequent reorientations of their displacements. This phenomenon is complex, involving the sensing of one cell by the other one and their subsequent repolarizations. Although it has been described long ago in the case of fibroblasts migrating on a surface [20, 162], the mechanistic basis of CIL that involve different signaling pathways is still not fully understood [163, 18, 164, 165]. Contact inhibition would make one anticipate a complete arrest of motion for a cell in a monolayer since there is no direction of motion free of cells. However, this is not what is generally observed. As a matter of fact, cells remain motile even in confluent monolayers where there does not remain areas free of cells. Cells move within these monolayers by developing lamellipodia but, since there is no free space, these lamellipodia develop under the nearby cells (cryptic lamellipodia) [68]. It is observed however that movements gradually slow down as density increases because of cell proliferation. Of course, the situations where the monolayer presents a free edge for instance after a wound, is different and the edge itself acts as a cue for migration [9].

5.2. Jamming of a cell monolayer

One generally observes that the average velocity of cells in a monolayer progressively decreases after they reach confluence, a property that amounts to a generalized CIL (the situation is different before confluence where cells collectively migrate on the cell-free areas). Initially, cells significantly move in groups but at long times, these displacements freeze and become more local. Since theoretical models and numerical simulations have shown that self-propelled

particles jam at high density [166], it is tempting to interpret these observations in the framework of the jamming theory classically used to describe granular material or concentrated colloidal systems.

As a matter of fact, the changes in collective cell dynamics are reminiscent of the transition observed in granular systems with increasing density. In these materials, the jamming transition - associated with the glass transition in other types of materials - involves clusters of particles whose characteristic size increases with crowding, and the slowing down of movements [167]. In other words, as volume fraction increases, the movements freeze and the associated correlation length increases [168]. Because of the analogy between stress in granular media and temperature in glasses, a 3-axes representation has been proposed with stress and temperature as independent axes, the third axis being the inverse of the volume fraction [167, 169](Figure 5A). In such a diagram, the so-called jamming surface separates a fluid phase (above it) and a jammed solid phase (below it, close to origin). For active systems, the temperature is an effective temperature set by the activity itself [170]. As previously mentioned, crossing this surface goes with large spatial heterogeneities, with large density fluctuations and clustering of the fastest particles in large domains [94]. This framework can be applied to describe the change of behavior observed in Vicsek-like models [75] (section 3.2.1) as their parameters are varied. The density and noise intensity are then, respectively, the analogs of the volume fraction and temperature.

The transposition to biological active matter such as cell monolayers although tempting, necessitates some important assumptions. For instance, the system is usually treated as a 2D incompressible material and the cell density is the equivalent of the surface fraction. However, real cells are not purely 2D. Their height increases as their density increases and their projected area decreases, amounting to a finite 2D compressibility. These questions which are already a concern in the description of soft colloids [171], become critical in this context.

The analogy with the jamming transition was explicitly proposed and investigated with keratocytes monolayers [91] and with MDCK monolayers plated on soft polyacrylamide substrates [12]. In this last example, the speed of the cells is spatially very heterogeneous with fast cells regrouping in clusters. This allows one to define a heterogeneity length as the typical size of clusters of highest speed. As time goes on, cell density increases because of proliferation, and the cell mean speed decreases. In parallel, the heterogeneity length increases. This behavior is typical of a system approaching the jamming transition via an increase in cell density. This conclusion is backed by the observed reduction of diffusive motion with cell density as cells get caged by their neighbors. It has to be noted that the behavior is strikingly different when cells of the same type are plated on rigid glass slides [149, 172]. In that case, the heterogeneity length *decreases* as density *increases*. On soft substrates, part of the intercellular interactions may be mediated via the substrate itself [149]. The observed difference between hard and soft substrates may also be the consequence of a modulation of the cell-substrate adhesions that in turn may impact the cell-cell adhesions [157].

The framework of the jamming transition can also be used to interpret the collective behavior of monolayers of MCF-10A breast cancer cells [173]. In this case too, spatially heterogeneous dynamics at the multi-cellular scale are observed in parallel with a slow-down of all movements with time, as cell density increases. Furthermore, as in the previous example, the dynamics of individual cells at high density appears controlled by transient trapping in cages formed by their neighbors. The complex dynamics of relaxation times involve the deformable nature of MCF-10A cells whose rigidity is also a function of density, similarly to what is observed with soft colloids [171]. Moreover, in the last stages of a wound healing assay, when two identical MCF-10A monolayers fuse, the interface between the two initial monolayers remains well defined. No mixing of cells originating from the two opposite monolayers occurs, regardless of their homotypic adhesion [174]. This absence of mixing can be interpreted as a resultant of the jamming of the cells at this interface when the directed motion of the cells at the two front edges is hindered.

This analogy between collective cell behavior and a system close to its jamming transition has also been tested in zebrafish embryonic tissues aggregates where caging of the cells by their neighbors is observed [175]. The particle-based mechanical model developed to interpret these experiments shows that although the system is fluid, it is close to its jamming transition, suggesting that the viscoelastic rheology observed in such systems is controlled by this proximity to the transition. A similar effect could potentially impact the interpretation of wound-healing experiments where gradients of density naturally form (low cell density at the front edge and high density in the monolayer) [173, 176]. More generally, it is interesting to note that the proximity of a transition has been argued to be important in different biological contexts (see [177] for a recent discussion).

In order to go beyond these dynamical observations, a series of experiments was performed in which the stress field within the monolayer was carefully measured by MSM [153]. They demonstrate that the stress

field is also spatially heterogeneous and dynamically fluctuating with characteristics that are common to rat pulmonary microvascular endothelial cells (RPME) as well as MDCK and MCF-10A epithelial cells [153]. The high intercellular stress cooperativity in these monolayers increases with time and cell density. In parallel, as the system progressively evolves from fluid to solid, the movements of the cells gradually freeze while their velocity aligns with the local direction of principal stress. These observations confirm the analogy with a system close to its jamming transition. The dynamic heterogeneities observed in the stress field and in the velocity field were also analyzed for the MCF-10A cell line and two derived MCF-10A cell lines [153]. Compared to wild-type, the degree of local alignment of the velocity with the direction of principal stress is favored when the proliferation is increased and almost vanishes when adhesion between cells decreases.

The analogy to jamming has pushed several groups to try and adapt the classical three-axes jamming diagram to the particular case of cell monolayers. It was, for instance, proposed [176], that on the three-axes jamming phase diagram (Figure 5A), the equivalent of temperature is the cell motility, the inverse of cell-cell adhesion plays the role of stress, and the cell density is the counterpart of the volume fraction. Such a phase diagram can be used to interpret the dynamics of the MCF-10A epithelial cell line and its two derived cell lines by positioning them with respect to the jamming surface : the wild type is unjammed but close to the transition, the cell type for which the cell-cell adhesion is degraded is unjammed and more fluid, and the one for which the proliferation is enhanced is jammed.

The role of density *per se* as a relevant parameter in the jamming of an epithelial monolayer appears, however, questionable [178, 179, 172]. In an epithelial monolayer, there are no gaps between cells and the analogy between cell-density and volume fraction does not have a firm basis, as stressed in [178, 117]. The question was investigated using a vertex model (22), approximating the monolayer as non-motile adjacent cells with identical cell elasticity, active contractility and interfacial tension [178]. Computing the values of the energy barriers opposing cell rearrangements in a disordered configuration shows that they are finite below a critical value $p_0^* \simeq 3.81$ of the shape factor p_0 of the cells (defined as the ratio of their preferred perimeter to the square root of their preferred area (22), $p_0 = P_0/\sqrt{A_0}$). In this case, the system is frozen, and $p_0 < p_0^*$ corresponds to the jammed phase. The cell-cell interfacial tension is dominated by cortical tension in this phase, whereas cell-cell adhesion dominates in the fluid regime.

The analysis was extended to motile cells with intrinsic velocity v_0 (14), using a vertex model based on a Voronoi construction to define the forces f_{ij} between pointlike cell 'centers' [117]. In this generalized model, the preferred shape factor $p_{0,c}(v_0)$ depends on the cell intrinsic motility. Quite remarkably however, at the jamming transition the mean shape factor of cells, based on observed perimeter P_i and areas A_i, is independent of cell velocity and take the same value as for non-motile cells, $\langle P_i/\sqrt{A_i}\rangle \simeq 3.81$.

These predictions and the jamming transition were investigated in several experiments dealing with primary non-proliferating bronchial epithelial cells (HBEC) from healthy and asthmatic patients [179]. At the same cell density, monolayers of cells from asthmatic patients remain fluid while the normal cells are already jammed, suggesting that the dysfunction itself can be linked to the distance to the jamming transition. Upon stress, normal cells fluidize before returning to their basal solid-like jammed state while this transition is considerably delayed for cells from asthmatic donors, contributing to a permanent remodeling of the tissue which is a landmark of the disease. Since these experiments were performed at constant cell density (these primary cells dont proliferate), they support the view that cell density is *per se* not a good control parameter of the jamming/unjamming transition. These experiments and the theoretical results led the authors to reconsider the analogy with jamming and to propose [117, 180] a phase diagram for monolayers (Figure 5B) where the three-axes are the preferred shape factor p_0, the intrinsic cell velocity which acts somehow as stress, and the directional persistence of cell motion (as measured by the parameter $1/\sigma^2$ (15,16)). Increased directional persistence is found to be associated with a more collective behavior of cells which is more effective at fluidizing the tissue.

Other experiments also downplayed the direct role of cell density in the jamming transition for cultured HBEC cell line [172] and found that in contrast, motility, is a good control parameter playing the role of an effective temperature. The velocity correlation length was shown to exhibit an unexpected non-monotonous behavior as a function of the r.m.s. cell velocity [172] also observed with MDCK cells [115]. This observation results from an intrinsic maturation of the system independent on the density which makes its representative point move in the three-axes jamming diagram. Indeed, in [115, 172, 179] both cell-cell adhesion and cell-substrate were shown to evolve with time. These biophysical parameters control the shape factor and the cell motility in the analysis of [117]. Analytic estimations and simulations of self-propelled interacting particles have confirmed the importance of these changing biophysical parameters in accounting

for the experimental observations [172].

5.3. Cell migration in confined environments

After cells reach confluence, but before they jam, cells move within the monolayer over large distances as compared to their size. Their displacements are then correlated over long distances (many cell sizes; see section 6.1). Confining the cells in well-defined micropatterns whose size is smaller than or comparable to this correlation length (around 150 μm for MDCK cells) gives an extra control parameter on the behavior of the cells (Figure 6A).

By chemically patterning the surface, one can confine cell cultures in well-defined domains of basically any shape and size with a resolution of typically 1 μm. When plated in circular domains, epithelial cells show large correlated movements in typically the first 30h after confluence [181, 182, 183] (Figure 6B-C), after which their displacements gradually freeze and become very local as described in the preceding part (section 5.2).

Averaging the *orthoradial* component of the velocity over all angles shows that, in average, its maximum amplitude is reached at the edge of the domains and is minimal at their center [181, 182], as shown in Figure 6C. In small domains, the cellular system approximately rotates as a solid body. The rotation can occasionally change direction but these changes are stochastic [182]. When the size of the domain becomes very small, down to a few cell sizes only, the discrete nature of cells manifests itself. In particular, the persistence of the angular motion increases with the number of cells but shows a discontinuity when the number of cells increases from 4 to 5 (while adjusting the radius of the pattern to keep the same cell density) [183]. This transition can be explained by a change in the arrangement of the cells. For 4 cells or less, all cells participate in the pattern boundary. For 5 cells or more, there has to be at least one cell in the center that does not interact directly with this boundary. This arrangement of cells is obviously very dependent on the exact shape of the domains [184]. More quantitatively, different theoretical models including Potts models [181], active particles models [182] or approaches combining vertex-like models and self-propelled particles [116] have been used to describe the global rotation in small and mesoscopic domains as well as the change of behaviors between 4 and 5 cells in small domains [183].

The angle-averaged *radial* component of the velocity is minimal at the center of the domains and at their edges [182] (Figure 6B). These two boundary conditions are expected from symmetry reasons. However, more surprisingly, the radial speed has a clear maximum at mid-radius. Phases where displacements are oriented outwards alternate with inward displacements. Averaging the radial component of the velocity over the radius and analyzing it by Fourier transform shows that these fluctuations have an oscillatory character with a well-defined frequency that decreases with the domain's radius. These "breathing oscillations" depend on cell-cell adhesion and on actomyosin contractility but not on cell proliferation. They are not a consequence of the jamming of the system [94] since they are observed while the cells are still very motile and explore large distances. Furthermore, the phase difference between different radial positions is close to zero. Thus, these oscillations appear distinct from the mechanically excited waves observed during wound healing of the same MDCK cells on soft Polyacrylamide gels [185] (section 6.1).

Cellular movements in a collectively migrating monolayer can be well-described by the particle-based model (17) where cells are persistent random walkers that tend to adapt their velocity to that of their neighbors [95] (section 3.2). The same model was used for simulations in circular domains, keeping the parameters of the model at the values that were extracted from the migration experiments [95]. This simple model recovers qualitatively and quantitatively the global rotation of the cells and their radial breathing oscillations (Figure 6D-E). These breathing oscillations therefore appear to result from the oscillatory modes caused by the stochastic motion of the cells in a confining domain. In this view, the observed oscillations can be interpreted as the filtering at a particular frequency of the stochastic noise generated by cell motion. It has been alternatively suggested [124] that they result from a real oscillatory bifurcation coming for a feedback loop between strain and contractibility, as previously proposed [123] for waves observed during wound healing [185] (section 6.1).

Very interestingly, the collective movement of the cells in mesoscopic well-defined domains clearly shows a Left-Right asymmetry which can be seen both on the cell displacements and on their alignment. Similarly, when plated on ring-shaped or stripe micropatterns, cells of various types exhibit an intrinsic chirality in their organization and displacements by favoring a particular direction of migration/rotation [186] (Figure 7). The cells align accordingly and adopt a chiral pattern with a well-defined angle between the cells main direction and the direction of the pattern [186, 187]. The phenomenon appears to be actin- but not tubulin-dependent; it also depends on cell contractility [187] and on cell-cell adhesion [188]. The preferred direction of rotation itself is fixed by the cell type. This "collective chirality" appears to result from single-cell

chirality. The centrosome of the edge cells is positioned between their nucleus and the edge of the pattern with a bias in one direction. MDCK cells in circular domains show a similar trend although not as pronounced [182], probably because the stagnation point at the center is not as favorable to the development of chirality as two parallel boundaries. Chirality in the structure of single cells confined to circular domains has been reported and shown to be the indirect consequence of the chirality of the actin filaments [189]. However, the mechanism extending this symmetry breaking to populations of cells remains unclear.

6. Collective migration on free surface: the wound-healing assay

We now consider the evolution of an epithelium when it faces free surface. Comparison between wound-healing experiments involving a scratch wound and a barrier assay allows one to answer a fundamental question: Is physical injury to the cells necessary to trigger their migration? The answer is very clear from a large number of experiments: free surface by itself is sufficient to trigger cell migration [132, 190, 97, 100, 191], confirming the classic dictum "An epithelium will not tolerate a free edge"[192, 193, 68].

Epithelial cells, such as MDCKs, progress in a highly collective way. In particular, there is no cell escaping from the monolayer front edge. A first observation of the migrating epithelial monolayer shows two striking behaviors:
- The displacements are not necessarily "productive", they are not all directed toward the free surface although of course, this remains the average direction. Locally, all directions of displacements are allowed, even occasionally in an anti-productive direction. Furthermore, cells displacements are correlated i.e. cells in the monolayer move in groups. The displacement map is complex and involves swirls and other patterns (Figure 8A). With time, the displacements of cells tend to become more productive.
- Pluricellular "migration fingers" appear at the edge of the monolayer. These fingers are preceded by a cell whose morphology is different from the others: it is more spread and it exhibits an active lamellipodium at its front-edge.

We now detail these two aspects, beginning by the simplest geometry where the front edge is initially linear and sufficiently long to be considered as infinite.

6.1. Correlated movements and cooperativity in the monolayer

The correlation in the displacements corresponding to the size of the swirls is best quantified by computing the velocity correlation function from the velocity field. Technically, the use of PIV (section 4.3) to map this field is critical since traditional tracking would not allow one to access these quantities with sufficient statistics in a reasonable time. For MDCK cells, prototypical of epithelial cells, with well-defined cadherin-mediated cell-cell adhesions, a correlation length of typically 150 μm is measured [142, 194, 195, 153] (Figure 8B). This means that displacements in the monolayer are independent when they are separated by more than about 10 cell sizes. This large value highlights the importance of the collective migration in experiments. When the migration is oriented by nanostructuring part of the surface, the physical signal of contact guidance propagates in the unguided epithelium over a distance of the order of this correlation length [196].

The correlation length is very dependent on the cell type. For the more independent fibroblast-like NRK cells, it is only 20 μm (about 2 cell diameters; Figure 8A-B)). For a given cell type, the correlation length is also dependent on other parameters such as cell density [115, 149], contractile activity [157, 194], or cell-cell adhesions [172, 157, 153, 140, 197, 179, 198] in the line of what has been described in the context of jamming (section 5.2).

The large correlation length of the velocity correlation is well reproduced by particle-based models [91, 93] and extended cell models [106, 107] based on alignment of the cell motility force with cell velocity. The use of a phenomenological Vicsek-like term [95] allows one to reproduce quantitatively characteristics of the velocity beyond the existence of a large correlation, such as the distribution of cell velocities or the temporal velocity autocorrelation (Figure 8D-G).

The Cellular Potts Model has also been used to analyze how the correlation length depends on the strength of adhesion and the cell motile force [107] (Figure 3C). For low motility forces, cells are trapped by adhesion with their neighbors. For strong motility force, a cell can deform its neighbors and adhesive bonds can be broken. As a result, cells do not move very coherently in this regime either. It is only at intermediate motility forces that adhesion and alignment of motility on cell velocity work in synergy to produce large correlation lengths [107], when the system is close enough to the jamming transition (section 5.2).

Importantly, experiments are often conducted on soft substrate (such as Polyacrylamide gels) in particular because it is the substrate used for measuring traction forces (section 4.4). In this case, the stress can propagate via the substrate and not only via the monolayer (as it is the case on rigid substrates). This cell-driven substrate deformation

contributes to the mechanical coupling between cells and to correlations in the migrating monolayer [153, 157, 149].

It is very instructive to measure the traction forces exerted by the cells in these monolayers when they migrate collectively to close the wound. As noted previously, space and time fluctuations of the forces are very large. In average, traction forces are maximal at the edge and oriented toward the bulk of the monolayer (they pull on the monolayer) [151, 148](Figure 8Ca-b). This observation allows one to conclude that it is active migration and not pressure, for instance due to proliferation, that drives the healing of the monolayer, a conclusion confirmed by experiments in which proliferation is inhibited [100].

To get a better insight on the situation in the monolayer, one can average the traction forces along the edge of the wound to overcome the intrinsic fluctuations of the system and treat the situation as a unidimensional problem. When such an averaging is performed, it is found that pulling forces decrease from the edge toward the bulk but do not vanish up to large distances (several 100 μm) from the edge [148]. In other words, cells in the monolayer contribute to collective migration even when localized many rows behind the edge. These traction forces must be balanced by the internal stress in the monolayer itself. The average internal stress within the monolayer is therefore tensile and increases from the edge.

More local information on the intercellular forces exerted in the monolayer can be obtained by analyzing the traction forces maps (Monolayer Stress Microscopy (MSM); Figure 8Cb,c; see section 4.4) [153]. The stresses in the monolayer are locally tensile and cells migrate along the direction of the local principal stress [153]. Spindle-shaped endothelial cells align physically with this maximal principal stress direction but MDCK cells also obey that rule while their cell geometry remains isotropic.

Dynamically monitoring the mechanical parameters (traction forces, monolayer stress and velocity) involved in the migration of MDCK cells shows the existence of propagating mechanical waves in millimeter-size cell stripes [185] (Figure 9A-B). These waves propagate from the edge toward the center of the stripe and back, at roughly twice the speed of the advancing front. They are dependent on cell-cell adhesion and on contractile activity. Although their origin is not completely clear, a model of mechanically excitable waves is consistent with the experimental data, assuming a complex rheology of the tissue that involves in particular a reinforcement/fluidization of the tissue at a critical strain threshold. An active gel model encapsulating contractile activity and polarization of the cells, and ignoring possible heterogeneities within the cell population, also describes the data provided that contractility is function of strain [123](Figure 9C-D). Interestingly, this feedback between contractility and local strain accounts for the periodic reinforcement/fluidization assumed in the previous model [185].

Patterning the surface with large non-adhesive patches that cannot be covered by the cells, amounts to placing obstacles on the path of the migrating monolayer [199]. The flow lines associated to displacements of the cells exhibit two expected stagnation points at the front and back of these obstacles. Far from one obstacle, the above-mentioned correlation between traction forces and displacements is well verified. However, this relationship breaks down close to the obstacle boundary. At this location, forces are systematically centripetal while the flows are not. Therefore, edge cells downstream the obstacle exhibit traction forces antiparallel to the actual flow. Consistently, displacements and maximal principal stress are also uncoupled close to the edge. This systematic orientation of the traction forces toward the center of the non-adhesive surface may be related to the acto-myosin cable developing at the free edge of an epithelium [200, 201] that we describe in another context in section 7.2. Alternatively, a particle-based model of cells interacting through CIL naturally gives particular properties to the edge cells since they have one side free of neighbors. Such a model also describes well the monolayer behavior next to the non-adherent obstacle [99].

6.2. Cell-cell adhesion and the importance of having a free edge

Weakly adherent cells can migrate collectively with a well-defined front even though single cells may occasionally escape from the monolayer [173]. In that case, the highly directed motion of the cells in the monolayer allows the monolayer to catch up with the escaping cells that have a lower persistence. Collective motion of non-adherent cells can be observed *in vivo*; it is attributed to the secretion of chemoattractants cues by the cells themselves [25, 29].

However, *in vitro*, most of collective migration studies deal with epithelial or endothelial cells, and emphasize the mechanical importance of strong cell-cell adhesions in the behavior of these systems. On top of their adhesion properties per se, the mechanical function of adhesion proteins (in particular cadherins at cell-cell junctions or integrins at cell-substrate adhesion sites), their role as mechanotransducers and the interplay between mechanical forces and biochemical signals, involving in particular the Rho GTPases are now well-accepted [202, 203].

Indeed, several high-throughput migration assays have identified cadherins and other proteins involved

in cell-cell adhesion as major players in collective migration [139, 140, 158]. Selectively knocking down the cadherins subtypes one at a time shows that although they are somewhat functionally redundant, their response to a mechanical stimulation is different when they are co-expressed. Some of these proteins respond to the level of force while others are sensitive to the rate at which the intercellular stress builds up, which allows for a particularly efficient control strategy [158]. Moreover, the dynamics of these cell-cell contacts themselves plays an important role in the cohesion of cells monolayers during their migration [118]. Periodic cadherin "fingers" at the cell-cell boundary of migrating VE-cadherin containing cells have been reported some years ago [204]. Recently, these cadherin fingers have been observed to be polarized relative to the cell motion in HUVECs and to link the back of one moving cell to the front of its immediate follower [98]. The finger structure has been found to consist of a double-membrane tube extending from the front cell and engulfed by the follower cell, triggered by RhoA activation in the front cell [98]. Moreover, the finger formation rate was observed to correlate well with the coordination of the two cell movements [98]. The role of another protein, Merlin, as a mechanotransducer (upon application of a mechanical force, Merlin translocates from the cell junctions to the cytoplasm) and its interactions with Rac1 have been identified [194] and shown to be consistent with the local alignment of cell motion with the previously mentioned direction of maximal principal stress [153]. The role of cell adhesion proteins and their crosstalk with integrins appears therefore central in collective migration via the modulation of concentration and/or activity of signaling molecules such as the Rho GTPases.

The importance of cell-cell adhesions also allows one to understand the particular situation of the edge cells. They have fewer neighbors and are engaged in adhesive interactions on a fraction of their contour only. By analogy with conventional liquids, an effective line tension can be associated to the monolayer edge. By sensing their physical cellular environment, edge cells act as cues for collective motility. Moreover, their localization at the free edge allows the activation of particular growth factor receptors [191, 190] or the onset of waves of MAPK [205]. This directional cue is mechanically transmitted from the wound edge by cell-cell interactions [68, 140] with a coordination between cells propagating in the monolayer as time goes on [142, 95]. It is also possible that signaling (or lack of it due to absence of neighboring) plays a role in the particular behavior of edge cells. In that respect, the interface between two cell populations differing in their cell-cell adhesions is a somewhat similar situation that would be worth investigating further (see Perspectives section 9.2).

This influence of cell-cell adhesion was further quantified by monitoring the spreading of aggregates of cells with controlled cadherin levels on surfaces of various compositions [206] or rigidities [207](Figure 10). In the same way a simple liquid spreads on a solid surface [208], cellular aggregates spread into monolayers (the equivalent of a wetting film) . The dynamics of spreading and the wetting transition are largely controlled by the adhesion between cells that can be tuned via the amount of cadherins expressed in the cells [206]. In a striking parallel to classical wetting situations, the cell-cell and cell-surface interactions control the transient and final state of the monolayer from liquid where the cells collectively migrate, to gaseous where they scatter on the surface (Figure 10).

6.3. The migration fingers

6.3.1. Experimental observations As noted above, collectively migrating epithelial cells frequently exhibit a strong fingering of the front edge (Figure 11). These migration fingers have been observed *in vitro* with several cell types including IAR2 Rat liver epithelial cells [209], MDCK epithelial cells [100, 210] or endothelial HUVECs [140, 191]. They are led by "leader cells" which are phenotypically distinct from their direct followers: leader cells are very spread out, have a large active lamellipodium at their front-edge and develop more focal adhesions or focal complexes than the other cells of the finger. However, they maintain strong cadherin-mediated adhesions with their followers. It has been also noted that these cells do not physically divide after mitosis [100]. Therefore, these cells have a very peculiar "Janus" phenotype with a fibroblast-like front edge and the back edge of an epithelial cell. In a wound-healing assay, a leader cell is not necessarily positioned at the monolayer edge when the barrier is removed. It can be transported to this edge by the swirling flows described in the previous section, before acquiring a leader phenotype at the initial stages of migration.

There has been no evidence that leader cells are initially different from the others. In particular they recover their initial phenotype after fusion when the two edges of a wound meet and fuse. In terms of shape, mobility or biochemical signals such as the activity of GTPases, these cells are initially not discernable from the other cells of the monolayer [100, 142, 211]. Therefore, leaders appear to be driven to their particular phenotype/function by their cellular environment.

A pluricellular acto-myosin contractile "cable" is systematically present at the edge of the migration fingers [100, 211, 191](Figure 11B arrows). This cable

that appears to run from cell to cell, has a major role in the function of the migration fingers. This apparent continuity is confirmed mechanically by laser ablation [211]; it implies that the cable is mechanically relayed at cell-cell junctions. When severed by laser ablation, the cable retracts and a new leader has a high probability to start at this cutting point [211]. Similarly, the spontaneous outgrowth of a leader is well correlated with local discontinuities in the initial cable [142] for exemple after the division of an edge cell. The local curvature of the interface is another determinant of finger formation as will be described in section 6.3 below .

Cells pertaining to a migration finger are stretched along their long axes, their velocities point toward the leader and their centrosome is localized in front of their nucleus, which indicates an active migration [212, 213]. In contrast, in the bulk of the monolayer, none of these descriptors is oriented or polarized.

When a finger is stopped (but not killed) by locally destroying the actin of its lamellipodium with a laser, the order of the cell velocities in the finger gradually decreases as the cells continue to migrate causing their density to increase. After a few hours, density is high enough to trigger the formation of a new finger. This leader formation follows a pre-alignment of the velocities of the cells behind it. These cells are then incorporated in the developing finger [212]. Leaders are therefore the consequence of a prealignment of the displacements of the cells that then become followers.

6.3.2. Models of finger formation and dynamics The striking observations of leader cells and migration fingers have given rise to several models.

A simple approach is taken in [95] motivated by the very different phenotypes of leader cells. Without considering or modeling their formation [95], it investigates how faster cells moving in a very directional manner can guide "normal" cells modeled by (17) . In order to obtain leaders cells, guiding fingers with shapes comparable to experimental ones, three conditions are found necessary. First, it is concluded that normal cells should be able to reach on their own, velocities comparable to typical leader velocities. This is obtained when the noise amplitude in (17) increases as cell density decreases so that the velocity of more-spread out cells is larger, as seen in the experiments. The natural decrease of density behind a fast leader allows normal cells to follow in the leader's wake. Second, for realistic finger shapes, normal cells should not easily invade free space in the absence of guiding leaders, i.e. the motile force component towards free space should be reduced for cells at the epithelium border (an effect obtained in [95] by the addition of a repulsive force away from free space for epithelium border cells). This effect may arise from the above-described actin cable lining the interface. Third, leader cells need to decrease their velocity when they stretch to maintain an adhesive contact with their followers, an effect which again may arise from tension in the actin cable.

Other works have considered interface dynamics and mechanisms of finger formations. The role of a potential chemical substance diffusing in the epithelium has been considered both in [214] and [215]. Reference [214] assumes that the secretion of chemoattractant is inversely proportional to the local cell density. Cells at the epithelium boundary secrete more chemoattractant and polarize the motion of cells lying deeper in the epithelium toward the epithelium boundary. A Potts model implementation shows that the epithelium interface becomes corrugated when the chemoattractant degradation is large enough or its diffusion large enough. A precise criterion remains however to be worked out. In [215], it is supposed that cells deformation induces chemoattractant release. A vertex model with motile cells is used to analyze the effect of this positive feedback loop. The epithelium border is found to widen qualitatively similarly to the experimental ones although fingers themselves are not explicitly considered.

A more phenomenological approach has been taken by Mark *et al.* [216], taking inspiration from a model previously developed in the context of crystal growth [217]. The proposal is that cells in outward-pointing convex parts of the epithelium border, invade free space more easily that cells in concave parts. This is modeled by assuming that the normal velocity of the epithelium border is proportional to its curvature. This results in a positive feedback loop in which interface regions with high curvature invade free space faster than regions with lower curvature, thereby increasing their curvature. This renders a straight interface unstable to corrugations. A definite maximally growing wavelength is obtained when restabilizing terms at short wavelength are taken into account. Simulations of this geometric model produce interface protrusions with a definite resemblance to experimental fingers. While the mechanism relating cell velocity to interface curvature remains to be identified, this relation could result from a coupling between tension at the interface and lamellipodium dynamics. The postulated relation has also suggested to try and manipulate experimentally the epithelium interface curvature as further discussed below (section 7.3). Subsequent theoretical work [218] has investigated this particular epithelium border dynamics in a full epithelium model, described with the particle-based model of [95]. The instability in this more complete model is similar to the one obtained

with the purely geometric model [216]. The nonlinear development of the instability is also very comparable to the one previously obtained with extrinsically added leader cells [95], with the self-generated highly-curved epithelium border parts playing the role of added leader cells.

6.3.3. Force measurements The mechanical traction forces developed by the cells of the fingers are maximal at the tip (i.e. at the leader cell) meaning that the leader cell exerts a traction force on its followers [211]. Under the finger, forces are very heterogeneous and fluctuating (Figure 12A). Since cells migrate actively using their cryptic lamellipodia [68], they produce intermittent forces of positive or negative sign. However, an average over the width of the finger shows that the profile of the *longitudinal* component of the force presents a negative minimum close to the junction with the monolayer [211] (Figure 12B-C). The profile of the *transverse* of the force (across the finger) is symmetric and points inwards from both sides; it results directly from the tension of the acto-myosin cable at the edge of the finger. From these robust features, it can be concluded that migration fingers that can comprise up to 80 cells are coherent mechanical entities (Figure 12).

Furthermore, the longitudinal force profile with a clear positive maximum at the tip and a negative minimum at its back is the transposition at the multicellular scale of the force profile generated by a single cell (positive traction at the front-edge protrusions and negative retraction forces at the back; Figure 12D) [219]. Mechanically these structures therefore behave as "supercells" as coined in [220].

Experiments conducted with IAR-2 epithelial cells transfected with dominant negative or constitutively active RhoA constructs emphasize the role of this GTPase in fingers formation [209]. Moreover, the profile of RhoA differential activity measured with biosensors (section 4.5) mirrors the profile of traction forces [211]: Cells pertaining to a migrating finger are polarized with a larger RhoA activity at their backside; the leader presents a large RhoA activity at its lamella while Rac1 is more active at the lamellipodium of the leader cell [213]. On soft collagen substrates, MDCK aggregates exhibit very similar fingers preceded by a leader cell. In that case, Rac, Integrins and other kinases are upregulated [213], highlighting again the complex interplay between mechanical tension and the various GTPases at play. The proposed mechanisms involve integrated signaling pathways encapsulating molecular players and mechanical tensions. They focus in particular on the complex interplay between the spatial distribution of the active form of RhoA and Rac1 and a mechanical signaling between cells upon traction by the leader [211, 194, 213].

These migration fingers look very similar to structures commonly observed in embryonic development or in tumor maturation [4] (Figure 11). Such collectively migrating structures occupy an intermediate position between immobile assemblies of epithelial cells and individually migrating cells. This has led to propose that the important Epithelial-Mesenchymal transition (EMT) is more complex that the two-state transition implied by its name. The EMT should be seen as gradual and a better description of it should integrate the whole spectrum of collective migration phenotypes, including the migration fingers [221, 222].

It should be kept in mind that migration fingers *in vivo* and, more generally in 3D environments, have different features than the 2D *in vitro* models. For instance, in the case of tumor invasion in the surrounding matrix, the leader cell locally degrades the matrix by secreting metalloproteases (MMPs) and the following cells migrates in strands in this channel [223, 220, 221, 224]. The leading cell may even be of different nature such as a cancer-associated fibroblast [225]. In the *in vitro* 2D experiments, the contractile cable at the edge of the finger may play a role comparable to the confining structure in a 3D channel by preventing the follower cells to venture independently on the surface (Figure 12E-D).

7. Coping with geometry in wound-healing

7.1. Migration with confining borders

As previously mentioned, the migration fingers observed in wound healing assays define a self-generated confinement via the peripheral actin cable that prevents nucleation of new leaders. A more controlled confinement can be imposed by setting the cells to migrate along well-defined stripes printed on the surface (Figure 13). The stripe width provides an additional control parameter which allows, for instance, the testing of theoretical models and predictions. [226, 195, 227, 228].

As a matter of fact, when the stripe is much wider than the velocity correlation length, behaviors are similar to the ones observed for infinitely long front edges, with the typical swirls in the epithelium and leader cells at the front edge [195, 228] (section 6.2). For stripes narrower than this typical length ($\sim 150\,\mu$m for MDCK cells), the cell displacements orient in the direction of the stripe (Figure 13). The cell flow is then well described by a plug flow [227]. A phenomenological description based on a reaction-diffusion equation describes well the behavior of the cells with an effective diffusive behavior superimposed to a drift.

In very narrow stripes ($\sim 20\mu$m), the migration

is more irregular and is described by contraction-extension flows [195]. These different modes of migration are also observed on the traction forces with the force profile in thin stripes much more irregular than in wide stripes where it decays smoothly from the front edge toward the bulk, as with semi-infinite wounds. A similar behavior (faster and more irregular) is observed on monolayers migrating on wires whose perimeter is comparable to the width of these stripes, suggesting that, despite the rather strong influence of the physical borders on the flows in the monolayer [227, 229], it is the confinement and not this influence of the edges that causes the difference of behaviors between thin and wide stripes.

Finally, confining weakly adhering cells onto stripes whose width is one cell size helps deciphering the importance of CIL in collective migration by transposing the situation to a one-dimensional problem. Under these conditions, the cells migrate and repolarize when they meet. They are observed to generate trains of cells moving collectively even though these cells dont develop cell-cell adhesions. Carefully monitoring the probabilities of collision and repolarization allows concluding that CIL can coexist with collective migration and control the EMT to some extent [226, 230]

Interestingly, some features of 3D migration are better recapitulated in migration experiments on very thin lines ("1D migration") than in classical 2D migration experiments [231]. This geometry encapsulates the propensity of the cells *in vivo* to migrate along heterogeneities (fibers, bundles) as will be discussed in the last part (section 9.3).

7.2. Closed-contour wound

In vivo, many situations deal with the closing of finite apertures within an epithelium. For instance, dorsal closure in Drosophila embryo has received a lot of attention as recalled in section 2. In the closure of this epithelial layer, an important role is played by the contraction of the continuous acto-myosin cable present at its edge [71]. This mechanism of closure is called purse string closure [70]. A similar purse-string closure is at play at cell extrusion events when single cells get expelled from very dense monolayers [232].

Since the presence of an acto-myosin cable is ubiquitous at the free edge of epithelial monolayers, it is interesting to mimic this situation with "closed contour" wounds by using a barrier-like assay to control the initial size of the wound. These experiments bridge the gap between "open wounds" (no curvature) and experiments dealing with cell-size wounds created by laser ablation (closed-contour wounds, very high curvature) [130].

In these experiments, arrays of circular mesoscopic pillars whose tops are initially in contact with the substrate prevent cells migration. Removing the pillars triggers the collective migration of the cells. Using pillars of large radius ($R > 100\,\mu$m) leads to the appearance of migration fingers analogous to the ones observed at the edge of linear wounds. In contrast, smaller wounds close with no finger and remain globally circular [200, 233]. As expected, upon removal of the pillar, an actomyosin cable quickly develops at the edge (Figure 14A). This cable is contractile and under tension as shown by laser ablation experiments [200]. This cable closely resembles the one observed *in vivo* during epithelial closure by a purse-string process after a wound or during embryogenesis [30]. However, impacting the cable contractility via RhoA inhibition has little influence on the closure process, whereas Rac inhibition slows down drastically the closure and, in extreme situations, even prevents the closure altogether [200, 233]. These results show that, despite the presence of the acto-myosin cable at the edge, epithelialization is driven by the protrusive activity at the free edge and that the purse-string mechanism is only secondary. This conclusion holds down to radii of the order of a typical cell size. Modeling the tissue as an incompressible fluid (which is consistent with the velocity profile measured away from the front edge), the fluid viscosity is found to play a negligible role and the closure time can be analytically expressed as a function of three parameters: the initial wound radius, an epithelialization coefficient defined as the ratio of the protrusive stress to the effective friction, and a cut-off length of the order of the velocity correlation length [200](Figure 14B). In another approach, particle-based simulations with local rules of coordination [93] also describe very well the experimental results (Figure 14C-D) and confirm in particular the secondary importance of the purse string mechanism [234]. The function of this cable in these experiments, as well as along the migration fingers described above, is to restrict uncontrolled forward movements of the leading edge. It is also one of its functions in the Drosophila dorsal closure [71].

Mapping the traction forces during the closure of small wounds largely confirms the previous analyses [201]: as the wound closes, traction forces initially point away from the cell-free area which is characteristic of the migration driven by protrusive activity. As time goes on and the wound closes, the curvature at the free edge becomes more important and the force resulting from the purse string contraction increases until it eventually outgrows the contribution of protrusive activity. The average force due to the cable points toward the wound. It also interacts strongly with the gel surface at focal adhesions and generates tangential forces that participate to the closure process on soft substrates.

7.3. The impact of the local curvature of the wound

Coming back to the leader cells and their associated migration fingers, the visual resemblance with physical hydrodynamic or solidification instabilities has initiated the idea they may be correlated with local curvature of the front edge [216], as previously described (section 6.3.2). Barrier assays are not restricted to circular or linear wounds and can be used to try and test this hypothesis. The use of microfabrication/micropatterning techniques allows one to design barriers of basically any geometry, and to shape the initial front-edge accordingly. In order to test the influence of the local curvature of the edge of the epithelium, the previously-described pillar assay has been extended to pillars of complex shapes where the curvature varies and can be positive or negative (i.e. combining concave and convex portions) [233, 235]. An analysis of the dynamics of the front edge in parallel with the traction forces developed on the underlying substrate, shows that protrusive forces at the edge are present at all curvatures and dominate the closure mechanism when the curvature is positive (convex shapes). This mechanism coexists with the purse-string contraction at large negative curvature (concave shapes of small radii), confirming its importance in the closing of cell-size wounds [130, 201] or in other physiological events such as cell extrusion [232]. Numerical simulations including these two contributions, show that the purse string acts as a mechanical regulator coordinating the global progression of the tissue [235]. Interestingly, the emergence of leader cells coupled to migration fingers correlates very well with the initial curvature of the front edge with much more of these structures emerging from highly convex "spikes".

A similar conclusion is reached by using a patterned photoswitchable surface [134], or adequately tailored stencils [236] (Figure 15A). In both situations, by modulating the global and/or local curvatures, the emergence of leader cells correlates well with high positive curvatures (Figure 15B). Coupling these experiments with traction force measurements shows that large traction forces develop even before the finger begins to develop, in good agreement with the pattern of forces observed at the spontaneous emergence of leader cells [211]. Models have been developed that include at the convex parts of the epithelium edge, protruding forces increasing with the local edge curvature [216, 218]. This positive feedback between motility and outward pointing curvature results renders a straight epithelium edge unstable and produces digitations resembling the experimentally observed ones (Figure 15C).

7.4. Purse-string driven wound closure on non-adherent substrates

Since the purse-string mechanism is thought to play an important role in many *in vivo* situations, it is surprising to conclude that it is only secondary in the *in vitro* epithelial closures of openings larger than a few cell sizes. The predominance of the protrusive activity in these experiments is explained by the large adhesions that cells develop with their substrate via FAs or FCs including direct interaction between the cable itself and the surface [201].

Therefore, to study the purse string contribution, monolayers must be plated on surfaces with which they do not develop adhesive interactions. This can be obtained by chemically treating areas of the substrate with a non-adherent coating. On such surfaces, monolayers of keratinocytes can bridge over mesoscopic non adhesive stripes patterned on an otherwise adhesive substrate [237]. Cells on these bridges cannot develop adhesions with the substrate; they are held together by cell-cell adhesions. The particular geometry of these experiments imposes a large tension to the suspended epithelium. The shape of the edge of the suspended tissue suggests that under these conditions, the monolayer behaves as an elastic medium.

A monolayer can bridge over a non-adhesive mesoscopic patch imprinted on the surface, as long as the patch is smaller than a critical size, measured to be of the order of 150 μm for keratinocytes [238] and 60 μm for MDCK cells [239]. This difference that may reflect the different origins of these cells (respectively skin and kidney). For these small-size patches, the closure of the wound is actually driven by acto-myosin purse-string contractility (Figure 14E), as shown by experiments conducted in presence of specific inhibitors.

For the same initial radius, wounds close much more slowly over non-adhesive disks than on uniformly adherent surfaces (up to 10 times more slowly [239]). Closure is also much "noisier" over non-adhesive surfaces, with a large dispersion of the closure times for a given initial radius, and very jerky trajectories of the radius with time (Figure 14F). These features illustrate the importance of active epithelial fluctuations in the closure process in these particular conditions. A stochastic model encapsulating a line tension, a friction force and tissue fluctuations allows a quantitative description of these results. The solution of the allied Fokker-Planck equation for the wound radius distribution shows a very good agreement with the experimental data [239] (Figure 14F). It demonstrates that this stochastic model provides a good description of the closing dynamics, with only two adjustable parameters. From this analysis, it can be concluded

that, although epithelial tension itself is negligible in this context, its active fluctuations are an essential ingredient of this mode of closure. As a matter of fact, fluctuations are even dominant over the purse-string contractility in the early dynamics and they speed up the closure throughout the process. These conclusions may hold for more complex situations including *in vivo* tissue fusion. However, a full analysis would require a better description of the tissue viscoelastic rheology, including in particular the non-linearities evidenced in [238].

8. Collective taxis

8.1. Collective chemotaxis

The question of the motility of aggregates is of particular interest. Aggregates of cells of the Xenopus neural crest have been observed to migrate collectively up a gradient of the chemokine Sdf1 [23]. A similar gradient is thought to underlie the migration of border cells (Figure 1B) in the Drosophila egg chamber but the hypothesized gradient remains to be directly evidenced *in vivo* [8]. *In vitro*, recent observations show that chemokine gradients can provide directional motility to clusters of malignant lymphocytes [240]. The directionality of cluster motion is much higher than for single cells and clusters are more sensitive to shallow gradients (Figure 16AB). Interestingly, the aggregates are always observed to move up-the-gradient (toward the high concentrations of chemokines) in [240] while single cells respond differently to the chemokine gradient at low and high chemokine concentrations. They actually move down-the-gradient at high chemokine concentration (away from the source), a phenomenon called chemorepulsion, that is bypassed when cells move collectively (Figure 16B). The migrating structures formed by these malignant lymphocytes are very dynamic. Unlike the previously described leader cells in wound healing [211] (section 6.3), the cells that exert the largest traction forces at the front edge exchange their position during motion. This leader cell turnover results from global rotation of the clusters between two directed "runs" in a mechanism reminiscent of single cell bacterial chemotaxis [241], and from loss of polarity following internalization of the receptors of the chemokine. By frequently exchanging leaders, clusters are not prone to chemorepulsion, in contrast with single cells. A similar phenomenon was also noted in invasion of 3D hydrogels [242].

All these results demonstrate that chemotactic migration of clusters is not merely the juxtaposition of single cell chemotaxis but that other mechanisms must be at play. This has been conceptualized as "collective guidance" [243, 244] with the principle that, when migrating collectively in a chemotactic gradient, the cells located at the boundary of the cluster respond to the local concentration of attractant and not to its local gradient.

Several mechanisms by which edge cells convert the information of the local concentration across a cluster to the directed movement of this cluster have been proposed [240]. They amount to a regulation of CIL in which the radial polarization of the edge cells away from the cluster is function of the chemokine local concentration [240, 245]. The imbalance of chemokine concentrations at the front and back of the cluster results in a difference of forces and thus in a directed motion (Figure 14C).

Although these models capture the essential features of the observations, they do not reproduce all their details and in particular the dependence on cluster size. In this context, a generalization of the LEGI (Local Excitation/ Global Inhibition) model that has been shown to account for the chemotaxis and adaptation of single cells [246], describes well the saturation effect observed for large clusters [247, 248]. In this model, cells remain cohesive and communicate via biochemical signals.

Finally, some *in vivo* observations involve cells that do not adhere together but still display a collective response to chemotaxis for instance in the neural crest [25]. In this last case, similar to collective bacterial chemotaxis [249, 250], it has been concluded that cells secrete a chemoattractant in the medium that keeps the cells together. There are therefore two fields of chemoattractants in this case : the chemokine itself and the secreted attractant that results in an effective attractive interaction between cells [251] that keeps them in clusters even in the absence of stable cell-cell adhesion.

8.2. Galvanotaxis

The presence of endogenous electric fields at the edge of wounded tissues has been observed *in vivo* and *in vitro* [252, 253]. The question of the possible functions of such electric fields in the range of a few 10 V/m in the healing process remains an open question. Therefore, several works have studied the response of cells in isolation or within a monolayer upon the application of an exogenous electric field, a process named galvanotaxis.

It is observed that modest exogenous electric fields (typically 40-200 V/m) have a clear accelerating effect on the migration of cells [252, 254]. Interestingly, the direction of migration itself (toward the anode or the cathode) is cell-type dependent. For some cells, this direction is even function of the field strength. For example, lens cells migrate toward the cathode at low field and toward the anode at high field [252,

255]. The exact mechanism underlying galvanotaxis is still not fully understood. However, it is clear that electric fields do not act on the cells by applying an electrophoretic force on them. Rather, they appear to redistribute membrane components of the cells such as growth factor receptors [256]. The transduction of this electric field-induced polarization is ensured by the same signaling pathways as those involved in chemotaxis. In this spirit, electric fields have been used as cues to guide migration, just as chemical gradient have been used to the same purpose.

Upon the application of an electric field, cells in monolayers migrate more efficiently than when in isolation [257, 254]. As with chemotactic cues, larger clusters are more responsive to the field compared to small ones [257, 258]. This response and even its sign are cell-type dependent. The cadherin-mediated cell-cell junctions are critical in this coordination but gap junctions are not. When changing the direction of the electric field, cells do not repolarize but make a U-turn (Figure 17). When engaged in a monolayer, they coordinate in clusters to rapidly perform this U-turn (within minutes). The size of these clusters is fixed by the velocity correlation length. After this step, the orientation of the cells becomes uniform again by fusion of these domains [258] (Figure 17).

The response of the cells belonging to a free edge is very sensitive to the details of the experiment as some reports show an enhanced response with forces larger than in the bulk [257] and others a decreased sensitivity compared to the bulk cells [258]. In particular, leader cells appear insensitive to electric fields.

8.3. Durotaxis

The effect of substrate stiffness on single cell migration has been shown for some time [259]. On rigidity gradients, cells migrate from soft to rigid substrates, in a process called "durotaxis" [260]. In monolayers, cells maintain contacts with their neighbors; this cellular environment provides them with another scale of stiffness. As a result, phenotypic differences (eg. spreading area) that appear for cells in isolation on substrates of different stiffness disappear in a confluent monolayer [261]. In terms of collective migration, although cancer invasion in 3D gels is dominated by collagen degradation and not directly by the rigidity of the matrix [262], it has been shown that cancer cells follow paths of least resistance [263] (Figure 18), meaning that cells migrating collectively or in isolation are sensitive to gradients of rigidity. When plated on planar surfaces, MDCK clusters have different phenotypes depending on the substrate rigidity: on soft collagen substrates, the leader cell phenotype is enhanced and the migration fingers are larger compared to collagen-coated glass [210]. It is suggested that this observation results from an alignment of the collagen fibers caused by the cell traction forces. However, the downregulation of adhesion proteins observed on soft substrates is also probably at play [259, 261, 264]. Furthermore, the forces developed by the cells also increase with rigidity [264, 211].

In any case, a systematic study of the effect of stiffness on MCF10A cell layers in a wound-healing assay shows a dependence of speed, persistence and directionality with the stiffness [157]. These experiments also show an increase of the correlation length on stiff substrates. This phenotype is well correlated with the activity and the distribution of myosin II in the monolayer. As the stiffness increases, myosin II is more active at the edge and this activity propagates further in the monolayer. This mechanosensitivity is relayed by cadherin-mediated cell-cell junctions.

Related experiments exploring the spreading of spheroid cells aggregates have shown that the spreading parameter - that corresponds to the difference between the cell-cell and the cell-substrate adhesion energies per unit area - is function of the substrate rigidity [207, 265]. For very soft substrates, the aggregates are in a partial wetting situation and, above a rigidity threshold, there is a transition to total wetting with the presence of a "precursor" cell monolayer. The dynamics of spreading is then itself affected by the rigidity.

Collective durotaxis has been reported with MCF-10A or MDCK cells that do not exhibit durotaxis in isolation (or exhibit it too weakly to be measured) [266]. When placed on a gradient of stiffness, a stripe of cells tends to expend more in the direction of high stiffness, with the result that its center of mass migrates in the same direction. The generated traction forces on both sides of the stripe are found to be of the same amplitude; these forces are transmitted across the monolayer with a negligible contribution of the monolayer interaction with the substrate in the bulk. A generalized clutch model [267] in which the same forces are applied on both sides of the cluster and hence on different rigidities, accounts for the collective response of the cell cluster.

9. Concluding remarks and perspectives

Understanding the collective migration of cells is an exciting endeavor which should help elucidating several key steps in development and pathology. We have tried to show in this review that a physics approach leads to an analysis of the subject with a perspective that differs from the more traditional biological approach and that complements it. The focus is more on phenomenological descriptions of basic

mechanisms at the cell and tissue levels than on their detailed molecular implementation. It also leads to use complementary tools such as quantitative mechanical measurements and theoretical modeling.

A complete description of collective cell motion will, of course, only be obtained by a synthesis of the two approaches. Both biochemical signaling and mechanical interaction should be included in a single description. On the one hand, definite proteins, signaling pathways and precise molecular mechanisms need to be assigned to the parameters of the physics description. On the other hand, the actual cell-based models or continuous descriptions are certainly oversimplified. Supplementary regulatory mechanisms need to be taken into account. Their consequences on collective dynamics will have to be experimentally tested and theoretically assessed by appropriately including them in the mathematical descriptions. Comparison with the dynamics of synthetic active particles should also be fruitful. It may serve to elucidate general features of non-equilibrium collective motion and how cells have taken advantage of them or, on the contrary, have learned to overcome them. This may in turn serve to design more sophisticated synthetic active matter. In the following, we highlight a few illustrative questions and directions that we find of particular interest.

9.1. Some open issues in single cell motion

Collective migration of cells relies on single cell dynamics and its regulation through interaction with other cells. In this respect, its study highlights the fact that we are still lacking a fairly complete description of single cell motion [2]. Even at the level of the simple Fürths's description, (1) or (3,4), there remain outstanding questions. What is the real source of noise? Is molecular noise amplified in some way to be significant at the level of the single cell? Does this make use in part of some periodic or chaotic deterministic process at the scale of the single cell? There have been some suggestive theoretical proposals and interesting observations in this direction. More than 15 years ago, Meinhardt [268] proposed a model of cell orientation based on reaction-diffusion along the cell membrane. Local auto-activation together with long-range inhibition create a few activated patches along the cell membrane. In addition, delayed local inhibition endows the created patches with a finite lifetime and allows for their repeated renewals in space and time. In subsequent works, (e.g.[269, 270]), this has been promoted to a model of ameboid motility by assuming that the activated patches correspond to pseudopods and membrane protrusions. Alternatively, it has been proposed [271] that random membrane protrusions arise from the stochastic emergence of excited localized patches in an underlying noisy excitable system. On the experimental side, fascinating observations of actin waves have also been made in single cells [272], even taking the form of spiral waves [273], as commonly seen in excitable systems. Further work is needed to develop a firmly grounded cell model describing these data. The reduced description of an extended cell as a point-like object also deserves further scrutiny. Are cell velocity and polarization sufficient with the allied simple split between motility and friction forces or does one need to keep further variables such as other determinants of cell shapes? Do these supplementary variables provide some oscillatory characters to protrusion generation and cell locomotion? Again interesting experimental and theoretical works exist but need to be pursued further.

Cell interaction and CIL play an important role for collective dynamics. A related question for single cells concerns their interaction with obstacles. Random walkers moving under the action of a persistent force can develop an accumulation layer near obstacles [274, 275] contrary to the equilibrium case for which a repulsive potential produce a depletion layer. What about cells? Some observations [272] show that cells can repolarize away from an obstacle in a mechanism akin to CIL. It seems probable that cell interaction with obstacles generally include both mechanical and signaling interactions that could depend for instance on the obstacle surface moiety, combined in different ways. Is a simple Fürths-like model sufficient to describe the observed behaviors? Further studies would help to better understand cell motion under external influence and may be useful in the description of cell-cell interactions.

9.2. Collective motion in 2D

The collective migration of cells is a very rich phenomenon, even in the "simplest" case dealing with cells with identical genotype migrating on a flat substrate. Although much progress has been made in recent years, many different aspects need to be further studied.

The relative contributions of mechanics and signaling in coordinating cell motion need to be better assessed as well as the different ways in which intercellular-signaling can affect the motion of two cells [96, 97, 98]. How this coordination is best described mathematically should also be further clarified.

Cell proliferation is an important topic that we have left aside. It is known that cell density impacts cell proliferation at long times, a process described under the heading of "contact inhibition of proliferation", the loss of which is a hallmark of

tumoregenicity. The axis of division of a cell is also affected by its interaction with neighboring cells (see e.g. [276] for a recent study). Reciprocally, cell division can affect tissue flows. These questions have started to be considered from a physics perspective [125, 115] but they obviously deserve much further scrutiny.

Another topic that appears of special interest for future studies is collective migration with different cell types. We have discussed the case of leader cells which transiently phenotypically differentiate from other cells, a transformation which remains to be better understood. In this direction, recent efforts have been made to characterize the transcriptional profile of leader or "trailblazer" cells in neural crest migration [277, 278](section 2). Guidance of cell cohorts, in this case by cells with a different genotype, takes place in the case of CAFs which guide tumor invasion (see Figure 11A). The coordination between a leader and its cohort of followers has been studied in simple models [95, 277] but further experimental and theoretical investigations are certainly needed. More generally, the coordination or the competition between different cell types is seen in developmental events, e.g. the chase-and-run between neural-crest and placode cells [24] during neural crest migration , as well as in pathology. A few studies have started to consider it, for instance the spontaneous segregation between non-motile and motile cells [107, 279, 275] but much remain to be studied and discovered.

9.3. Toward the third dimension

The model systems described in this review deal mostly with collective migration on planar substrates. Indeed, many cellular systems are bidimensional *in vivo* (epitheliums or endotheliums for instance) and are therefore close to these model systems. However, in many circumstances, collective migration involves the third dimension.

A spectacular example of collective migration in development is provided by border cell migration between nurse cells during Drosophila oogenesis (Figure 1B). As the border cell cluster approach the oocyte, its motion alternates linear migration and global rotations [280]. Another well-known example of collective migration in a 3D environment is the migration of the neural crest cells (Figure 1A). These cell clusters travel collectively until they dissociate to colonize tissues and organs in the embryo. In the case of Xenopus neural crest migration, N-cadherin mediated cell-cell adhesion are short-lived and cell clusters migrate by collective chemotaxis [23]. Other types of interactions such as another chemotactic field mediated by secreted soluble cues, may keep the cells together [25].

Consideration of the third dimension is also important for collective migration during cancer development. As a matter of fact, there are many correspondences regarding the different modes of migration between embryonic development, cancer and tissue repair [4]. The recent progress of intravital imaging techniques, using in particular multi-photon excitation, allows imaging both the cells and their microenvironment *in vivo* [263] (Figure 18). These detailed observations have allowed the classification of the various types of migration [221] and the observations of the modes of guidance of migrating cell populations in various environments [281]. In particular, the crucial role of heterogeneities and interfaces can be evidenced in spectacular intravital observations [263, 282].

In an effort to mimic some of the behaviors in controlled 3D environments, cells have been put in culture in hydrogels (mostly collagen or Matrigel). In such matrices, cells migrate by a combination of matrix degradation and traction forces. For example, in collective migration of cancer cells, the successive steps of matrix proteolysis involving cell-surface proteinases and in particular metalloproteinases (MMPs) have been characterized. The first cell acts as a leader and creates a "channel" in the matrix by degrading it. As the followers enter this channel and form a strand, they further expand it by combining forces and degradation [223]. When cancer cells cannot degrade the matrix, for instance in the case of squamous cells carcinoma, the function of the leader cell in terms of degradation is ensured by a CAF, a cell of another type, that becomes the pilot-fish of the cancer cells [225]. In the channels created by the leaders, the followers also develop mechanical forces that can be probed by having the cells migrating in 3D microtracks generated by laser photoablation in collagen gels, while inhibiting MMPs [283]. In these conditions, cancer cells can progress in these tracks down to a width of about 3 μm. Migration in the smallest channels requires the cells to squeeze. Moreover, the colony can generate secondary tracks from these preformed channels, using forces alone.

It is difficult to measure the forces developed by the cells in 3D in this context, not so much because of a technical difficulty that would hinder the transposition of TFM in 3D but precisely because the gel is constantly remodeled and therefore its local rheology is ill-defined, in particular next to the cells. A qualitative picture has been obtained by plating cells in microfabricated wells in a collagen matrix seeded with latex beads [284]. By analyzing the strain field, it is observed that epithelial cell clusters generate multicellular protrusions in the gel by developing tensile mechanical forces. These pulling forces not only control the progression of the cells in the gel, they

also remodel its structure into ordered oriented fibrils that in turn control the direction of migration of the migrating cohorts [285].

These studies confirm the importance of the interfaces and, more generally, of the matrix heterogeneities that were previously observed *in vivo* with tumor cells following the paths of least resistance between tissues [263]. This particular role of the interfaces has been further evidenced in experiments involving two non-mixing gels in contact, using a microfluidic strategy [286]. The geometry of the interface then directs the migration from the soft to the rigid gel.

The architecture of the cell assemblies may be more complex and organized than the spheroids described above. For example, epithelial cells such as MDCK assemble in polarized cysts when in collagen or Matrigel [287]; mammary epithelial cells organize in acini [288, 289]. In contrast, cancer cells lose this organization and assemble in disorganized clusters. Furthermore, the acini of normal cells show very coherent rotation modes [290], absent in the case of cancer cells. These rotation modes are reminiscent of the ones observed for cells in confined 2D disks [182] or during the migration of the border cells in Drosophila oogenesis [280]. The organization of cells in these acini and cysts makes it clear that 3D architectures cannot be reduced to cell clusters. In many situations, in particular those involving epithelial or endothelial tissues, cells adopt a 2D configuration, itself folded in the 3D space. To mimic some aspects of this complexity, one has to rely on topologically complex environments. As well, the organization of endothelial cells can be reproduced in cylindrical channels within a collagen matrix [291]. Such complex environments also allow discriminating normal and cancer cells when they are challenged by large diameter pillars [292]. These two examples illustrate the degree of complexity of such experiments as even the sign of the out-of-plane curvature is different in these two situations.

By plating cells on model glass fibers, the effect of the out-of-plane curvature can be tested on endotheliums [293] or epitheliums [228] (Figure 19). Epithelial cells organize on these fibers similarly to the cancer cells engulfing and migrating on vessels, nerves or muscle fibers [263]. The effect of the curvature on the dynamics of the cells reduces to the inherent confinement of this geometry down to submicron fibers, at which point the migration stops. Another hallmark of epithelial migration on these particular substrates is the spontaneous frequent detachment of the leading cell from the monolayer at radii smaller than typically 5 μm. These detachments may mimic the behavior of tumor cells migrating on collagen bundles or other types of fibers *in vivo*. Further works in this line may help understand the different modes of cancer invasion that are largely controlled by the microenvironment and the organization of the stroma [294].

Acknowlegdments We wish to thank for collaboration and discussions on the subject of this review, I Bonnet, A Buguin, O Cochet-Escartin, S Coscoy, M Deforet, G Duclos, S Garcia, N Gov, E Grasland-Mongrain, L Petitjean, M Poujade, M Reffay-Beugnon, N Sepúlveda, H Yevick as well as all members of the "Biology-inspired physics at mesoscales" group. We are also grateful to E Theveneau and X Trepat for their comments on a previous version of this manuscript and to J Fredberg for pointing out Figure 5B . Funding from ARC, DIM C'nano, FP44, FPGG and Labex CelTisPhysBio is also gratefully acknowledged.

[1] Bruce Alberts, Alexander Johnson, Julian Lewis, Martin Raff, Keith Roberts, and Peter Walter. *Molecular Biologyi of the Cell*. Garland Science, 2008.

[2] G. Danuser, J. Allard, and A. Mogilner. Mathematical modeling of eukaryotic cell migration: insights beyond experiments. *Annu. Rev. Cell Dev. Biol.*, 29:501–528, 2013.

[3] MC Marchetti, JF Joanny, S Ramaswamy, TB Liverpool, J Prost, Madan Rao, and R Aditi Simha. Hydrodynamics of soft active matter. *Reviews of Modern Physics*, 85(3):1143, 2013.

[4] Peter Friedl and Darren Gilmour. Collective cell migration in morphogenesis, regeneration and cancer. *Nat. Rev. Mol. Cell Biol.*, 10(7):445–57, 2009.

[5] P. Rorth. Collective cell migration. *Annu. Rev. Cell Dev. Biol.*, 25:407–429, 2009.

[6] E. Scarpa and R. Mayor. Collective cell migration in development. *J. Cell Biol.*, 212(2):143–155, Jan 2016.

[7] Pernille Rørth. Fellow travellers: emergent properties of collective cell migration. *EMBO reports*, 13(11):984–991, 2012.

[8] Denise J. Montell, Wan Hee Yoon, and Michelle Starz-Gaiano. Group choreography: mechanisms orchestrating the collective movement of border cells. *Nat. Rev. Mol. Cell Biol.*, 13(10):631–45, oct 2012.

[9] Roberto Mayor and Sandrine Etienne-Manneville. The front and rear of collective cell migration. *Nat. Rev. Mol. Cell Biol.*, 17(2):97–109, jan 2016.

[10] Előd Méhes and Tamas Vicsek. Collective motion of cells: from experiments to models. *Integrative Biology*, 6(9):831–854, 2014.

[11] Jin-Ah Park, Jeffrey J. Fredberg, and Jeffrey M. Drazen. Putting the Squeeze on Airway Epithelia. *Physiology*, 30(4):293–303, 2015.

[12] Thomas E. Angelini, Edouard Hannezo, Xavier Trepat, Manuel Marquez, Jeffrey J. Fredberg, and David A. Weitz. Glass-like dynamics of collective cell migration. *Proc. Natl. Acad. Sci.*, 108(12):4714–4719, mar 2011.

[13] J Prost, F Jülicher, and JF Joanny. Active gel physics. *Nature Physics*, 11(2):111–117, 2015.

[14] Y. Arai and A. Pierani. Development and evolution of cortical fields. *Neurosci. Res.*, 86:66–76, Sep 2014.

[15] K. Toma and C. Hanashima. Switching modes in corticogenesis: mechanisms of neuronal subtype transitions and integration in the cerebral cortex. *Front Neurosci*, 9:274, 2015.

[16] A. Griveau, U. Borello, F. Causeret, F. Tissir, N. Boggetto, S. Karaz, and A. Pierani. A novel role for Dbx1-derived Cajal-Retzius cells in early regionalization of the cerebral cortical neuroepithelium. *PLoS Biol.*, 8(7):e1000440, 2010.

[17] Verona Villar-Cerviño, Manuel Molano-Mazón, Timothy Catchpole, Miguel Valdeolmillos, Mark Henkemeyer, Luis M Martínez, Víctor Borrell, and Oscar Marín. Contact repulsion controls the dispersion and final distribution of cajal-retzius cells. *Neuron*, 77(3):457–471, 2013.

[18] C. Carmona-Fontaine, H. K. Matthews, S. Kuriyama, M. Moreno, G. A. Dunn, M. Parsons, C. D. Stern, and R. Mayor. Contact inhibition of locomotion in vivo controls neural crest directional migration. *Nature*, 456(7224):957–961, Dec 2008.

[19] R. Mayor and C. Carmona-Fontaine. Keeping in touch with contact inhibition of locomotion. *Trends Cell Biol.*, 20(6):319–328, Jun 2010.

[20] Michael Abercrombie and Joan E. M. Heaysman. Observations on the social behaviour of cells in tissue culture. I speed of movement of chick heart fibroblasts in relation to their mutual contacts. *Exp. Cell Res.*, 5:111, may 1953.

[21] Nicole Le Douarin and Chaya Kalcheim. *The neural crest*. Number 36. Cambridge University Press, 1999.

[22] E. Theveneau and R. Mayor. Neural crest migration: interplay between chemorepellents, chemoattractants, contact inhibition, epithelial-mesenchymal transition, and collective cell migration. *Wiley Interdiscip Rev Dev Biol*, 1(3):435–445, 2012.

[23] Eric Theveneau, Lorena Marchant, Sei Kuriyama, Mazhar Gull, Barbara Moepps, Maddy Parsons, and Roberto Mayor. Collective Chemotaxis Requires Contact-Dependent Cell Polarity. *Dev. Cell*, 19(1):39–53, jul 2010.

[24] Eric Theveneau, Benjamin Steventon, Elena Scarpa, Simon Garcia, Xavier Trepat, Andrea Streit, and Roberto Mayor. Chase-and-run between adjacent cell populations promotes directional collective migration. *Nat. Cell Biol.*, 15(7):763–72, jul 2013.

[25] Carlos Carmona-Fontaine, Eric Theveneau, Apostolia Tzekou, Masazumi Tada, Mae Woods, Karen M Page, Maddy Parsons, John D Lambris, and Roberto Mayor. Complement fragment C3a controls mutual cell attraction during collective cell migration. *Dev. Cell*, 21(6):1026–37, dec 2011.

[26] Cornelis J Weijer. Collective cell migration in development. *Journal of cell science*, 122(18):3215–3223, 2009.

[27] William F Loomis. Genetic control of morphogenesis in dictyostelium. *Developmental biology*, 402(2):146–161, 2015.

[28] Jocelyn A McDonald, Elaine M Pinheiro, Lisa Kadlec, Trudi Schupbach, and Denise J Montell. Multiple egfr ligands participate in guiding migrating border cells. *Developmental biology*, 296(1):94–103, 2006.

[29] Erika Donà, Joseph D Barry, Guillaume Valentin, Charlotte Quirin, Anton Khmelinskii, Andreas Kunze, Sevi Durdu, Lionel R Newton, Ana Fernandez-Minan, Wolfgang Huber, Michael Knop, and Darren Gilmour. Directional tissue migration through a self-generated chemokine gradient. *Nature*, 503(7475):285–9, dec 2013.

[30] Paul Martin and Susan M Parkhurst. Parallels between tissue repair and embryo morphogenesis. *Development*, 131(13):3021–34, jul 2004.

[31] Y. Toyama, X. G. Peralta, A. R. Wells, D. P. Kiehart, and G. S. Edwards. Apoptotic force and tissue dynamics during Drosophila embryogenesis. *Science*, 321(5896):1683–1686, Sep 2008.

[32] A. R. Wells, R. S. Zou, U. S. Tulu, A. C. Sokolow, J. M. Crawford, G. S. Edwards, and D. P. Kiehart. Complete canthi removal reveals that forces from the amnioserosa alone are sufficient to drive dorsal closure in Drosophila. *Mol. Biol. Cell*, 25(22):3552–3568, Nov 2014.

[33] P Martin and R Nunan. Cellular and molecular mechanisms of repair in acute and chronic wound healing. *British Journal of Dermatology*, 173(2):370–378, 2015.

[34] ED Hay. An overview of epithelio-mesenchymal transformation. *Cells Tissues Organs*, 154(1):8–20, 1995.

[35] Raghu Kalluri and Robert A Weinberg. The basics of epithelial-mesenchymal transition. *The Journal of clinical investigation*, 119(6):1420–1428, 2009.

[36] M Angela Nieto, Ruby Yun-Ju Huang, Rebecca A Jackson, and Jean Paul Thiery. Emt: 2016. *Cell*, 166(1):21–45, 2016.

[37] Kari R Fischer, Anna Durrans, Sharrell Lee, Jianting Sheng, Fuhai Li, Stephen TC Wong, Hyejin Choi, Tina El Rayes, Seongho Ryu, Juliane Troeger, et al. Epithelial-to-mesenchymal transition is not required for lung metastasis but contributes to chemoresistance. *Nature*, 527(7579):472–476, 2015.

[38] Xiaofeng Zheng, Julienne L Carstens, Jiha Kim, Matthew

Scheible, Judith Kaye, Hikaru Sugimoto, Chia-Chin Wu, Valerie S LeBleu, and Raghu Kalluri. Epithelial-to-mesenchymal transition is dispensable for metastasis but induces chemoresistance in pancreatic cancer. *Nature*, 2015.

[39] Kazuki Nabeshima, T Inoue, Y Shimao, H Kataoka, and M Koono. Cohort migration of carcinoma cells: differentiated colorectal carcinoma cells move as coherent cell clusters or sheets. *Histology and histopathology*, 14(4):1183–1187, 1999.

[40] Raghu Kalluri and Michael Zeisberg. Fibroblasts in cancer. *Nature Reviews Cancer*, 6(5):392–401, 2006.

[41] Reinhold Fürth. Die brownsche bewegung bei berücksichtigung einer persistenz der bewegungsrichtung. mit anwendungen auf die bewegung lebender infusorien. *Zeitschrift für Physik A Hadrons and Nuclei*, 2(3):244–256, 1920.

[42] Mitchell H Gail and Charles W Boone. The locomotion of mouse fibroblasts in tissue culture. *Biophysical journal*, 10(10):980, 1970.

[43] LS Ornstein. On the brownian motion. In *Proc. Amst*, volume 21, pages 96–108, 1919.

[44] D. Selmeczi, S. Mosler, P. H. Hagedorn, N. B. Larsen, and H. Flyvbjerg. Cell motility as persistent random motion: theories from experiments. *Biophys. J.*, 89(2):912–931, Aug 2005.

[45] H. Takagi, M. J. Sato, T. Yanagida, and M. Ueda. Functional analysis of spontaneous cell movement under different physiological conditions. *PLoS ONE*, 3(7):e2648, 2008.

[46] L. Li, E. C. Cox, and H. Flyvbjerg. 'Dicty dynamics': Dictyostelium motility as persistent random motion. *Phys Biol*, 8(4):046006, Aug 2011.

[47] Takao Ohta and Takahiro Ohkuma. Deformable self-propelled particles. *Physical review letters*, 102(15):154101, 2009.

[48] S. M. Rafelski and J. A. Theriot. Crawling toward a unified model of cell mobility: spatial and temporal regulation of actin dynamics. *Annu. Rev. Biochem.*, 73:209–239, 2004.

[49] L. Blanchoin, R. Boujemaa-Paterski, C. Sykes, and J. Plastino. Actin dynamics, architecture, and mechanics in cell motility. *Physiol. Rev.*, 94(1):235–263, Jan 2014.

[50] V. Achard, J. L. Martiel, A. Michelot, C. Guerin, A. C. Reymann, L. Blanchoin, and R. Boujemaa-Paterski. A "primer"-based mechanism underlies branched actin filament network formation and motility. *Curr. Biol.*, 20(5):423–428, Mar 2010.

[51] Pascal Vallotton, Stephanie L Gupton, Clare M Waterman-Storer, and Gaudenz Danuser. Simultaneous mapping of filamentous actin flow and turnover in migrating cells by quantitative fluorescent speckle microscopy. *Proceedings of the National Academy of Sciences of the United States of America*, 101(26):9660–9665, 2004.

[52] T. Mitchison and M. Kirschner. Cytoskeletal dynamics and nerve growth. *Neuron*, 1(9):761–772, Nov 1988.

[53] G. Giannone, R. M. Mege, and O. Thoumine. Multi-level molecular clutches in motile cell processes. *Trends Cell Biol.*, 19(9):475–486, Sep 2009.

[54] M. L. Gardel, B. Sabass, L. Ji, G. Danuser, U. S. Schwarz, and C. M. Waterman. Traction stress in focal adhesions correlates biphasically with actin retrograde flow speed. *J. Cell Biol.*, 183(6):999–1005, Dec 2008.

[55] G. I. Bell. Models for the specific adhesion of cells to cells. *Science*, 200(4342):618–627, May 1978.

[56] Benoit Ladoux and Alice Nicolas. Physically based principles of cell adhesion mechanosensitivity in tissues. *Reports on Progress in Physics*, 75(11):116601, 2012.

[57] Ulrich S Schwarz and Samuel A Safran. Physics of adherent cells. *Reviews of Modern Physics*, 85(3):1327, 2013.

[58] Martin Lenz. Geometrical origins of contractility in disordered actomyosin networks. *Physical Review X*, 4(4):041002, 2014.

[59] A. Zumdieck, K. Kruse, H. Bringmann, A. A. Hyman, and F. Julicher. Stress generation and filament turnover during actin ring constriction. *PLoS ONE*, 2(8):e696, 2007.

[60] I. Mendes Pinto, B. Rubinstein, A. Kucharavy, J. R. Unruh, and R. Li. Actin depolymerization drives actomyosin ring contraction during budding yeast cytokinesis. *Dev. Cell*, 22(6):1247–1260, Jun 2012.

[61] M. P. Murrell and M. L. Gardel. F-actin buckling coordinates contractility and severing in a biomimetic actomyosin cortex. *Proc. Natl. Acad. Sci. U.S.A.*, 109(51):20820–20825, Dec 2012.

[62] M. Lenz, T. Thoresen, M. L. Gardel, and A. R. Dinner. Contractile units in disordered actomyosin bundles arise from F-actin buckling. *Phys. Rev. Lett.*, 108(23):238107, Jun 2012.

[63] Pierre Ronceray, Chase P Broedersz, and Martin Lenz. Fiber networks amplify active stress. *Proceedings of the National Academy of Sciences*, page 201514208, 2016.

[64] Adam C Martin, Matthias Kaschube, and Eric F Wieschaus. Pulsed contractions of an actin–myosin network drive apical constriction. *Nature*, 457(7228):495–499, 2009.

[65] Kai Dierkes, Angughali Sumi, Jérôme Solon, and Guillaume Salbreux. Spontaneous oscillations of elastic contractile materials with turnover. *Physical review letters*, 113(14):148102, 2014.

[66] Paolo Maiuri, Jean-François Rupprecht, Stefan Wieser, Verena Ruprecht, Olivier Bénichou, Nicolas Carpi, Mathieu Coppey, Simon De Beco, Nir Gov, Carl-Philipp Heisenberg, et al. Actin flows mediate a universal coupling between cell speed and cell persistence. *Cell*, 161(2):374–386, 2015.

[67] Matthias Krause and Alexis Gautreau. Steering cell migration: lamellipodium dynamics and the regulation of directional persistence. *Nature reviews Molecular cell biology*, 15(9):577–590, 2014.

[68] Rizwan Farooqui and Gabriel Fenteany. Multiple rows of cells behind an epithelial wound edge extend cryptic lamellipodia to collectively drive cell-sheet movement. *J. Cell Sci.*, 118(1):51–63, 2005.

[69] M. Rauzi, P. Verant, T. Lecuit, and P. F. Lenne. Nature and anisotropy of cortical forces orienting Drosophila tissue morphogenesis. *Nat. Cell Biol.*, 10(12):1401–1410, Dec 2008.

[70] Paul Martin and Julian Lewis. Actin cables and epidermal movement in embryonic wound healing. *Nature*, 360(6400):179–183, nov 1992.

[71] Antonio Jacinto, William Wood, Sarah Woolner, Charlotte Hiley, Laura Turner, Clive Wilson, Alfonso Martinez-Arias, and Paul Martin. Dynamic analysis of actin cable function during Drosophila dorsal closure. *Curr. Biol.*, 12(14):1245–50, jul 2002.

[72] A. Cavagna, A. Cimarelli, I. Giardina, G. Parisi, R. Santagati, F. Stefanini, and M. Viale. Scale-free correlations in starling flocks. *Proc. Natl. Acad. Sci. U.S.A.*, 107:11865–11870, Jun 2010.

[73] D. J. Sumpter, J. Krause, R. James, I. D. Couzin, and A. J. Ward. Consensus decision making by fish. *Curr. Biol.*, 18:1773–1777, Nov 2008.

[74] A. J. Ward, D. J. Sumpter, I. D. Couzin, P. J. Hart, and J. Krause. Quorum decision-making facilitates information transfer in fish shoals. *Proc. Natl. Acad. Sci. U.S.A.*, 105:6948–6953, May 2008.

[75] Tamás Vicsek, András Czirók, Eshel Ben-Jacob, Inon Cohen, and O. Shochet. Novel type of phase transition in a system of self-driven particles. *Phys. Rev. Lett.*, 75(6):1226, 1995.

[76] Craig W Reynolds. Flocks, herds and schools: A distributed behavioral model. In *ACM SIGGRAPH computer graphics*, volume 21, pages 25–34. ACM, 1987.

[77] N David Mermin and Ho Wagner. Absence of ferromagnetism or antiferromagnetism in one-or two-dimensional isotropic heisenberg models. *Physical Review Letters*, 17(22):1133, 1966.

[78] PC Hohenberg. Existence of long-range order in one and two dimensions. *Physical Review*, 158(2):383, 1967.

[79] John Toner and Yuhai Tu. Long-range order in a two-dimensional dynamical xy model: how birds fly together. *Physical Review Letters*, 75(23):4326, 1995.

[80] John Toner and Yuhai Tu. Flocks, herds, and schools: A quantitative theory of flocking. *Physical review E*, 58(4):4828, 1998.

[81] Maximino Aldana, Victor Dossetti, Christian Huepe, VM Kenkre, and Hernán Larralde. Phase transitions in systems of self-propelled agents and related network models. *Physical review letters*, 98(9):095702, 2007.

[82] Tamás Vicsek and Anna Zafeiris. Collective motion. *Physics Reports*, 517(3):71–140, 2012.

[83] Guillaume Grégoire and Hugues Chaté. Onset of collective and cohesive motion. *Physical review letters*, 92(2):025702, 2004.

[84] Alexandre P Solon, Hugues Chaté, and Julien Tailleur. From phase to microphase separation in flocking models: the essential role of nonequilibrium fluctuations. *Physical review letters*, 114(6):068101, 2015.

[85] H. Chate, F. Ginelli, G. Gregoire, and F. Raynaud. Collective motion of self-propelled particles interacting without cohesion. *Phys Rev E Stat Nonlin Soft Matter Phys*, 77:046113, Apr 2008.

[86] Sriram Ramaswamy, R Aditi Simha, and John Toner. Active nematics on a substrate: Giant number fluctuations and long-time tails. *EPL (Europhysics Letters)*, 62(2):196, 2003.

[87] J. Deseigne, O. Dauchot, and H. Chate. Collective motion of vibrated polar disks. *Phys. Rev. Lett.*, 105:098001, Aug 2010.

[88] Antoine Bricard, Jean-Baptiste Caussin, Nicolas Desreumaux, Olivier Dauchot, and Denis Bartolo. Emergence of macroscopic directed motion in populations of motile colloids. *Nature*, 503(7474):95–98, 2013.

[89] G. Gregoire, H. Chate, and Y. Tu. Moving and staying together without a leader. *Physica D*, 181:157–170, 2003.

[90] Brian Camley and Wouter-Jan Rappel. Physical models of collective cell motility: from cell to tissue. *Journal of Physics D: Applied Physics*, 2017.

[91] B. Szabó, G. Szöllösi, B. Gönci, Zs. Jurányi, David Selmeczi, and Tamás Vicsek. Phase transition in the collective migration of tissue cells: Experiment and model. *Phys. Rev. E*, 74(6):1–5, 2006.

[92] Pawel Romanczuk, Markus Bär, Werner Ebeling, Benjamin Lindner, and Lutz Schimansky-Geier. Active brownian particles. *The European Physical Journal Special Topics*, 202(1):1–162, 2012.

[93] Markus Basan, Jens Elgeti, Edouard Hannezo, Wouter-Jan Rappel, and Herbert Levine. Alignment of cellular motility forces with tissue flow as a mechanism for efficient wound healing. *Proc. Natl. Acad. Sci. U. S. A.*, 110(7):2452–9, feb 2013.

[94] Silke Henkes, Yaouen Fily, and M. Cristina Marchetti. Active jamming: Self-propelled soft particles at high density. *Phys. Rev. E*, 84(4):84–87, oct 2011.

[95] Néstor Sepúlveda, Laurence Petitjean, Olivier Cochet-Escartin, Erwan Grasland-Mongrain, Pascal Silberzan, and Vincent Hakim. Collective cell motion in an epithelial sheet can be quantitatively described by a stochastic interacting particle model. *PLoS Comput. Biol.*, 9(3):e1002944, jan 2013.

[96] Danfeng Cai, Shann-Ching Chen, Mohit Prasad, Li He, Xiaobo Wang, Valerie Choesmel-Cadamuro, Jessica K Sawyer, Gaudenz Danuser, and Denise J Montell. Mechanical feedback through e-cadherin promotes direction sensing during collective cell migration. *Cell*, 157(5):1146–1159, 2014.

[97] Asha M Das, Alexander M M Eggermont, and Timo L M ten Hagen. A ring barrierbased migration assay to assess cell migration in vitro. *Nat. Protoc.*, 10(6):904–915, 2015.

[98] Arnold Hayer, Lin Shao, Mingyu Chung, Lydia-Marie Joubert, Hee Won Yang, Feng-Chiao Tsai, Anjali Bisaria, Eric Betzig, and Tobias Meyer. Engulfed cadherin fingers are polarized junctional structures between collectively migrating endothelial cells. *Nature Cell Biology*, 18(12):1311–1323, 2016.

[99] Juliane Zimmermann, Brian A Camley, Wouter-jan Rappel, and Herbert Levine. Contact inhibition of locomotion determines cellcell and cellsubstrate forces in tissues. *Proc. Natl. Acad. Sci.*, page 201522330, feb 2016.

[100] Mathieu Poujade, Erwan Grasland-Mongrain, A Hertzog, J Jouanneau, Philippe Chavrier, Benoît Ladoux, Axel Buguin, and Pascal Silberzan. Collective migration of an epithelial monolayer in response to a model wound. *Proc. Natl. Acad. Sci. U. S. A.*, 104(41):15988–93, oct 2007.

[101] Malcolm S Steinberg. Reconstruction of tissues by dissociated cells. *Science*, 141(3579):401–408, 1963.

[102] François Graner and James A Glazier. Simulation of biological cell sorting using a two-dimensional extended potts model. *Physical review letters*, 69(13):2013, 1992.

[103] James A Glazier and François Graner. Simulation of the differential adhesion driven rearrangement of biological cells. *Physical Review E*, 47(3):2128, 1993.

[104] James A Glazier, Ariel Balter, and Nikodem J Popławski. Magnetization to morphogenesis: a brief history of the glazier-graner-hogeweg model. In *Single-Cell-Based Models in Biology and Medicine*, pages 79–106. Springer, 2007.

[105] Wouter-Jan Rappel, Alastair Nicol, Armand Sarkissian, Herbert Levine, and William F Loomis. Self-organized vortex state in two-dimensional dictyostelium dynamics. *Physical review letters*, 83(6):1247, 1999.

[106] András Szabó, R Unnep, Eld Méhes, W O Twal, W S Argraves, Y Cao, and András Czirók. Collective cell motion in endothelial monolayers. *Phys. Biol.*, 7(4):046007, jan 2010.

[107] Alexandre J. Kabla. Collective cell migration: leadership, invasion and segregation. *J. R. Soc. Interface*, 9(77):3268–78, dec 2012.

[108] H. Honda. Description of cellular patterns by dirichlet domains: The two-dimensional case. *J. theor. Biol.*, 72:523–543, 1978.

[109] L. Hufnagel, A. A. Teleman, H. Rouault, S. M. Cohen, and B. I. Shraiman. On the mechanism of wing size determination in fly development. *Proc. Natl. Acad. Sci. U.S.A.*, 104(10):3835–3840, Mar 2007.

[110] R. Farhadifar, J.-C. Röper, B. Aigouy, S. Eaton, and F. Jülicher. The influence of cell mechanics, cell-cell interactions, and proliferation on epithelial packing. *Current Biology*, 17:2095–2104, 2007.

[111] Shraiman BI Chiou KK, Hufnagel L. Mechanical stress inference for two dimensional cell arrays. *PLoS Comput*

Biol, 8(5):e1002512, 2012.

[112] K. Sugimura and S. Ishihara. The mechanical anisotropy in a tissue promotes ordering in hexagonal cell packing. *Development*, 140(19):4091–4101, Oct 2013.

[113] Vincent Nier, Shreyansh Jain, Chwee Teck Lim, Shuji Ishihara, Benoit Ladoux, and Philippe Marcq. Inference of Internal Stress in a Cell Monolayer. *Biophys. J.*, 110(7):1625–1635, apr 2016.

[114] Nebojsa Murisic, Vincent Hakim, Ioannis G Kevrekidis, Stanislav Y Shvartsman, and Basile Audoly. From discrete to continuum models of three-dimensional deformations in epithelial sheets. *Biophysical journal*, 109(1):154–163, 2015.

[115] Alberto Puliafito, Lars Hufnagel, Pierre Neveu, Sebastian Streichan, Alex Sigal, D. Kuchnir Fygenson, and Boris I. Shraiman. Collective and single cell behavior in epithelial contact inhibition. *Proc. Natl. Acad. Sci. U. S. A.*, 109(3):739–744, jan 2012.

[116] Bo Li and Sean X Sun. Coherent Motions in Confluent Cell Monolayer Sheets. *Biophys. J.*, 107(7):1532–1541, oct 2014.

[117] Dapeng Bi, Xingbo Yang, M Cristina Marchetti, and M Lisa Manning. Motility-driven glass and jamming transitions in biological tissues. *Physical Review X*, 6(2):021011, 2016.

[118] Florent Peglion, Flora Llense, and Sandrine Etienne-Manneville. Adherens junction treadmilling during collective migration. *Nat. Cell Biol.*, 16(7):639–51, 2014.

[119] Pierre C Hohenberg and Bertrand I Halperin. Theory of dynamic critical phenomena. *Reviews of Modern Physics*, 49(3):435, 1977.

[120] Eric Bertin, Michel Droz, and Guillaume Grégoire. Hydrodynamic equations for self-propelled particles: microscopic derivation and stability analysis. *Journal of Physics A: Mathematical and Theoretical*, 42(44):445001, 2009.

[121] John Toner. Reanalysis of the hydrodynamic theory of fluid, polar-ordered flocks. *Physical Review E*, 86(3):031918, 2012.

[122] Pilhwa Lee and Charles W Wolgemuth. Crawling cells can close wounds without purse strings or signaling. *PLoS Comput Biol*, 7(3):e1002007, 2011.

[123] Shiladitya Banerjee, Kazage J. C. Utuje, and M. Cristina Marchetti. Propagating Stress Waves During Epithelial Expansion. *Phys. Rev. Lett.*, 114(June):228101, 2015.

[124] J. Notbohm, S. Banerjee, K. J. Utuje, B. Gweon, H. Jang, Y. Park, J. Shin, J. P. Butler, J. J. Fredberg, and M. C. Marchetti. Cellular Contraction and Polarization Drive Collective Cellular Motion. *Biophys. J.*, 110(12):2729–2738, Jun 2016.

[125] Jonas Ranft, Markus Basan, Jens Elgeti, Jean-François Joanny, Jacques Prost, and Frank Jülicher. Fluidization of tissues by cell division and apoptosis. *Proceedings of the National Academy of Sciences*, 107(49):20863–20868, 2010.

[126] Michael H. Köpf and Len M. Pismen. A continuum model of epithelial spreading. *Soft Matter*, 9(14):3727, 2013.

[127] PC Martin, O Parodi, and Peter S Pershan. Unified hydrodynamic theory for crystals, liquid crystals, and normal fluids. *Physical Review A*, 6(6):2401, 1972.

[128] Pierre-Gilles de Gennes and Jacques Prost. The physics of liquid crystals (international series of monographs on physics). *Oxford University Press, USA*, 1995.

[129] Justin C Yarrow, Zachary E Perlman, Nicholas J Westwood, and Timothy J Mitchison. A high-throughput cell migration assay using scratch wound healing, a comparison of image-based readout methods. *BMC Biotechnol.*, 4:21, 2004.

[130] Masako Tamada, Tomas D Perez, W. James Nelson, and Michael P Sheetz. Two distinct modes of myosin assembly and dynamics during epithelial wound closure. *J. Cell Biol.*, 176(1):27–33, 2007.

[131] Andries D van der Meer, Kim Vermeul, André a Poot, Jan Feijen, and István Vermes. A microfluidic wound-healing assay for quantifying endothelial cell migration. *Am. J. Physiol. Heart Circ. Physiol.*, 298(2):H719–H725, 2010.

[132] Ethan R. Block, Abigail R Matela, Nirmala SundarRaj, Erik R Iszkula, and Jes K Klarlund. Wounding induces motility in sheets of corneal epithelial cells through loss of spatial constraints: role of heparin-binding epidermal growth factor-like growth factor signaling. *J. Biol. Chem.*, 279(23):24307–12, 2004.

[133] A-K Marel, A Piera Alberola, and JO Rädler. Proliferation and collective migration of small cell groups released from circular patches. *Biophysical Reviews and Letters*, 7(01n02):15–28, 2012.

[134] Claudio G Rolli, Hidekazu Nakayama, Kazuo Yamaguchi, Joachim Pius Spatz, Ralf Kemkemer, and Jun Nakanishi. Switchable adhesive substrates: revealing geometry dependence in collective cell behavior. *Biomaterials*, 33(8):2409–18, mar 2012.

[135] M N Yousaf, B T Houseman, and M Mrksich. Using electroactive substrates to pattern the attachment of two different cell populations. *Proc. Natl. Acad. Sci.*, 98(11):5992–5996, may 2001.

[136] Nir S. Gov. Collective Cell Migration. In Roland Kaunas and Assaf Zemel, editors, *Cell Matrix Mech.*, chapter Collective, pages 219–238. CRC Press, Boca Raton, 2014.

[137] Anna Tourovskaia, Thomas Barber, Bronwyn T. Wickes, Danny Hirdes, Boris Grin, David G. Castner, Kevin E. Healy, and Albert Folch. Micropatterns of Chemisorbed Cell Adhesion-Repellent Films Using Oxygen Plasma Etching and Elastomeric Masks. *Langmuir*, 19(11):4754–4764, may 2003.

[138] George M Whitesides, Emanuele Ostuni, Xingyu Jiang, and Donald E. Ingber. Soft Lithography in Biology and Biochemistry. *Annu. Rev. Biomed. Eng.*, 3:335–73, 2001.

[139] Kaylene J Simpson, Laura M Selfors, James Bui, Angela Reynolds, Devin Leake, Anastasia Khvorova, and Joan S Brugge. Identification of genes that regulate epithelial cell migration using an siRNA screening approach. *Nat. Cell Biol.*, 10(9):1027–38, sep 2008.

[140] Philip Vitorino and Tobias Meyer. Modular control of endothelial sheet migration. *Genes Dev.*, 22(23):3268–81, dec 2008.

[141] M. Raffel, C. E. Willert, and J. Kompenhans. *Particle Image Velocimetry. A practical guide.* Springer Verlag, Berlin, 1998.

[142] Laurence Petitjean, Myriam Reffay, Erwan Grasland-Mongrain, Mathieu Poujade, Benoît Ladoux, Axel Buguin, and Pascal Silberzan. Velocity fields in a collectively migrating epithelium. *Biophys. J.*, 98(9):1790–800, may 2010.

[143] Willy Supatto, Delphine Débarre, Bruno Moulia, Eric Brouzés, Jean-louis Martin, Emmanuel Farge, and Emmanuel Beaurepaire. In vivo modulation of morphogenetic movements in Drosophila embryos with femtosecond laser pulses. *Proc. Natl. Acad. Sci. U. S. A.*, 102(4):1047–52, 2005.

[144] Maxime Deforet, Maria Carla Parrini, Laurence Petitjean, Marco Biondini, Axel Buguin, Jacques Camonis, and Pascal Silberzan. Automated velocity mapping of migrating cell populations (AVeMap). *Nat. Methods*, 9(11):1081–1083, oct 2012.

[145] Micah Dembo, T Oliver, A Ishihara, and Ken Jacobson. Imaging the traction stresses exerted by locomoting

cells with the elastic substratum method. *Biophys. J.*, 70:2008–2022, 1996.

[146] James P. Butler, Iva Marija Tolić-Nørrelykke, Ben Fabry, and Jeffrey J. Fredberg. Traction fields, moments, and strain energy that cells exert on their surroundings. *Am. J. Physiol. Cell Physiol.*, 282(3):C595–605, mar 2002.

[147] Benedikt Sabass, Margaret L. Gardel, Clare M. Waterman, and Ulrich S. Schwarz. High Resolution Traction Force Microscopy Based on Experimental and Computational Advances. *Biophys. J.*, 94(1):207–220, jan 2008.

[148] Xavier Trepat, Michael R. Wasserman, Thomas E. Angelini, Emil Millet, David A. Weitz, James P. Butler, and Jeffrey J. Fredberg. Physical forces during collective cell migration. *Nat. Phys.*, 5(6):426–430, 2009.

[149] Thomas E. Angelini, Edouard Hannezo, Xavier Trepat, Jeffrey J. Fredberg, and David a. Weitz. Cell Migration Driven by Cooperative Substrate Deformation Patterns. *Phys. Rev. Lett.*, 104(16):1–4, apr 2010.

[150] John L. Tan, Joe Tien, Dana M Pirone, Darren S. Gray, Kiran Bhadriraju, and Christopher S. Chen. Cells lying on a bed of microneedles: an approach to isolate mechanical force. *Proc. Natl. Acad. Sci. U. S. A.*, 100(4):1484–9, feb 2003.

[151] Olivia du Roure, Alexandre Saez, Axel Buguin, Robert H. Austin, Philippe Chavrier, Pascal Silberzan, and Benoît Ladoux. Force mapping in epithelial cell migration. *Proc. Natl. Acad. Sci. U. S. A.*, 102(7):2390–5, feb 2005.

[152] Michel Moussus, Christelle der Loughian, David Fuard, Marie Courçon, Danielle Gulino-Debrac, Hélène Delanoë-Ayari, and Alice Nicolas. Intracellular stresses in patterned cell assemblies. *Soft Matter*, 10(14):2414–2423, dec 2013.

[153] Dhananjay T. Tambe, C. Corey Hardin, Thomas E. Angelini, Kavitha Rajendran, Chan Young Park, Xavier Serra-Picamal, Enhua H. Zhou, Muhammad H. Zaman, James P. Butler, David a. Weitz, Jeffrey J. Fredberg, and Xavier Trepat. Collective cell guidance by cooperative intercellular forces. *Nat. Mater.*, 10(6):469–475, jun 2011.

[154] Dhananjay T. Tambe, Ugo Croutelle, Xavier Trepat, Chan Young Park, Jae Hun Kim, Emil Millet, James P. Butler, and Jeffrey J. Fredberg. Monolayer Stress Microscopy: Limitations, Artifacts, and Accuracy of Recovered Intercellular Stresses. *PLoS One*, 8(2), 2013.

[155] Juliane Zimmermann, Ryan L. Hayes, Markus Basan, José N. Onuchic, Wouter Jan Rappel, and Herbert Levine. Intercellular Stress Reconstitution from Traction Force Data. *Biophys. J.*, 107(3):548–554, 2014.

[156] Alexandre Saez, Marion Ghibaudo, Axel Buguin, Pascal Silberzan, and Benoît Ladoux. Rigidity-driven growth and migration of epithelial cells on microstructured anisotropic substrates. *Proc. Natl. Acad. Sci. U. S. A.*, 104(20):8281–6, 2007.

[157] Mei Rosa Ng, Achim Besser, Gaudenz Danuser, and Joan S Brugge. Substrate stiffness regulates cadherin-dependent collective migration through myosin-II contractility. *J. Cell Biol.*, 199(3):545–63, oct 2012.

[158] Elsa Bazellières, Vito Conte, Alberto Elosegui-Artola, Xavier Serra-Picamal, María Bintanel-Morcillo, Pere Roca-Cusachs, José J. Muñoz, Marta Sales-Pardo, Roger Guimerà, and Xavier Trepat. Control of cellcell forces and collective cell dynamics by the intercellular adhesome. *Nat. Cell Biol.*, 17(4):409–420, mar 2015.

[159] Anne J Ridley. Rho gtpase signalling in cell migration. *Current opinion in cell biology*, 36:103–112, 2015.

[160] Kazuhiro Aoki and Michiyuki Matsuda. Visualization of small GTPase activity with fluorescence resonance energy transfer-based biosensors. *Nat. Protoc.*, 4(11):1623–31, jan 2009.

[161] Olivier Pertz, Louis Hodgson, Richard L Klemke, and Klaus M Hahn. Spatiotemporal dynamics of RhoA activity in migrating cells. *Nature*, 440(7087):1069–72, apr 2006.

[162] Michael Abercrombie and Joan E. M. Heaysman. Observations on the social behaviour of cells in tissue culture II monolayering of fibroblasts. *Exp. Cell Res.*, 6:293–306, 1954.

[163] NA Gloushankova, MF Krendel, NO Alieva, EM Bonder, HH Feder, JM Vasiliev, and IM Gelfand. Dynamics of contacts between lamellae of fibroblasts: essential role of the actin cytoskeleton. *Proceedings of the National Academy of Sciences*, 95(8):4362–4367, 1998.

[164] Jonathan W Astin, Jennifer Batson, Shereen Kadir, Jessica Charlet, Raj A Persad, David Gillatt, Jon D Oxley, and Catherine D Nobes. Competition amongst eph receptors regulates contact inhibition of locomotion and invasiveness in prostate cancer cells. *Nature Cell Biology*, 12(12):1194–1204, 2010.

[165] John R Davis, Andrei Luchici, Fuad Mosis, James Thackery, Jesus A Salazar, Yanlan Mao, Graham A Dunn, Timo Betz, Mark Miodownik, and Brian M Stramer. Inter-cellular forces orchestrate contact inhibition of locomotion. *Cell*, 161(2):361–373, 2015.

[166] Tamás Vicsek and Anna Zafeiris. Collective motion. *Phys. Rep.*, 517(3-4):71–140, aug 2012.

[167] Andrea J. Liu and Sidney R. Nagel. Nonlinear dynamics: Jamming is not just cool any more. *Nature*, 396(6706):21–22, nov 1998.

[168] O Pouliquen. Velocity Correlations in Dense Granular Flows. *Phys. Rev. Lett.*, 93(24):248001, dec 2004.

[169] Corey S. O'Hern, Leonardo E Silbert, Andrea J Liu, and Sidney R Nagel. Jamming at zero temperature and zero applied stress: The epitome of disorder. *Phys. Rev. E*, 68(1):011306, jul 2003.

[170] C. Song, P. Wang, and H. A. Makse. Experimental measurement of an effective temperature for jammed granular materials. *Proc. Natl. Acad. Sci.*, 102(7):2299–2304, feb 2005.

[171] Johan Mattsson, Hans M Wyss, Alberto Fernandez-Nieves, Kunimasa Miyazaki, Zhibing Hu, David R Reichman, and David A. Weitz. Soft colloids make strong glasses. *Nature*, 462(7269):83–6, nov 2009.

[172] Simon Garcia, Edouard Hannezo, Jens Elgeti, Jean-François Joanny, Pascal Silberzan, and Nir S. Gov. Physics of active jamming during collective cellular motion in a monolayer. *Proc. Natl. Acad. Sci.*, 112(50):15314–15319, dec 2015.

[173] Kenechukwu David Nnetu, Melanie Knorr, Josef a. Käs, and Mareike Zink. The impact of jamming on boundaries of collectively moving weak-interacting cells. *New J. Phys.*, 14(11):115012, nov 2012.

[174] Kenechukwu David Nnetu, Melanie Knorr, Steve Pawlizak, Thomas Fuhs, and Josef a. Käs. Slow and anomalous dynamics of an MCF-10A epithelial cell monolayer. *Soft Matter*, 9(39):9335, 2013.

[175] E.-M. Schotz, Marcos Lanio, Jared a Talbot, and M. Lisa Manning. Glassy dynamics in three-dimensional embryonic tissues. *J. R. Soc. Interface*, 10(89):20130726–20130726, sep 2013.

[176] Monirosadat Sadati, Nader Taheri Qazvini, Ramaswamy Krishnan, Chan Young Park, and Jeffrey J. Fredberg. Collective migration and cell jamming. *Differentiation*, 86(3):121–125, oct 2013.

[177] Thierry Mora and William Bialek. Are biological systems poised at criticality? *Journal of Statistical Physics*,

144(2):268–302, 2011.

[178] Dapeng Bi, J. H. Lopez, J. M. Schwarz, and M. Lisa Manning. A density-independent rigidity transition in biological tissues. *Nat. Phys.*, 11(12):1074–1079, sep 2015.

[179] Jin-Ah Park, Jae Hun Kim, Dapeng Bi, Jennifer A. Mitchel, Nader Taheri Qazvini, Kelan Tantisira, Chan Young Park, Maureen McGill, Sae-Hoon Kim, Bomi Gweon, Jacob Notbohm, Robert Steward Jr, Stephanie Burger, Scott H. Randell, Alvin T. Kho, Dhananjay T. Tambe, Corey Hardin, Stephanie A. Shore, Elliot Israel, David A. Weitz, Daniel J. Tschumperlin, Elizabeth P. Henske, Scott T. Weiss, M. Lisa Manning, James P. Butler, Jeffrey M. Drazen, and Jeffrey J. Fredberg. Unjamming and cell shape in the asthmatic airway epithelium. *Nat. Mater.*, 14(10):1040–1048, 2015.

[180] Jin-Ah Park, Lior Atia, Jennifer A Mitchel, Jeffrey J Fredberg, and James P Butler. Collective migration and cell jamming in asthma, cancer and development. *J Cell Sci*, 129(18):3375–3383, 2016.

[181] Kevin Doxzen, Sri Ram Krishna Vedula, Man Chun Leong, Hiroaki Hirata, Nir S. Gov, Alexandre J. Kabla, Benoît Ladoux, and Chwee Teck Lim. Guidance of collective cell migration by substrate geometry. *Integr. Biol. (Camb).*, 5(8):1026–35, aug 2013.

[182] Maxime Deforet, V. Hakim, Hannah G. Yevick, Guillaume Duclos, and Pascal Silberzan. Emergence of collective modes and tri-dimensional structures from epithelial confinement. *Nat. Commun.*, 5(May):3747, jan 2014.

[183] Felix J Segerer, Florian Thüroff, Alicia Piera Alberola, Erwin Frey, and Joachim Oskar Rädler. Emergence and Persistence of Collective Cell Migration on Small Circular Micropatterns. *Phys. Rev. Lett.*, 114(22):228102, jun 2015.

[184] Matthias L. Zorn, Anna-Kristina Marel, Felix J. Segerer, and Joachim O. Rädler. Phenomenological approaches to collective behavior in epithelial cell migration. *Biochim. Biophys. Acta - Mol. Cell Res.*, 1853(11):3143–3152, nov 2015.

[185] Xavier Serra-Picamal, Vito Conte, Romaric Vincent, Ester Anon, Dhananjay T. Tambe, Elsa Bazellieres, James P. Butler, Jeffrey J. Fredberg, and Xavier Trepat. Mechanical waves during tissue expansion. *Nat. Phys.*, 8(8):628–634, jul 2012.

[186] Leo Q Wan, Kacey Ronaldson, Miri Park, Grace Taylor, Yue Zhang, Jeffrey M Gimble, and Gordana Vunjak-Novakovic. Micropatterned mammalian cells exhibit phenotype-specific left-right asymmetry. *Proc. Natl. Acad. Sci. U. S. A.*, 108(30):12295–300, jul 2011.

[187] T.-H. Chen, Jeffrey J Hsu, Xin Zhao, Chunyan Guo, Margaret N Wong, Yi Huang, Zongwei Li, Alan Garfinkel, C.-M. Ho, Yin Tintut, and Linda L Demer. Left-Right Symmetry Breaking in Tissue Morphogenesis via Cytoskeletal Mechanics. *Circ. Res.*, 110(4):551–559, feb 2012.

[188] Kathryn E Worley, David Shieh, and Leo Q Wan. Inhibition of cellcell adhesion impairs directional epithelial migration on micropatterned surfaces. *Integr. Biol.*, 7:580–590, 2015.

[189] Yee Han Tee, Tom Shemesh, Visalatchi Thiagarajan, Rizal Fajar Hariadi, Karen L Anderson, Christopher Page, Niels Volkmann, Dorit Hanein, Sivaraj Sivaramakrishnan, Michael M Kozlov, and Alexander D Bershadsky. Cellular chirality arising from the self-organization of the actin cytoskeleton. *Nat. Cell Biol.*, 17(4):445–457, mar 2015.

[190] Ethan R. Block, Michael A Tolino, Jennifer S Lozano, Kira L Lathrop, Rebecca S Sullenberger, Abigail R Mazie, and Jes K Klarlund. Free Edges in Epithelial Cell Sheets Stimulate Epidermal Growth Factor Receptor Signaling. *Mol. Biol. Cell*, 21:2172–2181, 2010.

[191] Jes K Klarlund. Dual modes of motility at the leading edge of migrating epithelial cell sheets. *Proc. Natl. Acad. Sci. U. S. A.*, 109(39):15799–804, sep 2012.

[192] Herbert W. Rand. Wound closure in actinian tentacles with reference to the problem of organization. *Rouxs Arch. Entwicklungsmech. Org.*, 41(1):159–214, 1915.

[193] J. P. Trinkaus. *Cells into Organs: The Forces that Shape the Embryo*. Prentice Hall, Englewood Cliffs, NJ, 1984.

[194] Tamal Das, Kai Safferling, Sebastian Rausch, Niels Grabe, Heike Boehm, and Joachim P Spatz. A molecular mechanotransduction pathway regulates collective migration of epithelial cells. *Nat. Cell Biol.*, (February), 2015.

[195] Sri Ram Krishna Vedula, Man Chun Leong, Tan Lei Lai, Pascal Hersen, Alexandre J. Kabla, Chwee Teck Lim, and Benoît Ladoux. Emerging modes of collective cell migration induced by geometrical constraints. *Proc. Natl. Acad. Sci. U. S. A.*, 109(32):12974–9, aug 2012.

[196] Camila Londono, M Jimena Loureiro, Benjamin Slater, Petra B Lücker, John Soleas, Suthamathy Sathananthan, J Stewart Aitchison, Alexandre J. Kabla, and Alison P. McGuigan. Nonautonomous contact guidance signaling during collective cell migration. *Proc. Natl. Acad. Sci. U. S. A.*, 111(5):1807–12, feb 2014.

[197] András Czirók, Katalin Varga, Eld Méhes, and András Szabó. Collective cell streams in epithelial monolayers depend on cell adhesion. *New J. Phys.*, 15(7):075006, jul 2013.

[198] Sei Kuriyama, Eric Theveneau, Alexandre Benedetto, Maddy Parsons, Masamitsu Tanaka, Guillaume Charras, Alexandre Kabla, and Roberto Mayor. In vivo collective cell migration requires an lpar2-dependent increase in tissue fluidity. *The Journal of cell biology*, 206(1):113–127, 2014.

[199] Jae Hun Kim, Xavier Serra-Picamal, Dhananjay T. Tambe, Enhua H. Zhou, Chan Young Park, Monirosadat Sadati, Jin-Ah Park, Ramaswamy Krishnan, Bomi Gweon, Emil Millet, James P. Butler, Xavier Trepat, and Jeffrey J. Fredberg. Propulsion and navigation within the advancing monolayer sheet. *Nat. Mater.*, 12(9):856–863, jun 2013.

[200] Olivier Cochet-Escartin, Jonas Ranft, Pascal Silberzan, and Philippe Marcq. Border forces and friction control epithelial closure dynamics. *Biophys. J.*, 106(1):65–73, jan 2014.

[201] Agustí Brugués, Ester Anon, Vito Conte, Jim H. Veldhuis, Mukund Gupta, Julien Colombelli, José J. Muñoz, G. Wayne Brodland, Benoît Ladoux, and Xavier Trepat. Forces driving epithelial wound healing. *Nat. Phys.*, 10(9):683–690, aug 2014.

[202] Caitlin Collins and W James Nelson. Running with neighbors: coordinating cell migration and cell-cell adhesion. *Curr. Opin. Cell Biol.*, 36:62–70, 2015.

[203] Sandrine Etienne-Manneville. Neighborly relations during collective migration. *Curr. Opin. Cell Biol.*, 30(1):51–59, 2014.

[204] H Delanoe-Ayari, P Lenz, J Brevier, M Weidenhaupt, M Vallade, D Gulino, JF Joanny, and D Riveline. Periodic adhesive fingers between contacting cells. *Physical review letters*, 93(10):108102, 2004.

[205] Djordje L Nikolić, Alistair N Boettiger, Dafna Bar-Sagi, Jeffrey D Carbeck, and Stanislav Y Shvartsman. Role of boundary conditions in an experimental model of epithelial wound healing. *Am. J. Physiol. Cell Physiol.*, 291(1):C68–75, 2006.

[206] Stéphane Douezan, Karine Guevorkian, Randa Naouar, Sylvie Dufour, Damien Cuvelier, and Françoise

Brochard-Wyart. Spreading dynamics and wetting transition of cellular aggregates. *Proc. Natl. Acad. Sci. U. S. A.*, 108(18):7315–20, may 2011.

[207] Stéphane Douezan, Julien Dumond, and Françoise Brochard-Wyart. Wetting transitions of cellular aggregates induced by substrate rigidity. *Soft Matter*, 8(17):4578, 2012.

[208] Pierre-Gilles De Gennes, Françoise Brochard-Wyart, and David Quéré. *Capillarity and wetting phenomena: drops, bubbles, pearls, waves*. Springer Science & Business Media, 2013.

[209] Tatiana Omelchenko, Jury M Vasiliev, I M Gelfand, H H Feder, and E M Bonder. Rho-dependent formation of epithelial "leader" cells during wound healing. *Proc. Natl. Acad. Sci. U. S. A.*, 100(19):10788–93, sep 2003.

[210] Hisashi Haga, Chikako Irahara, Ryo Kobayashi, Toshiyuki Nakagaki, and Kazushige Kawabata. Collective movement of epithelial cells on a collagen gel substrate. *Biophys. J.*, 88(3):2250–6, 2005.

[211] Myriam Reffay, Maria Carla Parrini, Olivier Cochet-Escartin, Benoît Ladoux, Axel Buguin, S. Coscoy, François Amblard, Jacques Camonis, and Pascal Silberzan. Interplay of RhoA and mechanical forces in collective cell migration driven by leader cells. *Nat. Cell Biol.*, 16(3):217–223, feb 2014.

[212] Myriam Reffay, Laurence Petitjean, S. Coscoy, Erwan Grasland-Mongrain, François Amblard, Axel Buguin, and Pascal Silberzan. Orientation and Polarity in Collectively Migrating Cell Structures: Statics and Dynamics. *Biophys. J.*, 100(11):2566–2575, jun 2011.

[213] Naoya Yamaguchi, Takeomi Mizutani, Kazushige Kawabata, and Hisashi Haga. Leader cells regulate collective cell migration via Rac activation in the downstream signaling of integrin β1 and PI3K. *Sci. Rep.*, 5:7656, 2015.

[214] Gaddiel Yonathan Ouaknin and Pinhas Zvi Bar-Yoseph. Stochastic collective movement of cells and fingering morphology: no maverick cells. *Biophysical journal*, 97(7):1811–1821, 2009.

[215] Marco Salm and LM Pismen. Chemical and mechanical signaling in epithelial spreading. *Physical biology*, 9(2):026009, 2012.

[216] Shirley Mark, Roie Shlomovitz, Nir S. Gov, Mathieu Poujade, Erwan Grasland-Mongrain, and Pascal Silberzan. Physical model of the dynamic instability in an expanding cell culture. *Biophys. J.*, 98(3):361–70, 2010.

[217] RC Brower, DA Kessler, J Koplik, and H Levine. Geometrical model of interface evolution. *Phys. Rev. A*, 29(3):1335–1342, 1984.

[218] Victoria Tarle, Andrea Ravasio, Vincent Hakim, and Nir S. Gov. Modeling the finger instability in an expanding cell monolayer. *Integr. Biol.*, 7(10):1218–1227, 2015.

[219] Micah Dembo and Yu-Li Wang. Stresses at the cell-to-substrate interface during locomotion of fibroblasts. *Biophysical journal*, 76(4):2307–2316, 1999.

[220] Antoine a Khalil and Peter Friedl. Determinants of leader cells in collective cell migration. *Integr. Biol. (Camb).*, 2(11-12):568–74, nov 2010.

[221] Peter Friedl, Joseph Locker, Erik Sahai, and Jeffrey E. Segall. Classifying collective cancer cell invasion. *Nat. Cell Biol.*, 14(8):777–783, aug 2012.

[222] Céline Revenu and Darren Gilmour. EMT 2.0: shaping epithelia through collective migration. *Curr. Opin. Genet. Dev.*, 19(4):338–42, aug 2009.

[223] Katarina Wolf, Yi I Wu, Yueying Liu, Jörg Geiger, Eric Tam, Christopher Overall, M Sharon Stack, and Peter Friedl. Multi-step pericellular proteolysis controls the transition from individual to collective cancer cell invasion. *Nat. Cell Biol.*, 9(8):893–904, 2007.

[224] Peter Friedl and Stephanie Alexander. Cancer invasion and the microenvironment: plasticity and reciprocity. *Cell*, 147(5):992–1009, nov 2011.

[225] Cedric Gaggioli, Steven Hooper, Cristina Hidalgo-Carcedo, Robert Grosse, John F Marshall, Kevin Harrington, and Erik Sahai. Fibroblast-led collective invasion of carcinoma cells with differing roles for RhoGTPases in leading and following cells. *Nat. Cell Biol.*, 9(12):1392–400, dec 2007.

[226] Ravi A Desai, Smitha B Gopal, S. Chen, and Christopher S. Chen. Contact inhibition of locomotion probabilities drive solitary versus collective cell migration. *J. R. Soc. Interface*, 10(88):20130717–20130717, sep 2013.

[227] Anna-Kristina Marel, Matthias Zorn, Christoph Klingner, Roland Wedlich-Söldner, Erwin Frey, and Joachim Oskar Rädler. Flow and Diffusion in Channel-Guided Cell Migration. *Biophys. J.*, 107(5):1054–1064, sep 2014.

[228] Hannah G. Yevick, Guillaume Duclos, Isabelle Bonnet, and Pascal Silberzan. Architecture and migration of an epithelium on a cylindrical wire. *Proc. Natl. Acad. Sci.*, 112(19):5944–5949, may 2015.

[229] Guillaume Duclos, Simon Garcia, Hannah G. Yevick, and Pascal Silberzan. Perfect nematic order in confined monolayers of spindle-shaped cells. *Soft Matter*, 10:2346–2353, 2014.

[230] Benjamin Lin, Taofei Yin, Yi I. Wu, Takanari Inoue, and Andre Levchenko. Interplay between chemotaxis and contact inhibition of locomotion determines exploratory cell migration. *Nat. Commun.*, 6:6619, apr 2015.

[231] Andrew D Doyle, Francis W Wang, Kazue Matsumoto, and Kenneth M Yamada. One-dimensional topography underlies three-dimensional fibrillar cell migration. *J. Cell Biol.*, 184(4):481–90, 2009.

[232] George T Eisenhoffer, Patrick D Loftus, Masaaki Yoshigi, Hideo Otsuna, Chi-bin Chien, Paul A Morcos, and Jody Rosenblatt. Crowding induces live cell extrusion to maintain homeostatic cell numbers in epithelia. *Nature*, 484(7395):546–9, apr 2012.

[233] Ester Anon, Xavier Serra-Picamal, Pascal Hersen, Nils C Gauthier, Michael P Sheetz, Xavier Trepat, and Benoît Ladoux. Cell crawling mediates collective cell migration to close undamaged epithelial gaps. *Proc. Natl. Acad. Sci. U. S. A.*, 109(27):10891–6, jul 2012.

[234] David S Li, Juliane Zimmermann, and Herbert Levine. Modeling closure of circular wounds through coordinated collective motion. *Phys. Biol.*, 13(1):016006, 2016.

[235] Andrea Ravasio, Ibrahim Cheddadi, Tianchi Chen, Telmo Pereira, Hui Ting Ong, Cristina Bertocchi, Agusti Brugues, Antonio Jacinto, Alexandre J. Kabla, Yusuke Toyama, Xavier Trepat, Nir Gov, Luís Neves de Almeida, and Benoît Ladoux. Gap geometry dictates epithelial closure efficiency. *Nat. Commun.*, 6:7683, jul 2015.

[236] Sebastian Rausch, Tamal Das, Jérôme Rd Soiné, Tobias W Hofmann, Christian HJ Boehm, Ulrich S. Schwarz, Heike Boehm, and Joachim Pius Spatz. Polarizing cytoskeletal tension to induce leader cell formation during collective cell migration. *Biointerphases*, 8(1):32, 2013.

[237] Sri Ram Krishna Vedula, Hiroaki Hirata, Mui Hoon Nai, Agustí Brugués, Yusuke Toyama, Xavier Trepat, Chwee Teck Lim, and Benoît Ladoux. Epithelial bridges maintain tissue integrity during collective cell migration. *Nat. Mater.*, 13(1):87–96, jan 2014.

[238] Sri Ram Krishna Vedula, Grégoire Peyret, Ibrahim Cheddadi, Tianchi Chen, Agustí Brugués, Hiroaki Hirata, Horacio Lopez-Menendez, Yusuke Toyama, Luís Neves de Almeida, Xavier Trepat, Chwee Teck Lim, and Benoît Ladoux. Mechanics of epithelial closure over non-adherent environments. *Nat. Commun.*, 6:6111, jan 2015.

[239] Vincent Nier, Maxime Deforet, Guillaume Duclos, Hannah G. Yevick, Olivier Cochet-Escartin, Philippe Marcq, and Pascal Silberzan. Tissue fusion over nonadhering surfaces. *Proc. Natl. Acad. Sci.*, 112(31):201501278, 2015.

[240] Gema Malet-Engra, Weimiao Yu, Amanda Oldani, Javier Rey-Barroso, Nir S. Gov, Giorgio Scita, and Loïc Dupré. Collective Cell Motility Promotes Chemotactic Prowess and Resistance to Chemorepulsion. *Curr. Biol.*, 25(2):242–250, jan 2015.

[241] Howard C. Berg. *E. coli in motion*. Springer-Verlag, New York, 2004.

[242] Liyu Liu, Guillaume Duclos, Bo Sun, Jeongseog Lee, Amy Wu, Yoonseok Kam, Eduardo D Sontag, Howard a Stone, James C Sturm, Robert a Gatenby, and Robert H. Austin. Minimization of thermodynamic costs in cancer cell invasion. *Proc. Natl. Acad. Sci. U. S. A.*, 110(5):1686–91, jan 2013.

[243] Pernille Rørth. Collective guidance of collective cell migration. *Trends Cell Biol.*, 17(12):575–9, 2007.

[244] M. Sarris and M. Sixt. Navigating in tissue mazes: chemoattractant interpretation in complex environments. *Curr. Opin. Cell Biol.*, 36:93–102, Oct 2015.

[245] Brian A Camley, Juliane Zimmermann, Herbert Levine, and Wouter-Jan Rappel. Emergent collective chemotaxis without single-cell gradient sensing. *Physical review letters*, 116(9):098101, 2016.

[246] Andre Levchenko and Pablo a Iglesias. Models of eukaryotic gradient sensing: application to chemotaxis of amoebae and neutrophils. *Biophys. J.*, 82(1 Pt 1):50–63, 2002.

[247] David Ellison, Andrew Mugler, Matthew Brennan, Sung Hoon Lee, Robert Huebner, Eliah Shamir, Laura A. Woo, Joseph Kim, Patrick Amar, Ilya Nemenman, Andrew J. Ewald, and Andre Levchenko. Cell-cell communication enhances the capacity of cell ensembles to sense shallow gradients during morphogenesis. *Proc. Natl. Acad. Sci.*, pages E1–30, aug 2015.

[248] Andrew Mugler, Andre Levchenko, and Ilya Nemenman. Limits to the precision of gradient sensing with spatial communication and temporal integration. *Proc. Natl. Acad. Sci.*, 113(6):E689–E695, feb 2016.

[249] E.F. Keller and L.A. Segel. Model for chemotaxis. *J. Theor. Biol.*, 30(2):225–34, feb 1971.

[250] Jonathan Saragosti, V. Calvez, Nikolaos Bournaveas, Benoît Perthame, Axel Buguin, and Pascal Silberzan. Directional persistence of chemotactic bacteria in a traveling concentration wave. *Proc. Natl. Acad. Sci. U. S. A.*, 108(39), sep 2011.

[251] Brian A. Camley, Juliane Zimmermann, Herbert Levine, and Wouter-Jan Rappel. Collective signal processing in cluster chemotaxis: roles of adaptation, amplification, and co-attraction in collective guidance. *ArXiv Prepr.*, pages 1–19, dec 2015.

[252] Richard Nuccitelli. A Role for Endogenous Electric Fields in Wound Healing. *Curr. Top. Dev. Biol.*, 58:1–26, 2003.

[253] Min Zhao, Bing Song, Jin Pu, Teiji Wada, Brian Reid, Guangping Tai, Fei Wang, Aihua Guo, Petr Walczysko, Yu Gu, Takehiko Sasaki, Akira Suzuki, John V Forrester, Henry R Bourne, Peter N Devreotes, Colin D McCaig, and Josef M Penninger. Electrical signals control wound healing through phosphatidylinositol-3-OH kinase-gamma and PTEN. *Nature*, 442(7101):457–460, 2006.

[254] Bing Song, Yu Gu, Jin Pu, Brian Reid, Zhiqiang Zhao, and Min Zhao. Application of direct current electric fields to cells and tissues in vitro and modulation of wound electric field in vivo. *Nat. Protoc.*, 2(6):1479–1489, jun 2007.

[255] E. Wang, M. Zhao, J. V. Forrester, and C. D. McCaig. Bi-directional migration of lens epithelial cells in a physiological electrical field. *Exp. Eye Res.*, 76(1):29–37, Jan 2003.

[256] Greg M. Allen, Alex Mogilner, and Julie a. Theriot. Electrophoresis of cellular membrane components creates the directional cue guiding keratocyte galvanotaxis. *Curr. Biol.*, 23(7):560–568, 2013.

[257] Li Li, Robert Hartley, Bjoern Reiss, Yaohui Sun, Jin Pu, Dan Wu, Francis Lin, Trung Hoang, Soichiro Yamada, Jianxin Jiang, and Min Zhao. E-cadherin plays an essential role in collective directional migration of large epithelial sheets. *Cell. Mol. Life Sci.*, 69(16):2779–2789, 2012.

[258] Daniel J Cohen, W. James Nelson, and Michel M Maharbiz. Galvanotactic control of collective cell migration in epithelial monolayers. *Nat. Mater.*, 13(4):409–17, apr 2014.

[259] R.J. Pelham and Yu-Li Wang. Cell locomotion and focal adhesions are regulated by substrate flexibility. *Proc. Natl. Acad. Sci. U. S. A.*, 94(25):13661, 1997.

[260] C.M. Lo, H.B. Wang, Micah Dembo, and Yu-Li Wang. Cell movement is guided by the rigidity of the substrate. *Biophys. J.*, 79(1):144–152, 2000.

[261] Tony Yeung, Penelope C Georges, Lisa a Flanagan, Beatrice Marg, Miguelina Ortiz, Makoto Funaki, Nastaran Zahir, Wenyu Ming, Valerie Weaver, and Paul a Janmey. Effects of substrate stiffness on cell morphology, cytoskeletal structure, and adhesion. *Cell Motil. Cytoskeleton*, 60(1):24–34, jan 2005.

[262] Anna Haeger, Marina Krause, Katarina Wolf, and Peter Friedl. Cell jamming: collective invasion of mesenchymal tumor cells imposed by tissue confinement. *Biochim. Biophys. Acta*, 1840(8):2386–95, aug 2014.

[263] Bettina Weigelin, Gert-Jan Bakker, and Peter Friedl. Intravital third harmonic generation microscopy of collective melanoma cell invasion. *IntraVital*, 1(1):32–43, jul 2012.

[264] Alexandre Saez, Axel Buguin, Pascal Silberzan, and Benoît Ladoux. Is the mechanical activity of epithelial cells controlled by deformations or forces? *Biophys. J.*, 89(6):L52–4, 2005.

[265] Grégory Beaune, Tomita Vasilica Stirbat, Nada Khalifat, Olivier Cochet-Escartin, Simon Garcia, Vasily Valérïévitch Gurchenkov, Michael P Murrell, Sylvie Dufour, Damien Cuvelier, and Françoise Brochard-Wyart. How cells flow in the spreading of cellular aggregates. *Proc. Natl. Acad. Sci. U. S. A.*, 111(22):8055–60, jun 2014.

[266] Raimon Sunyer, Vito Conte, Jorge Escribano, Alberto Elosegui-Artola, Anna Labernadie, Léo Valon, Daniel Navajas, José Manuel García-Aznar, José J Muñoz, Pere Roca-Cusachs, et al. Collective cell durotaxis emerges from long-range intercellular force transmission. *Science*, 353(6304):1157–1161, 2016.

[267] Clarence E Chan and David J Odde. Traction dynamics of filopodia on compliant substrates. *Science*, 322(5908):1687–1691, 2008.

[268] Hans Meinhardt. Orientation of chemotactic cells and growth cones: models and mechanisms. *J Cell Sci*, 112(17):2867–2874, 1999.

[269] Matthew P Neilson, Douwe M Veltman, Peter JM van Haastert, Steven D Webb, John A Mackenzie, and Robert H Insall. Chemotaxis: a feedback-based computational model robustly predicts multiple aspects of real cell behaviour. *PLoS Biol*, 9(5):e1000618, 2011.

[270] L. Tweedy, B. Meier, J. Stephan, D. Heinrich, and R. G. Endres. Distinct cell shapes determine accurate chemotaxis. *Sci Rep*, 3:2606, 2013.

[271] I. Hecht, M. L. Skoge, P. G. Charest, E. Ben-Jacob, R. A. Firtel, W. F. Loomis, H. Levine, and W. J. Rappel. Activated membrane patches guide chemotactic cell motility. *PLoS Comput. Biol.*, 7(6):e1002044, Jun 2011.

[272] Orion D Weiner, William A Marganski, Lani F Wu, Steven J Altschuler, and Marc W Kirschner. An actin-based wave generator organizes cell motility. *PLoS Biol*, 5(9):e221, 2007.

[273] D. Taniguchi, S. Ishihara, T. Oonuki, M. Honda-Kitahara, K. Kaneko, and S. Sawai. Phase geometries of two-dimensional excitable waves govern self-organized morphodynamics of amoeboid cells. *Proc. Natl. Acad. Sci. U.S.A.*, 110(13):5016–5021, Mar 2013.

[274] Jens Elgeti and Gerhard Gompper. Wall accumulation of self-propelled spheres. *EPL (Europhysics Letters)*, 101(4):48003, 2013.

[275] Xingbo Yang, M Lisa Manning, and M Cristina Marchetti. Aggregation and segregation of confined active particles. *Soft matter*, 10(34):6477–6484, 2014.

[276] Floris Bosveld, Olga Markova, Boris Guirao, Charlotte Martin, Zhimin Wang, Anaëlle Pierre, Maria Balakireva, Isabelle Gaugue, Anna Ainslie, Nicolas Christophorou, et al. Epithelial tricellular junctions act as interphase cell shape sensors to orient mitosis. *Nature*, 2016.

[277] Rebecca McLennan, Linus J Schumacher, Jason A Morrison, Jessica M Teddy, Dennis A Ridenour, Andrew C Box, Craig L Semerad, Hua Li, William McDowell, David Kay, et al. Neural crest migration is driven by a few trailblazer cells with a unique molecular signature narrowly confined to the invasive front. *Development*, 142(11):2014–2025, 2015.

[278] Rebecca McLennan, Linus J Schumacher, Jason A Morrison, Jessica M Teddy, Dennis A Ridenour, Andrew C Box, Craig L Semerad, Hua Li, William McDowell, David Kay, et al. Vegf signals induce trailblazer cell identity that drives neural crest migration. *Developmental biology*, 407(1):12–25, 2015.

[279] Eld Méhes, Enys Mones, Valéria Németh, and Tamás Vicsek. Collective Motion of Cells Mediates Segregation and Pattern Formation in Co-Cultures. *PLoS One*, 7(2):e31711, jan 2012.

[280] A. Combedazou, V. Choesmel-Cadamuro, G. Gay, J. Liu, L. Dupre, D. Ramel, and X. Wang. Myosin II governs collective cell migration behaviour downstream of guidance receptor signalling. *J. Cell Sci.*, pages 1–7, mar 2016.

[281] Anna Haeger, Katarina Wolf, Mirjam M. Zegers, and Peter Friedl. Collective cell migration: guidance principles and hierarchies. *Trends Cell Biol.*, 25(9):556–566, 2015.

[282] Stephanie Alexander, Bettina Weigelin, Frank Winkler, and Peter Friedl. Preclinical intravital microscopy of the tumour-stroma interface: invasion, metastasis, and therapy response. *Curr. Opin. Cell Biol.*, 25(5):659–71, oct 2013.

[283] Olga Ilina, Gert-Jan Bakker, Angela Vasaturo, Robert M Hoffman, and Peter Friedl. Two-photon laser-generated microtracks in 3D collagen lattices: principles of MMP-dependent and -independent collective cancer cell invasion. *Phys. Biol.*, 8(2):029501–029501, apr 2011.

[284] Celeste M. Nelson, Martijn M Vanduijn, Jamie L Inman, Daniel a Fletcher, and Mina J Bissell. Tissue geometry determines sites of mammary branching morphogenesis in organotypic cultures. *Science*, 314(5797):298–300, oct 2006.

[285] Nikolce Gjorevski, Alexandra S. Piotrowski, Victor D. Varner, and Celeste M. Nelson. Dynamic tensile forces drive collective cell migration through three-dimensional extracellular matrices. *Sci. Rep.*, 5(February):11458, jul 2015.

[286] Jiangrui Zhu, Long Liang, Yang Jiao, and Liyu Liu. Enhanced Invasion of Metastatic Cancer Cells via Extracellular Matrix Interface. *PLoS One*, 10(2):e0118058, feb 2015.

[287] Mirjam M.P. Zegers, Lucy E. O'Brien, Wei Yu, Anirban Datta, and Keith E. Mostov. Epithelial polarity and tubulogenesis in vitro. *Trends Cell Biol.*, 13(4):169–176, apr 2003.

[288] Pierre-Alexandre Vidi, Mina J. Bissell, and Sophie A. Lelièvre. Three-Dimensional Culture of Human Breast Epithelial Cells: The How and the Why. In *Methods Mol. Biol.*, volume 531, pages 193–219. 2012.

[289] O. W. Petersen, L. Ronnov-Jessen, A. R. Howlett, and M. J. Bissell. Interaction with basement membrane serves to rapidly distinguish growth and differentiation pattern of normal and malignant human breast epithelial cells. *Proc. Natl. Acad. Sci.*, 89(19):9064–9068, oct 1992.

[290] Kandice Tanner, Hidetoshi Mori, Rana Mroue, Alexandre Bruni-Cardoso, and Mina J Bissell. Coherent angular motion in the establishment of multicellular architecture of glandular tissues. *Proc. Natl. Acad. Sci. U. S. A.*, 109(6):1973–8, 2012.

[291] Ying Zheng, Junmei Chen, Michael Craven, Nak Won Choi, Samuel Totorica, Anthony Diaz-Santana, Pouneh Kermani, Barbara Hempstead, Claudia Fischbach-Teschl, José a López, and Abraham D Stroock. In vitro microvessels for the study of angiogenesis and thrombosis. *Proc. Natl. Acad. Sci. U. S. A.*, 109(24), may 2012.

[292] Liyu Liu, Bo Sun, Jonas N Pedersen, Koh-Meng Aw Yong, Robert H Getzenberg, Howard a Stone, and Robert H. Austin. Probing the invasiveness of prostate cancer cells in a 3D microfabricated landscape. *Proc. Natl. Acad. Sci. U. S. A.*, pages 1–4, apr 2011.

[293] Mao Ye, Henry M Sanchez, Margot Hultz, Zhen Yang, Max Bogorad, Andrew D Wong, and Peter C Searson. Brain microvascular endothelial cells resist elongation due to curvature and shear stress. *Sci. Rep.*, 4:4681, jan 2014.

[294] Andrew G Clark and Danijela Matic Vignjevic. Modes of cancer cell invasion and the role of the microenvironment. *Curr. Opin. Cell Biol.*, 36:13–22, oct 2015.

[295] Hai U Wang and David J Anderson. Eph family transmembrane ligands can mediate repulsive guidance of trunk neural crest migration and motor axon outgrowth. *Neuron*, 18(3):383–396, 1997.

[296] Xiaobo Wang, Li He, Yi I Wu, Klaus M Hahn, and Denise J Montell. Light-mediated activation reveals a key role for rac in collective guidance of cell movement in vivo. *Nature cell biology*, 12(6):591–597, 2010.

[297] Petra Haas and Darren Gilmour. Chemokine signaling mediates self-organizing tissue migration in the zebrafish lateral line. *Developmental cell*, 10(5):673–680, 2006.

[298] Antonio Jacinto, William Wood, Tina Balayo, Mark Turmaine, Alfonso Martinez-Arias, and Paul Martin. Dynamic actin-based epithelial adhesion and cell matching during drosophila dorsal closure. *Current Biology*, 10(22):1420–1426, 2000.

Figures

Figure 1. Different examples of collective cell motion *in vivo*. (A) Neural crest cells in the chick embryo, here marked by a HNK-1 antibody (left panel) migrate dorso-ventrally in corridors corresponding to rostral (r) somite halves. The corridors are delimited by expression of Eph ligands, such as Lerk2, in the caudal (c) somite halves, here visualized by a Lerk2 antibody (right panel). From [295]. (B) Border cells in *D. melanogaster* are a group of 4-8 migratory cells surrounding two non-motile polar cells. They migrate together between nurse cells from the anterior part of the Drosophila egg chamber toward the oocyte. (Top panels) Egg chambers at two stages are labelled with 4,6-diamidino-2-phenylindole (DAPI, blue) to stain all nuclei, Alexa 488-phalloidin (green) to mark actin filaments, and mCherry (red) expressed in border cells. Scale bars 20 μm (Bottom panels) Higher magnification views of border cells from each stage.From [296]. (C) (Top) The posterior lateral line organ primordium (pLLP) migration in zebrafish is visualized by expression of a membrane-tethered version of GFP expressed in every cell of the migrating pLLP as well as in the deposited neuromasts (pointed out by the white dashed lines) and connecting interneuromasts cells.The lateral line primordium migrates at a speed of $66\,\mu m/hr$ at 25^oC. The scale bar is $100\,\mu m$. (Bottom) Higher magnification of the migrating primordium. The scale bar is $20\,\mu m$.From [297]. (D) Dorsal closure in *D. melanogaster* . Scanning electron micrographs of embryos: (top left panel) during the zippering stage; and (top right panel) at the final stage of dorsal closure. (Bottom) High-magnification scanning electron micrographs of the corresponding boxed regions indicated in the top panels. From [298] .

Figure 2. Contact inhibition of locomotion. (A) CIL in isolated cells. (top) Sketch of a collision between two single cells showing the collapse of cell protrusion and a change in the direction of migration (green arrows). The four steps of CIL are shown with roman numerals. From [19]. (Bottom) Collision between two pseudo-colored neural crest cells *in vitro*.Time is shown in minutes. White arrows indicate the direction of migration; the red arrowhead indicates collision. From [18]. (B) CIL in a group of cells. CIL between inner cells leads to inhibition of protrusions, whereas CIL between the leader cells, at the free edge, can lead to cell polarization of the leaders (green arrows) and directional migration. From [19].

Figure 3. Some models of collective cell migration. (A) Simulation of the particle model described by (14,15) with particle confined to a square arena. The particle circular motion emerge over a wide range of model parameters. From [91] (B) Potts model simulation. (Top) An image of a motile tissue in the steady state, overlaid with the corresponding velocity field. Cell colors are arbitrary. (Bottom) Maps of the velocity correlations around a cell migrating from left to right. These have been obtained for populations of 1600 cells. The unit distance is the cell diameter. (C) A graph of the correlation length λ_c as a function of the motility parameter μ, for an energy parameter $J = 5$. Large correlation lengths are obtained for intermediate value of the motility parameter μ. For low values of μ/J, cells are essentially trapped while at large values of μ/J, the motility force is strong enough for a cell to disrupt adhesion between its neighbors and move through them. This jamming-like transition is discussed in section 5.2. From [107].

Figure 4. Mechanical measurements in a monolayer. (A) Displacement field measured by PIV. Rather than tracking each cell independently, one measures the cross correlation between subwindows from successive images. The maximum in the correlation plane corresponds to the average displacement. The procedure is reiterated for all subwindows and for all images of the movie [144]. (B) Traction force Microscopy (TFM) is performed by monitoring the displacement of beads (red) placed in a soft gel (blue). The cells placed on this substrate exert traction forces that can be inferred from the displacements of the beads. (C) An alternative technique uses micropillars on which cells are cultured. From the deflection of the micropillars, one can directly measure the local force. From [151]. (D) Once the traction forces are known by TFM, Monolayer Stress Microcopy (MSM) allows measuring the intracellular stresses by using Newton force balance. From [153].

Figure 5. Jamming of cell monolayers. A) Classical jamming phase diagram applicable to non-living systems such as glasses or colloidal suspensions. In this case the temperature, density and shear stress control the transition. The surface of jamming (yellow) separates jammed from unjammed regions. B) In the case of live cells, a strong analogy can be made with the jamming transition. The "motility" v_0 (14) plays the role of temperature; "persistence" ($1/D_r$ with D_r the rotational diffusion of the cell motility force) and preferred shape (p_0) are the two other control parameters. Depending on the phenotype of the cells, they can be positioned at different places in the diagram. The solid phase corresponds to the points close to the origin and the points above the jamming surface correspond to a fluid phase. From [117].

C) In dense conditions, a compressive stress mimicking a bronchospasm triggers the transition from jammed to unjammed states for bronchial HBEC cells. From [179]. D. Jamming transition in a vertex model (21) with non-motile cells and cell-independent parameters. The shape parameter p_0 denotes the ratio of the model preferred perimeter (P^0) to the square root of the preferred cell area (A^0), $p_0 = P^0/\sqrt{A^0}$, with $P^0 = -G/4H$ in the notations of (21). Critical collapse of the adimensionned averaged energy barrier $\overline{\Delta\epsilon}$ needed to induce a $T1$ transition between neighboring cells in the model ground state. The two branches of the scaling function are shown. The average energy barrier vanishes at the critical shape perimeter $p_0 = p_0^*$. E. The rigidity transition controlled by p_0 occurs at $p_0 = p_0^* \simeq 3.81$ corresponding to regular pentagons. If $p_0 < p_0^*$, the tissue is solid, it is fluid-like otherwise (the point $p_0 = 3.72$ corresponding to the loss of stability of regular hexagons is also indicated). From [178].

Figure 6. Effect of confinement on a MDCK epithelium. A) Confined epithelium on an adhesive disk. Cells do not escape on the surrounding non-adhesive surface for several weeks. B-C) Kymographs of the two components (radial (B) and orthoradial (C)) of the velocity after averaging over all angles. The orthoradial component describes the rotation of the cells in the disk. Changes of direction are stochastic. The radial component is maximal at mid-radius and exhibits a "breathing" oscillation whose period depends on the size of the domain. From [182].

Figure 7. Chirality in the orientation and displacements of myoblasts (C2C12 Cells). A) Phase contrast image. B) The green lines show the directions of the main axis of the cells. The chirality of the packing is clearly visible. C) the velocity field mirrors the orientation pattern. the insets show the angle-averaged orthoradial (v_θ) and radial (v_r) velocities as a function of the radial position. Scale bars = 100μm. From [186].

Figure 8. Collective migration following a model injury-free wound. A) Comparison between the collective displacements of epithelial MDCK cells (left) and fibroblast-like NRK cells (right). High velocity regions are distributed more uniformly for the MDCK cells. Scale bars 100 μm. B) the degree of collectiveness can be quantified from the velocity spatial correlation function. For MDCK cells, the correlation decrease over a characteristic distance of about 150 μm corresponding to about 10 cell diameters whereas for NRK cells, the correlation length is only 20 μm or two cell sizes. From [142] C) Stress maps for migrating mammary cells MCF10A (phase contrast (a); normal component of the traction forces exerted on the substrate measured by TFM (b) and normal component of the intercellular stress measured by MSM (c)). Vertical size of the images = 410μm. From [153]. D. Comparison between the experimental velocity field (left) and the simulated one (right). Box size = 1mm^2.E-G. The model accounts quantitatively for the different quantities measured in the experiments, including the wide distribution of the speeds (E), and the time and spatial correlation functions (F,G). Points are experimental points and black lines are the result of the simulations. From [95].

Figure 9. Mechanical waves during monolayer migration. The dynamical evolution of an initially 400 μm wide band of cells is represented as kymographs for the velocity (A) and the strain rate (B). on both kymographs, the waves appear as oblique bands in this representation. From [185].C. Schematic of the spreading monolayer. The stress σ is color coded. The polarization p has a sigmoidal shape of width λ. The boundaries of the monolayer are stress-free (σ=0). D. The theoretical model coupling the deformation in the monolayer to its contractile activity and to the polarization of the cells gives rise to mechanical waves consistent with the experimentally observed ones. From [123].

Figure 10. Spreading of a macroscopic murine sarcoma S-180 cell aggregate on a solid surface coated with fibronectin. The spreading parameter is controlled by the surface chemistry and the cohesion of the aggregate itself determined by the level of cadherins expressed at the surface of the cells. When a cell aggregate spreads on the surface, a monolayer of cells develops around it (A, green arrow). When the level of cadherins and hence the cohesiveness of the aggregate is high, the monolayer remains in a cohesive liquid form (B). In contrast, when the level of cadherins is low, the cells scatter on the surface and are best described as a gas (C). From [206].

Figure 11. (A) Heterotypic migration fingers. The Cancer-Associated Fibroblast (CAF) (in red) degrades the collagen matrix and generates a track in which the following squamous cell carcinoma (SCC) cells (in green) can follow. The SCC cells cannot invade the matrix by themselves. Scale bar= 20 μm. From [225]. (B) Migration finger at the front edge of a migrating MDCK monolayer. Actin green, phosphorylated myosin light chain red. Note the acto-myosin cable at the sides of the finger (arrows). Bar=50 μm. From [211]. (C) Similarly looking fingers are observed in 3D during invasion of collagen gels by HT-MT1 cells. The cells are initially in a spheroid (left) and migrate collectively in tracks where the collagen had been degraded. The arrow denotes the direction of migration. White triangles indicate high concentration of metalloproteases associated with the collagen matrix. Bar=20 μm. From [223].

Figure 12. The supercell analogy. The migration fingers at the front edge of a MDCK monolayer (Figure 11 B) are described by a traction force map dominated by fluctuations due to the active displacements of the individual cells that compose it (A). However when averaged across the finger, the longitudinal force behaves as a coherent mechanical entity that displays a high pulling force at its tip and a region of negative forces (friction forces) closer to the epithelium (B). Therefore, mechanically, the migrating fingers are characterized by force dipoles (red arrows) (C). From [211]. At a different scale, migrating single cells are also characterized by a force dipole (D) From [219]. The migration fingers that typically comprise 50 cells can therefore be considered as supercells. Laser ablation on the peripheral acto-myosin cable lining the edges of the migration fingers show that this pluricellular structure is under tension (E). Once severed, the alignment of the cells in the finger triggers the formation of a new leader at the cut (E),(F). Bar = 20 μm. From [211].

Figure 13. Migration in confining stripes. The migration of the epithelial MDCK cells is constrained in the micro-printed stripes (epithelium is on the right and cells migrate towards the left). For the widest stripes (400 μm (top)), the usual flows and swirls can be observed. However they disappear when the width decreases below 100 μm (middle and bottom). Scale bars=50 μm. From [195].

Figure 14. Effect of the adhesion on the substrate on the closing of circular wounds. A) When the underlying substrate is adhesive, cells close the wound by protrusive activity (stars) despite the presence of a pluricellular acto-myosin cable at the free edge. Bar = 20 μm. MDCK cells. Green: actin; red: myosin; blue: Nuclei. (B) A simple model including border forces, cell-substrate friction and tissue rheology accounts well the closure and allows quantitatively describing the trajectories of closures. R_0 is the initial radius of the wound. Dots: experimental points; lines: theoretical predictions. From [200]. (C) Alignment mechanism: cells switch from non-motile to motile states with a constant rate k_{mot}. The rate at which they switch back to a non-motile state depends on the degree of alignment of their velocity and motile force. (D) Results of the simulations for the convergent closure of a circular wound. Dashed lines are the theoretical fits from the continuous model of [200] (see panel (B)). The points results from the simulations of the model presented in panel (C) From [234]. (E) In contrast, when closing over a non-adherent surface (denoted by the white line), the cell actomyosin cable is instrumental in closing the aperture by a purse-string mechanism. (F) These wounds heal much slower than their counterpart on an adhesive surface and the closing is more jerky (compare the trajectories with panel B). The theoretical trajectories are simulated from a stochastic model including purse-string and tissue fluctuations. From [239].

Figure 15. High curvature of the front edge favors leader formation. (A) The initial shape of the MDCK monolayer is controlled by the stencil geometry. Leaders and migration fingers are more likely to develop at the spikes of high curvature (B). Scale bars =100 μm . From [236]. (C) Modelling of an expanding cell monolayer using the particle-based model (17) with velocity alignment supplemented with a curvature-dependent force at the border. These two ingredients give rise to migration fingers very similar to the ones observed experimentally. From [218].

Figure 16. Collective chemotaxis of malignant lymphocytes clusters in a gradient of the chemokine CCL-19. (A) The clusters migrate up the gradient. (B) Forward migration index (FMI) is positive and large for all values of gradients for clusters (black boxes). It is consistently smaller for single cells (Grey boxes). When gradients are too shallow, single cells do not chemotax. When it is too high, they migrate down the gradient (chemorepulsion).(C) In the model, the chemokine-dependent protrusive forces are located at the periphery of the cluster and are proportional to the local chemokine concentration. These forces are superimposed to random traction forces. From [240].

Figure 17. Collective galvanotaxis. A) Upon the application of a weak electric field, MDCK cells in a monolayer coordinate their migration toward the cathode. When the direction of the field is inverted, cells respond in minutes to change their direction. (B) Cells do not individually change their direction of migration but operate their U-turns in domains whose size is of the order of the correlation length. Width of panels 600 μm; time between frames: 6 min. From [258].

Figure 18. Role of the heterogeneities in *in vivo* collective migration. Melanoma invasion in the dermal tissue. (A) Tumor cells move in coherent and cohesive strands from the initial tumor into the deep dermis. In the inset an occasional detachment of tip cell. (C,D) cells remain confined by the heterogeneities of the tissue and guided by the interfaces. Intravital imaging performed in multiphoton microscopy (third harmonic generation and second harmonic generation). yellow, tumor cytoplasm; blue tumor nuclei; green, blood vessels; red, collagen. Scale bars =50 μm. From [263].

Figure 19. Collective migration on model glass fibers. (A) Glass fibers can be used to recapitulate some aspects of the heterogeneities of the *in vivo* environment. (A) MDCK cells migrate collectively on these substrates. (B) The architecture of the cell cytoskeleton is highly affected by the out-of-plane curvature and actin stress fibers display a marked orientation at the basal plane perpendicular to the fiber main axis. This circumferential orientation appears for radii smaller than typically 35 μm. These fibers appear continuous from one cell to its neighbor, demonstrating their mechanical continuity. From [228]

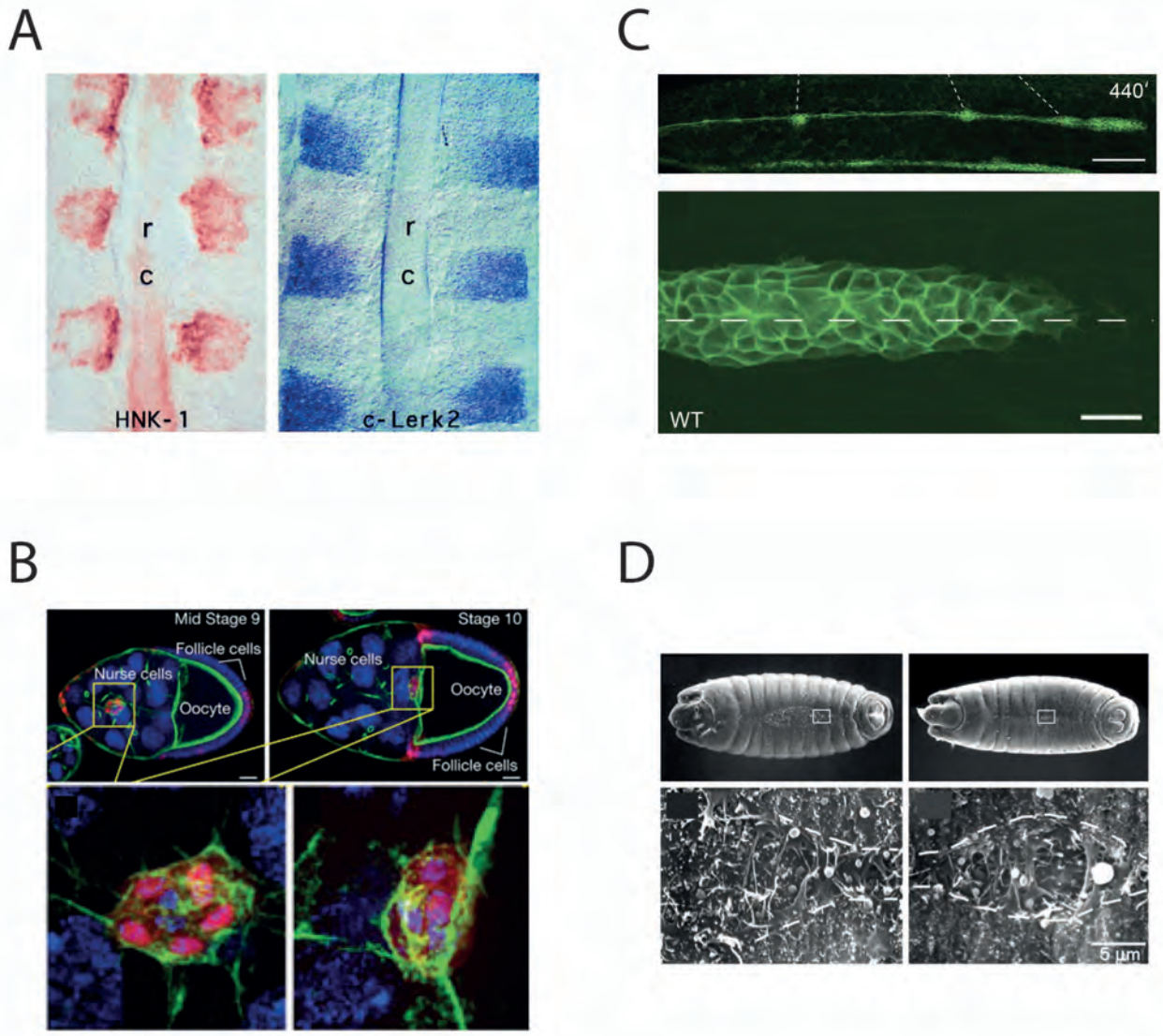
A
r
c
HNK-1
r
c
c-Lerk2
C
440'
WT
B
Mid Stage 9
Follicle cells
Nurse cells
Oocyte
Stage 10
Nurse cells
Oocyte
Follicle cells
D
5 µm

Figure 1

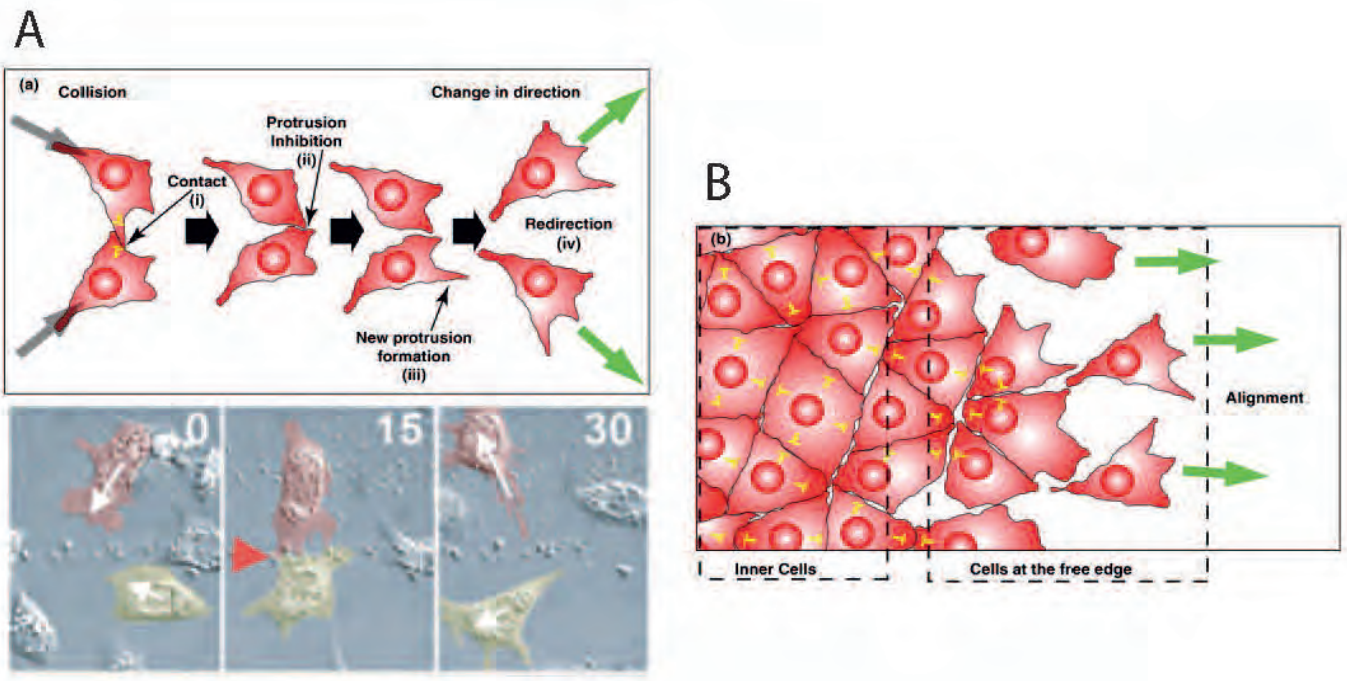
A
(a)
Collision
Change in direction
Protrusion
Inhibition
(ii)
Contact
(i)
Redirection
(iv)
New protrusion
formation
(iii)
0
15
30
B
(b)
Alignment
Inner Cells
Cells at the free edge

Figure 2

A

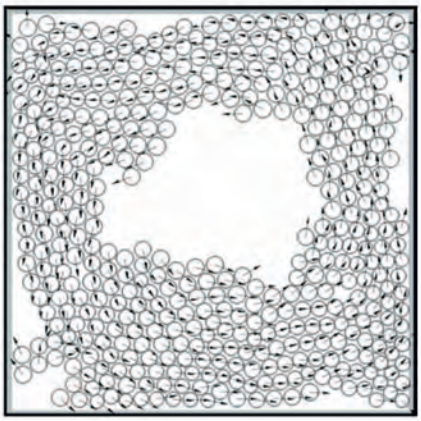

B

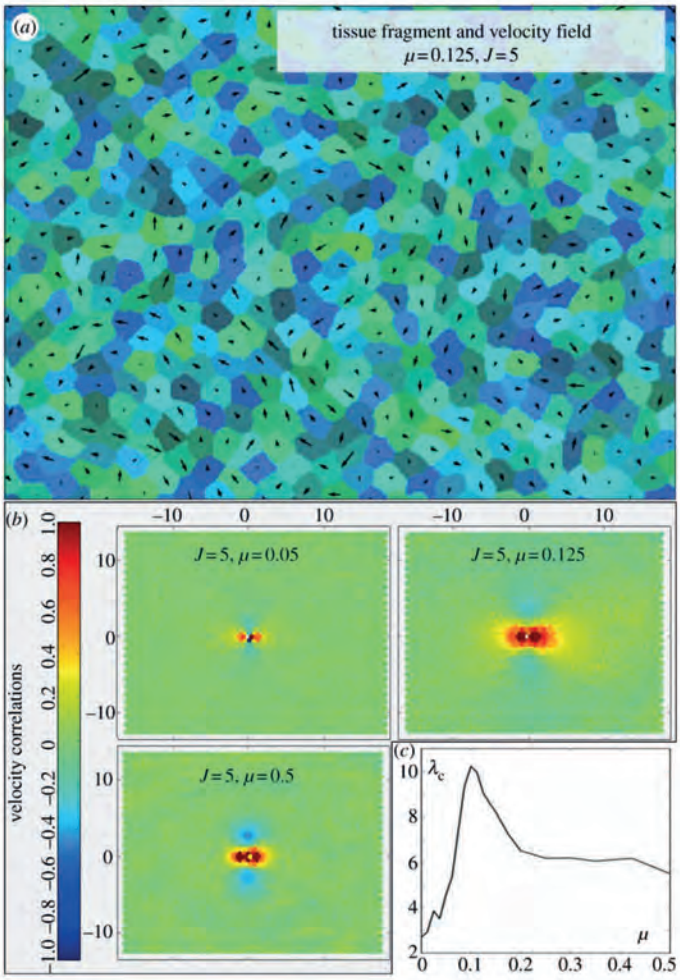
(a)
tissue fragment and velocity field
μ=0.125, J=5
(b)
velocity correlations
1.0
0.8
0.6
0.4
0.2
0
−0.2
−0.4
−0.6
−0.8
−1.0
−10
0
10
J=5, μ=0.05
J=5, μ=0.125
J=5, μ=0.5
(c)
λc
μ
2
4
6
8
10
0
0.1
0.2
0.3
0.4
0.5

Figure 3

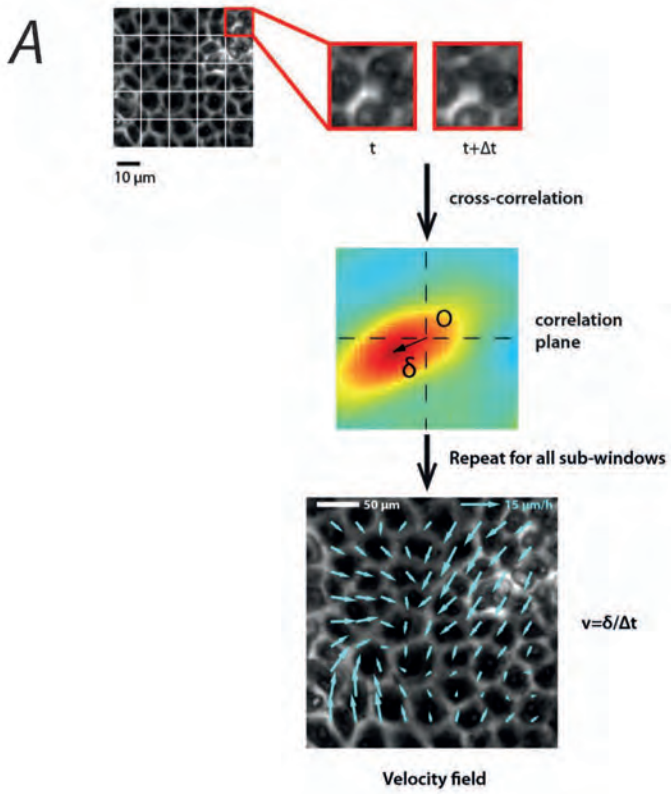
A
10 µm
t
t+Δt
cross-correlation
O
δ
correlation
plane
Repeat for all sub-windows
50 µm
15 µm/h
v=δ/Δt
Velocity field

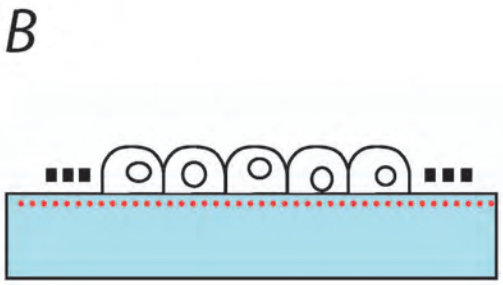
B

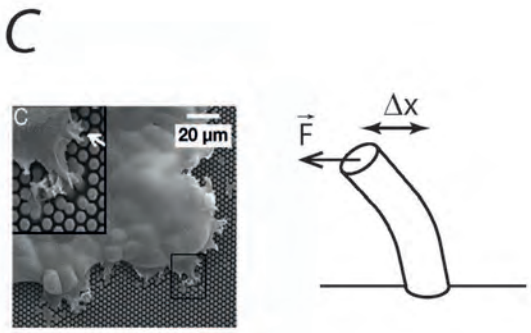
C
C
20 µm
F
Δx

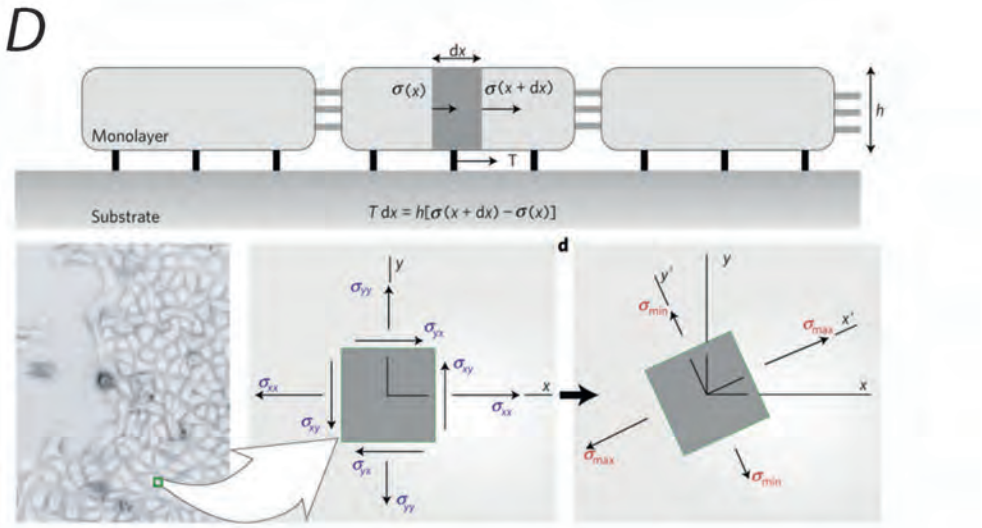
D
dx
σ(x)
σ(x + dx)
h
Monolayer
T
Substrate
T dx = h[σ(x + dx) − σ(x)]
d
y
x
σ_yy
σ_yx
σ_xy
σ_xx
σ_max
σ_min
x'
y'

Figure 4

A

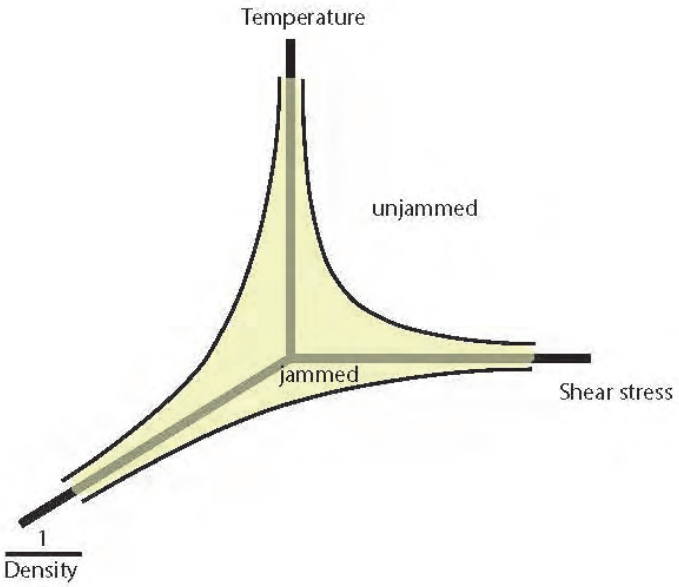

B

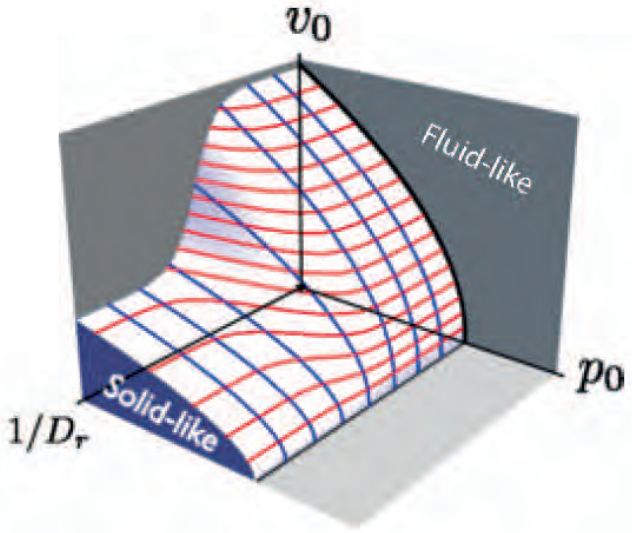

C

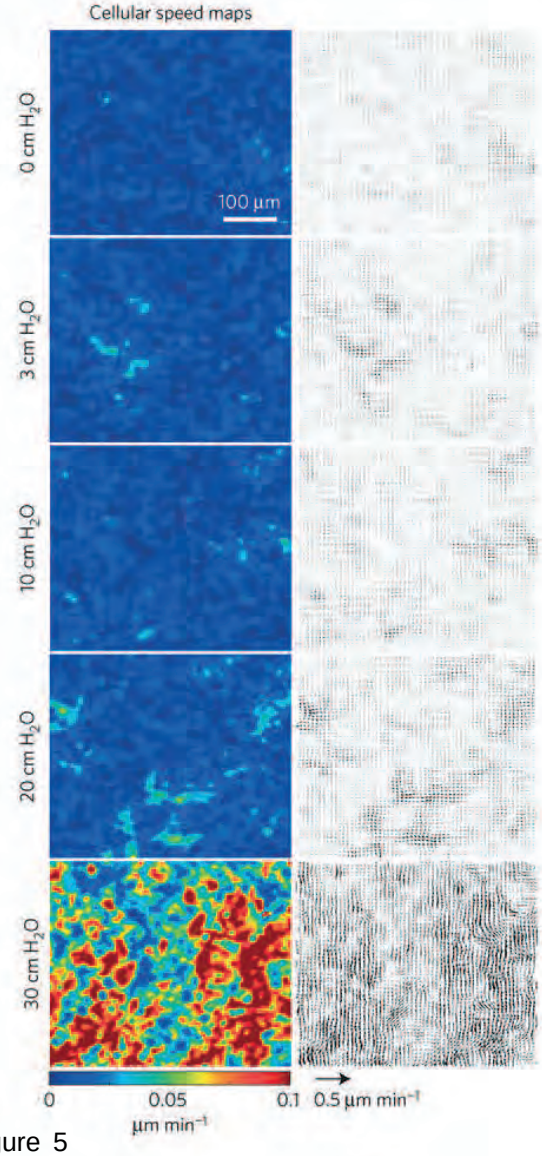

D

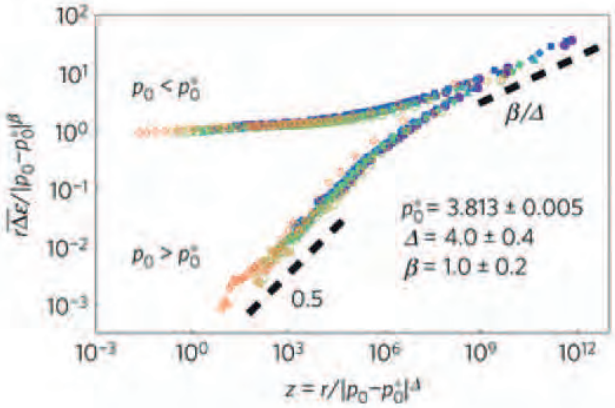

E

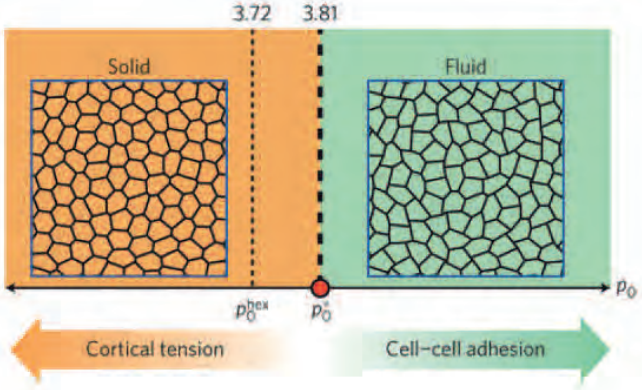

Figure 5

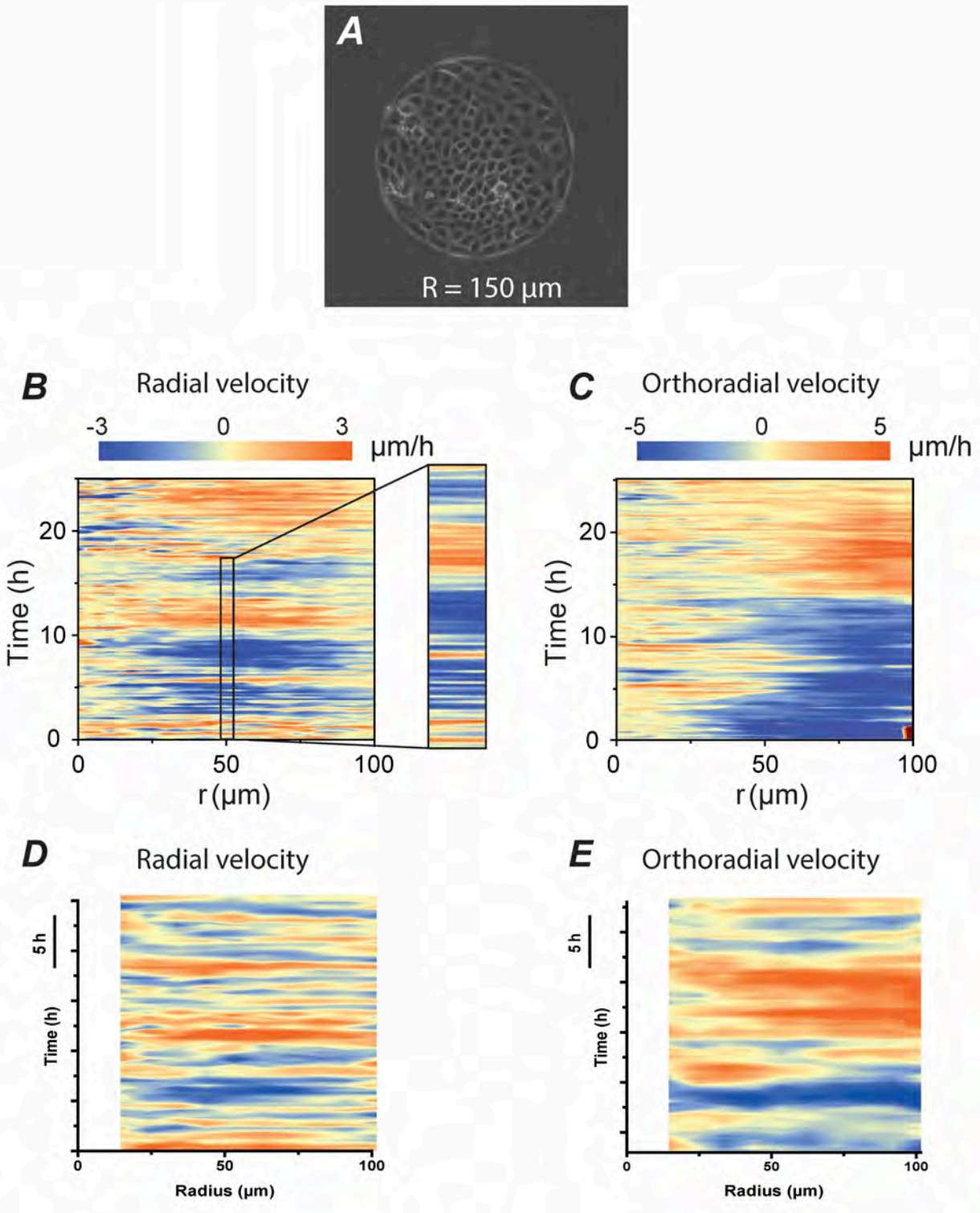
A
R = 150 µm
B
Radial velocity
-3
0
3
µm/h
Time (h)
r (µm)
C
Orthoradial velocity
-5
0
5
µm/h
Time (h)
r (µm)
D
Radial velocity
5 h
Time (h)
Radius (µm)
E
Orthoradial velocity
5 h
Time (h)
Radius (µm)

Figure 6

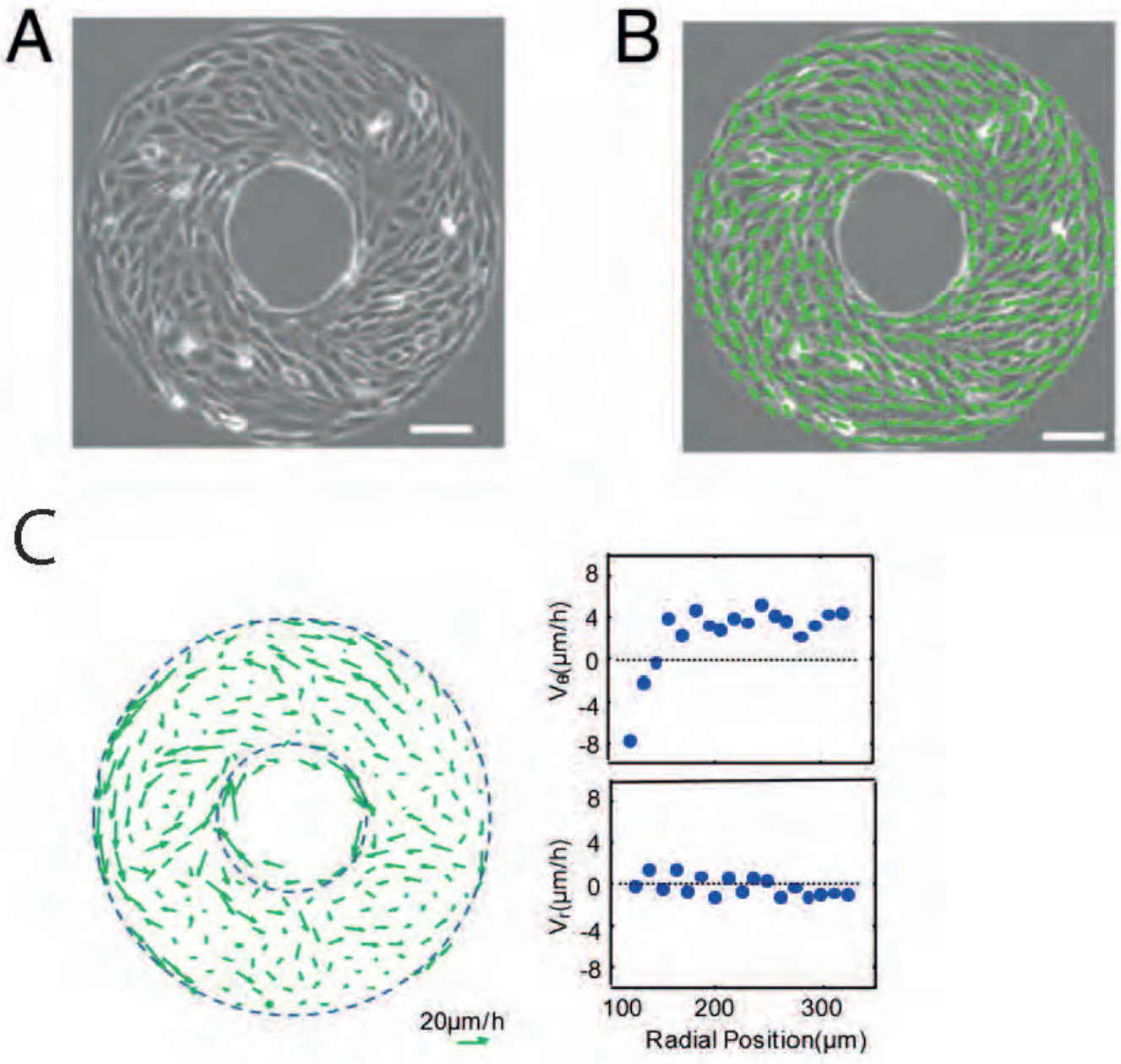
A
B
C
20μm/h
8
4
0
-4
-8
V_θ(μm/h)
8
4
0
-4
-8
V_r(μm/h)
100
200
300
Radial Position(μm)

Figure 7

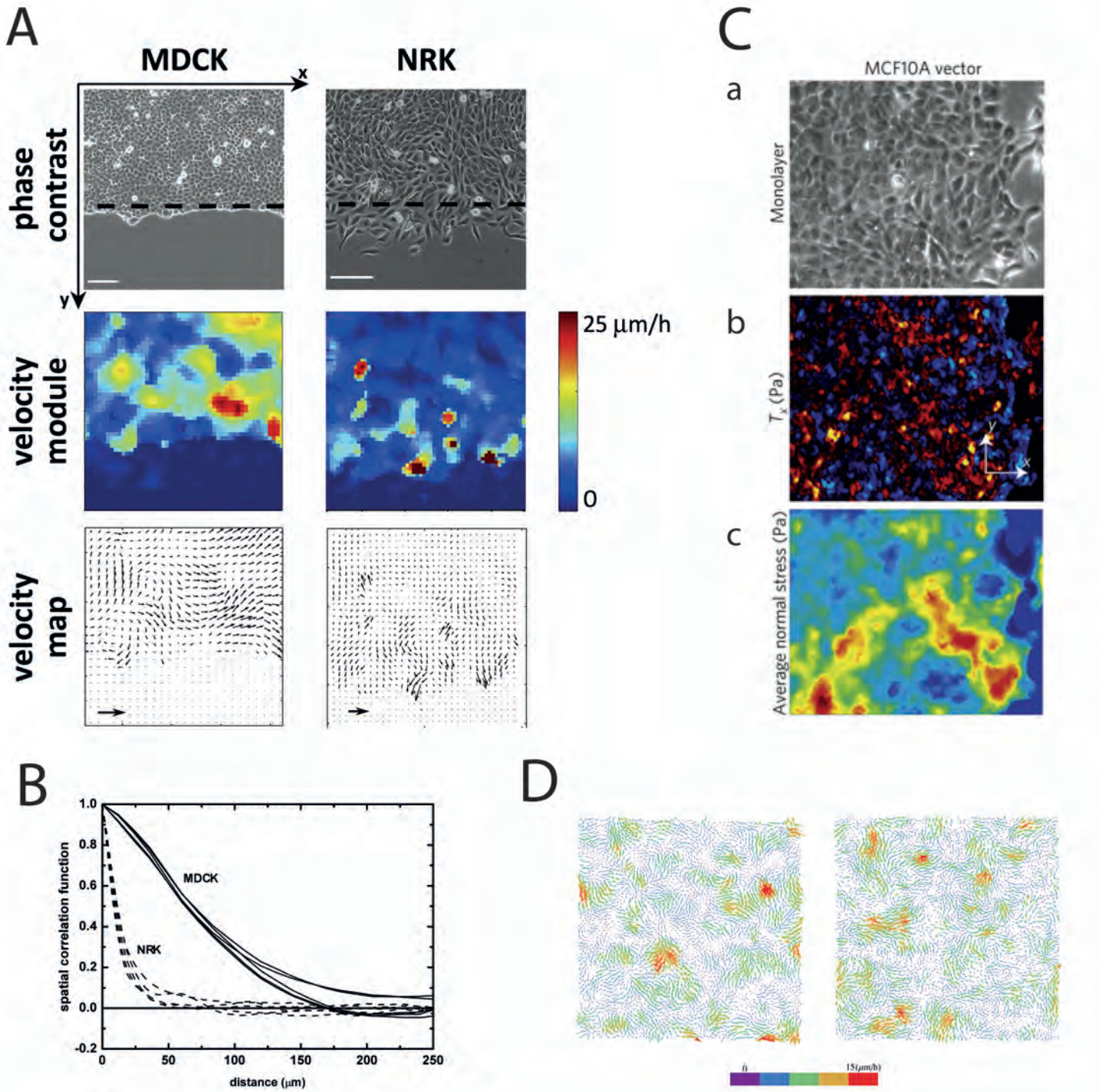
A
MDCK
NRK
phase contrast
x
y
velocity module
25 µm/h
0
velocity map
C
MCF10A vector
a
Monolayer
b
T_x (Pa)
c
Average normal stress (Pa)
B
spatial correlation function
MDCK
NRK
distance (µm)
D
0
15(µm/h)

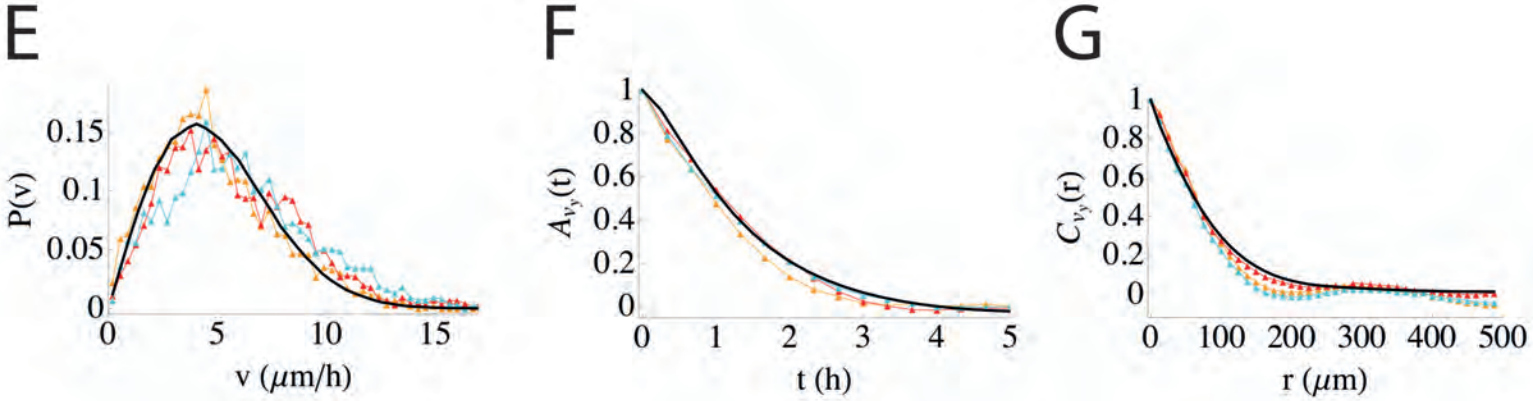
E
P(v)
v (µm/h)
F
$A_{v_y}(t)$
t (h)
G
$C_{v_y}(r)$
r (µm)

Figure 8

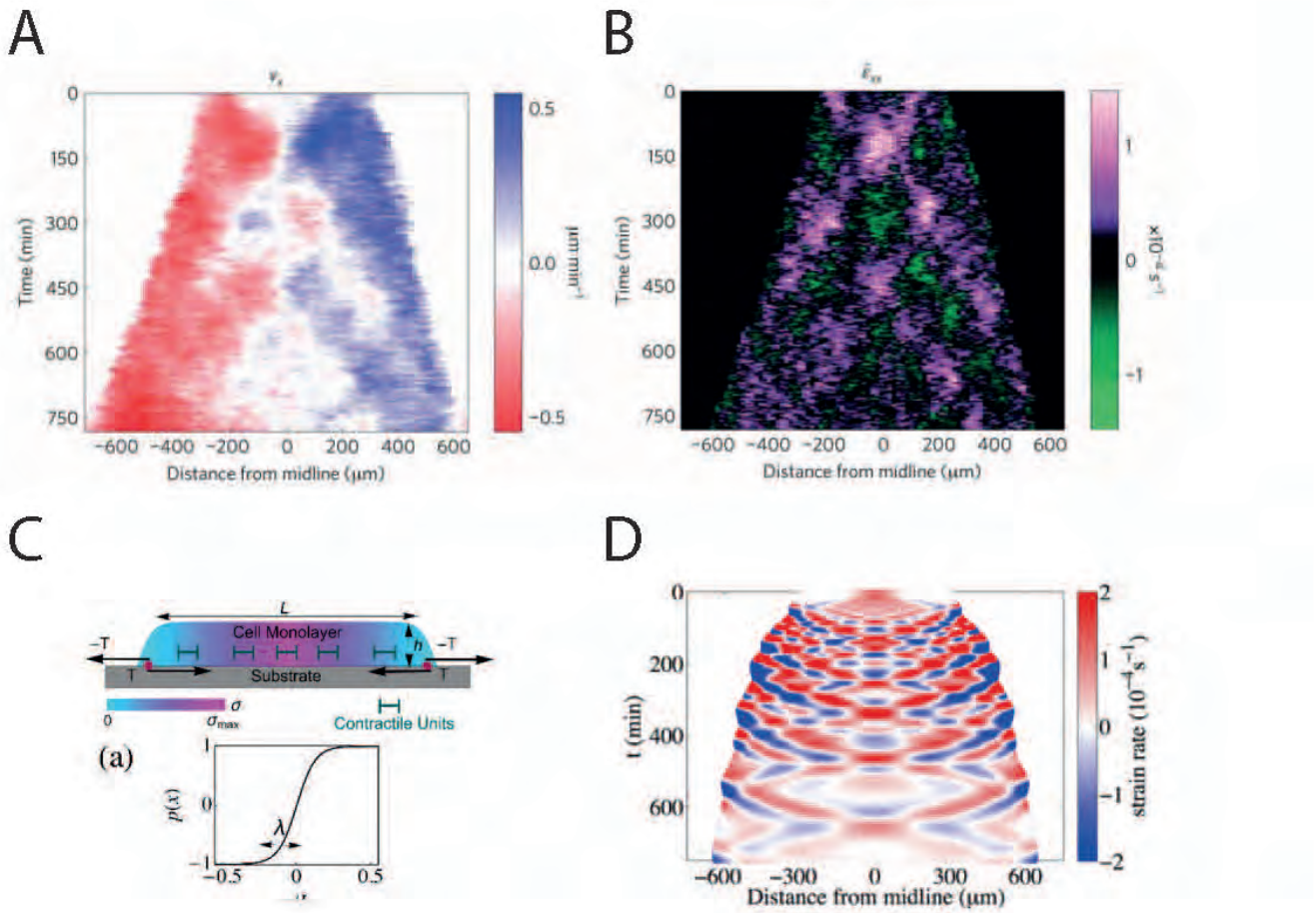
A
B
C
D
Time (min)
Distance from midline (μm)
Cell Monolayer
Substrate
Contractile Units
(a)
t (min)
strain rate (10⁻⁴ s⁻¹)

Figure 9

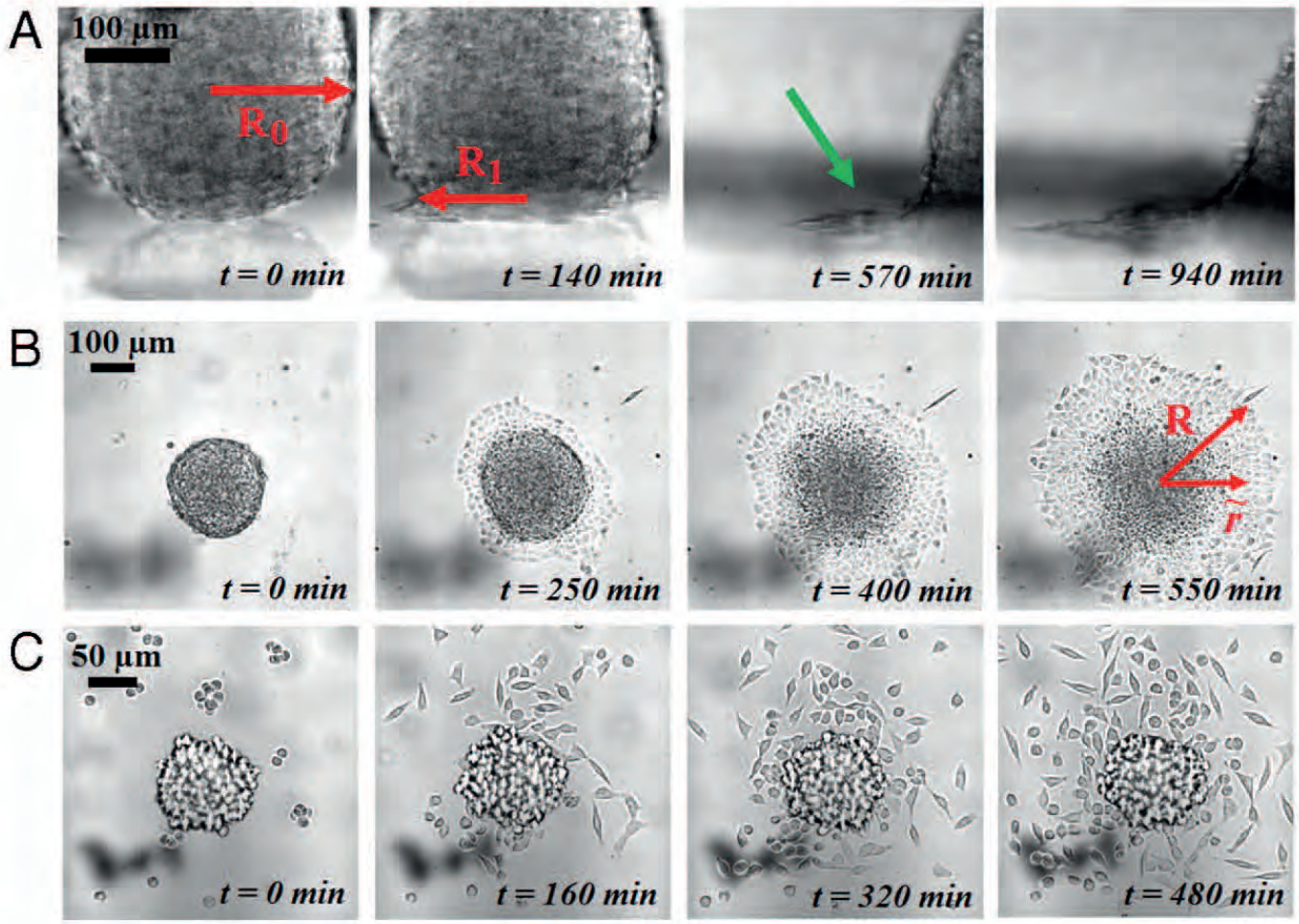
A
100 μm
R_0
R_1
t = 0 min
t = 140 min
t = 570 min
t = 940 min
B
100 μm
t = 0 min
t = 250 min
t = 400 min
R
r
t = 550 min
C
50 μm
t = 0 min
t = 160 min
t = 320 min
t = 480 min

Figure 10

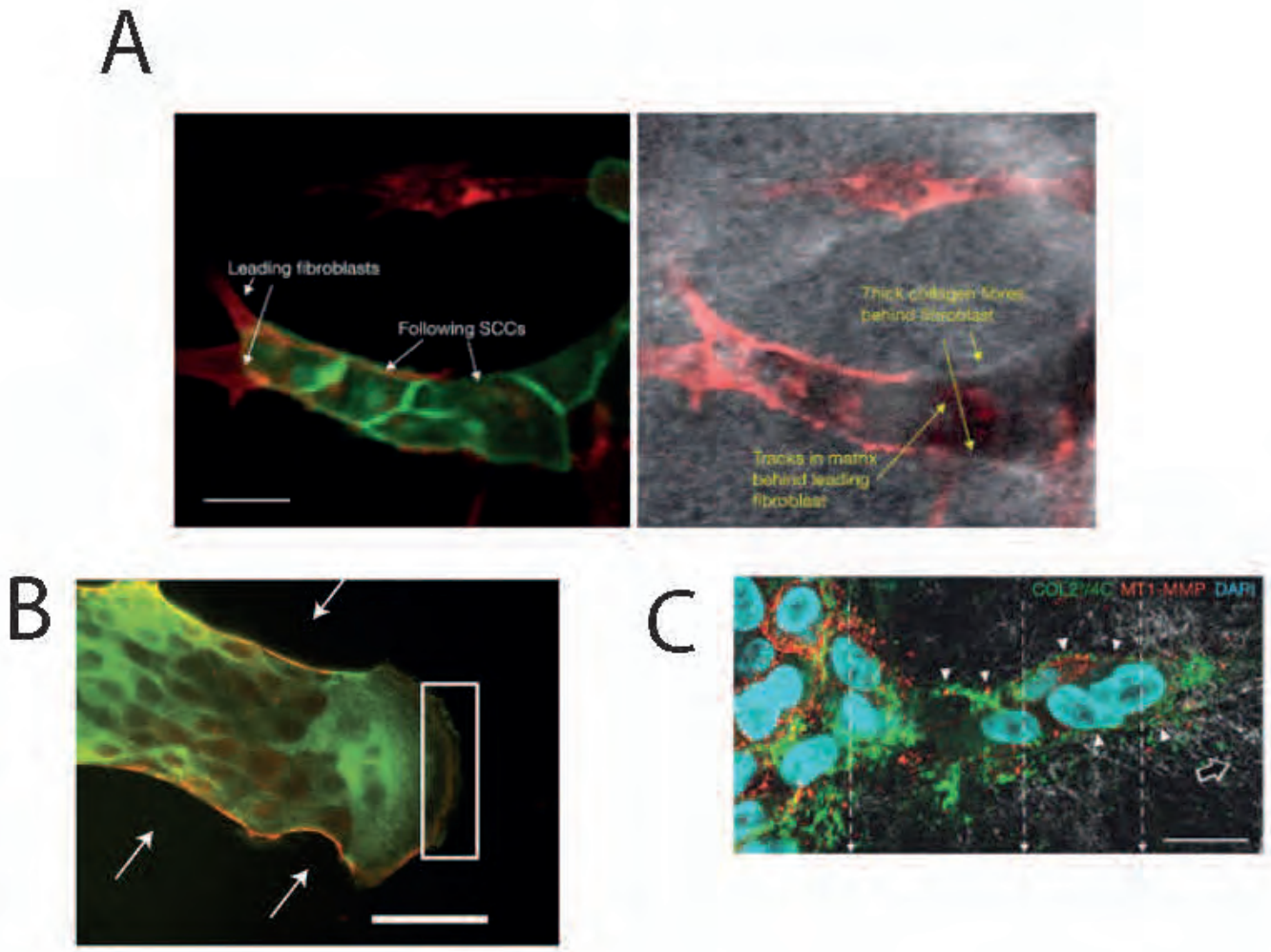
A
Leading fibroblasts
Following SCCs
Thick collagen fibres behind fibroblast
Tracks in matrix behind leading fibroblast
B
C
COL2/4C MT1-MMP DAPI

Figure 11

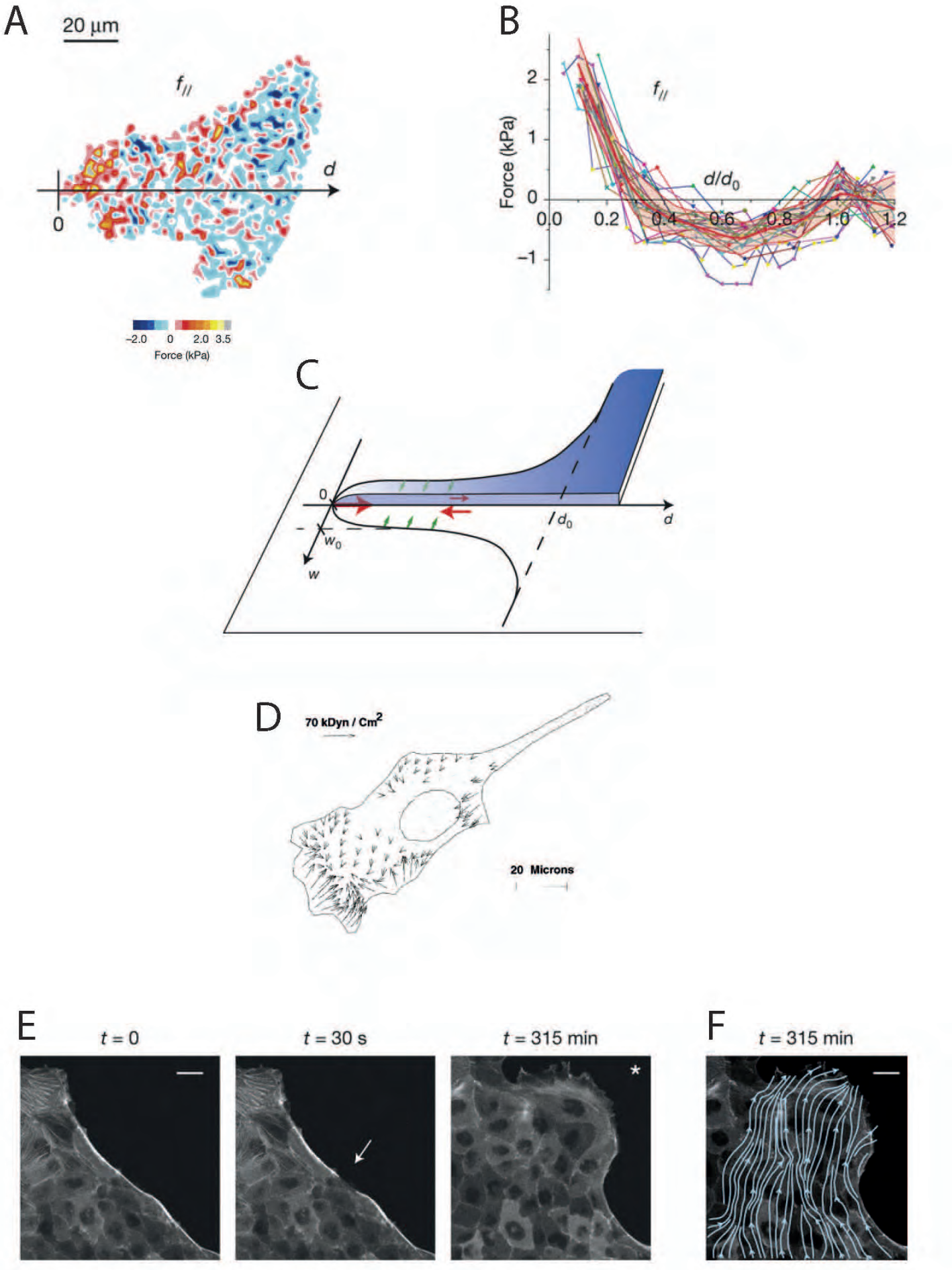
A
20 µm
$f_{//}$
d
0
−2.0 0 2.0 3.5
Force (kPa)
B
$f_{//}$
Force (kPa)
d/d_0
2
1
0
−1
0.0 0.2 0.4 0.6 0.8 1.0 1.2
C
0
w_0
w
$/d_0$
d
D
70 kDyn / Cm^2
20 Microns
E
t = 0
t = 30 s
t = 315 min
F
t = 315 min

Figure 12

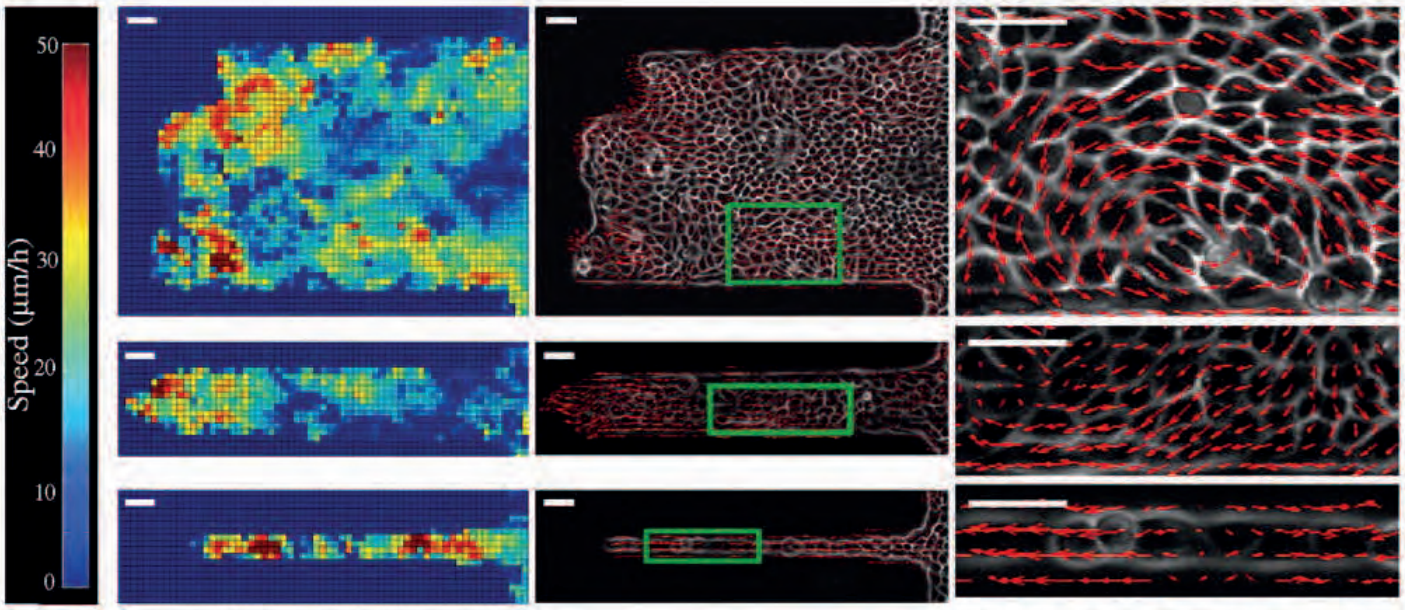

Figure 13

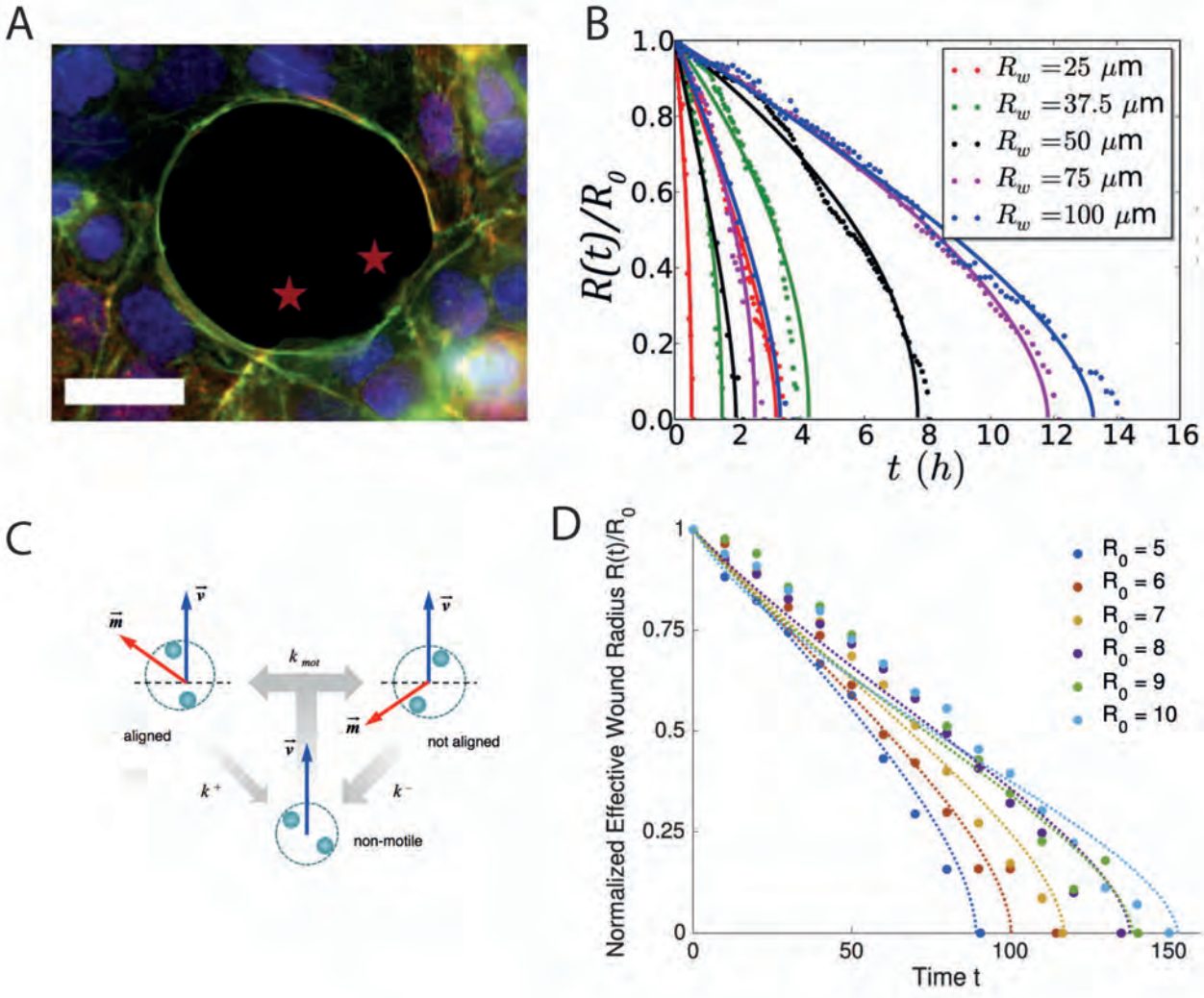
A
B
R_w =25 μm
R_w =37.5 μm
R_w =50 μm
R_w =75 μm
R_w =100 μm
R(t)/R0
t (h)
C
aligned
not aligned
non-motile
k mot
k+
k−
D
Normalized Effective Wound Radius R(t)/R0
R0 = 5
R0 = 6
R0 = 7
R0 = 8
R0 = 9
R0 = 10
Time t
E
50 μm
F
Experimental
Theoretical
R=25μm
R=35μm
R=45μm
Radius (μm)
Time (h)

Figure 14

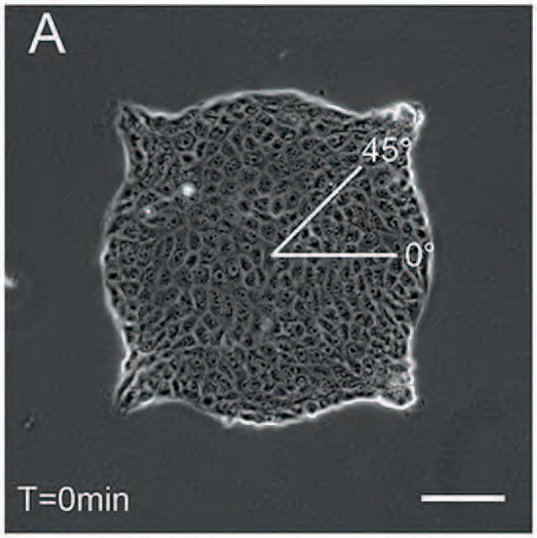
A
45°
0°
T=0min

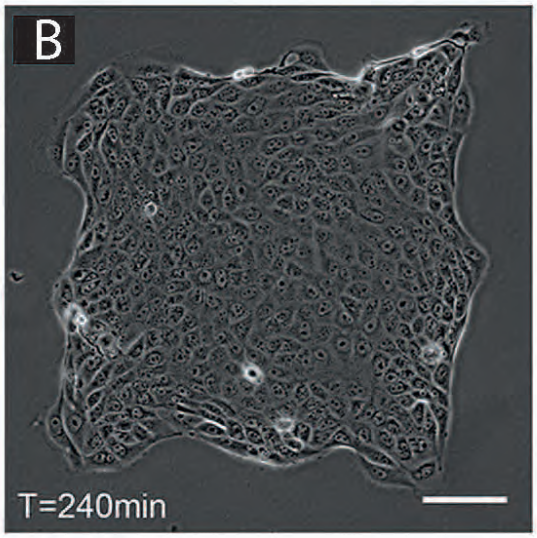
B
T=240min

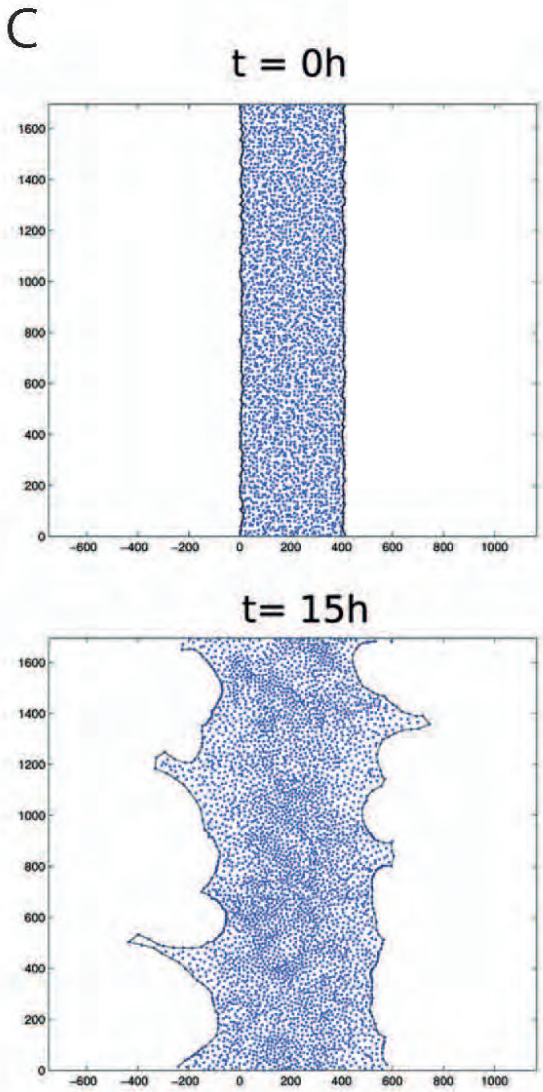
C
t = 0h
t= 15h
1600
1400
1200
1000
800
600
400
200
0
−600
−400
−200
0
200
400
600
800
1000

Figure 15

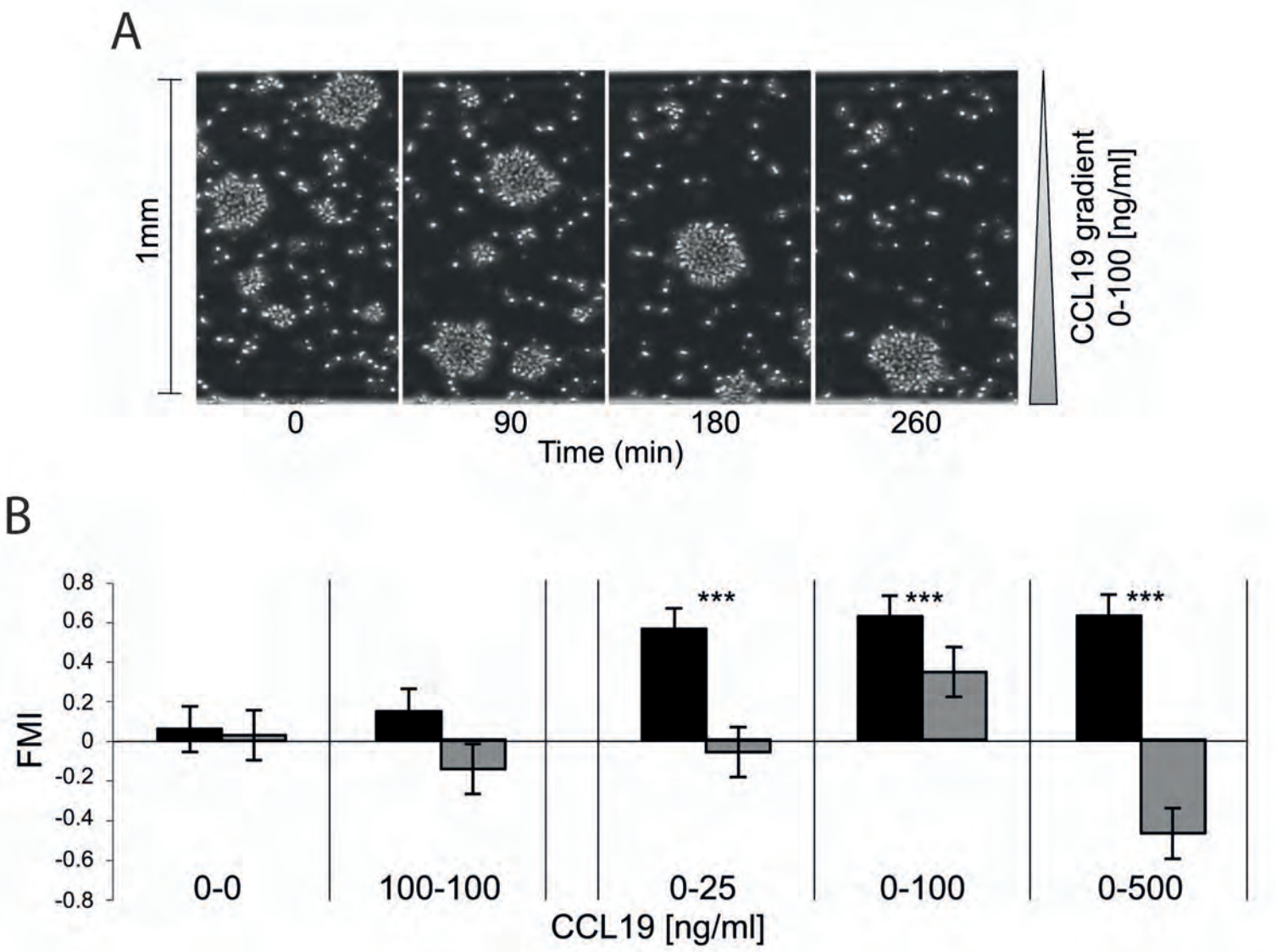
A
1mm
0
90
180
260
Time (min)
CCL19 gradient
0-100 [ng/ml]
B
FMI
0.8
0.6
0.4
0.2
0
-0.2
-0.4
-0.6
-0.8
***
***
***
0-0
100-100
0-25
0-100
0-500
CCL19 [ng/ml]
C
Protrusive
forces

Figure 16

A

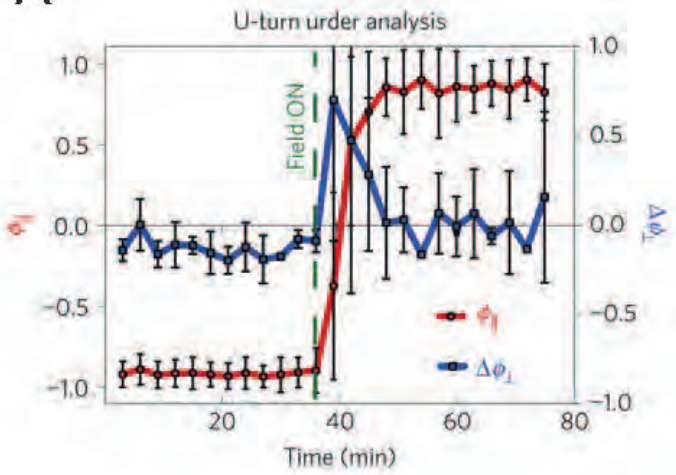
U-turn urder analysis
1.0
0.5
0.0
−0.5
−1.0
Field ON
20
40
60
80
Time (min)

B

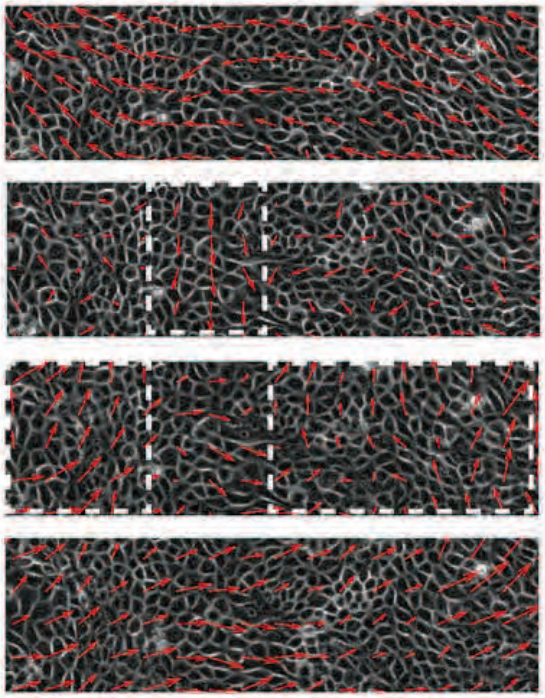

Figure 17

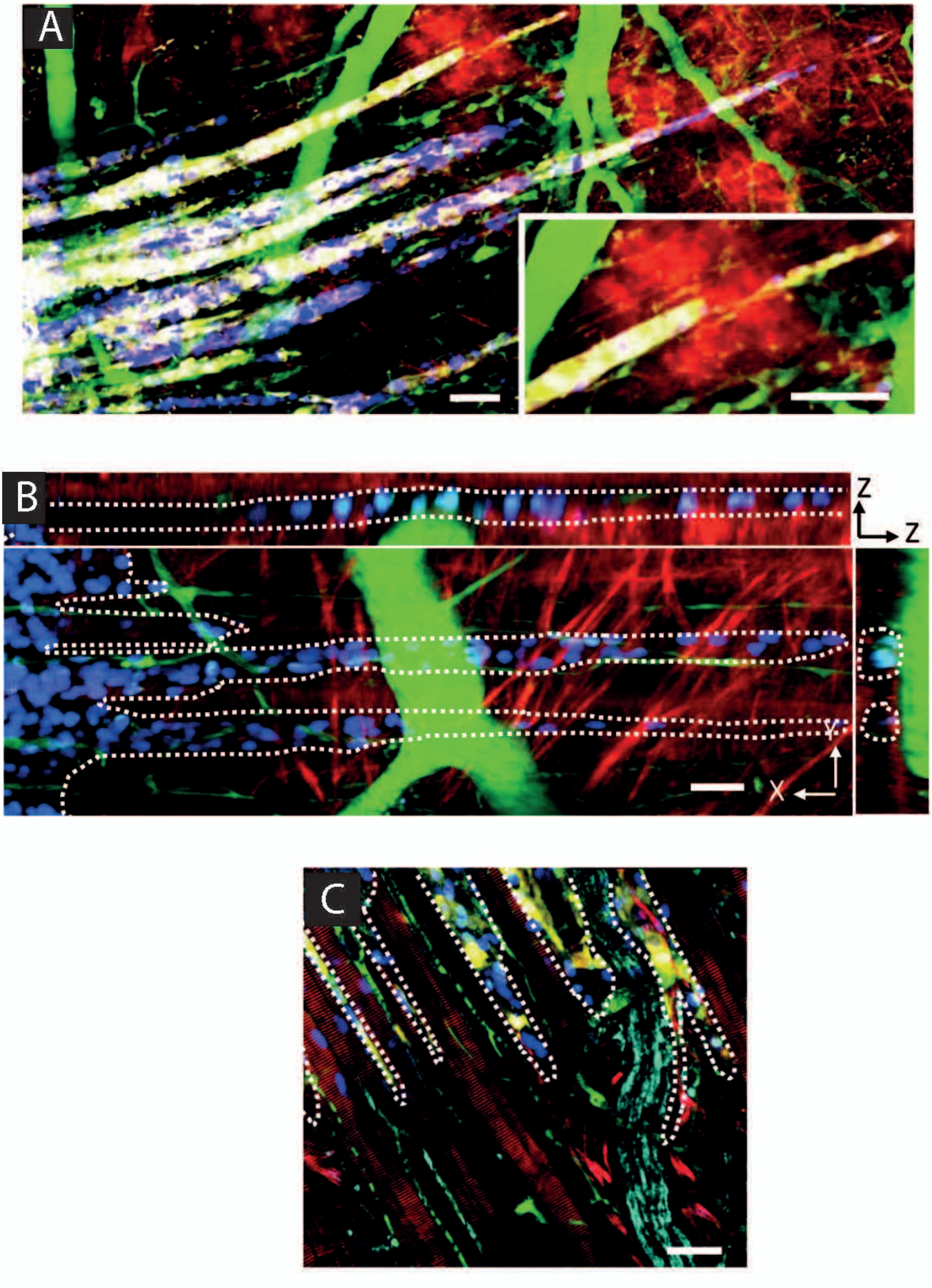

Figure 18

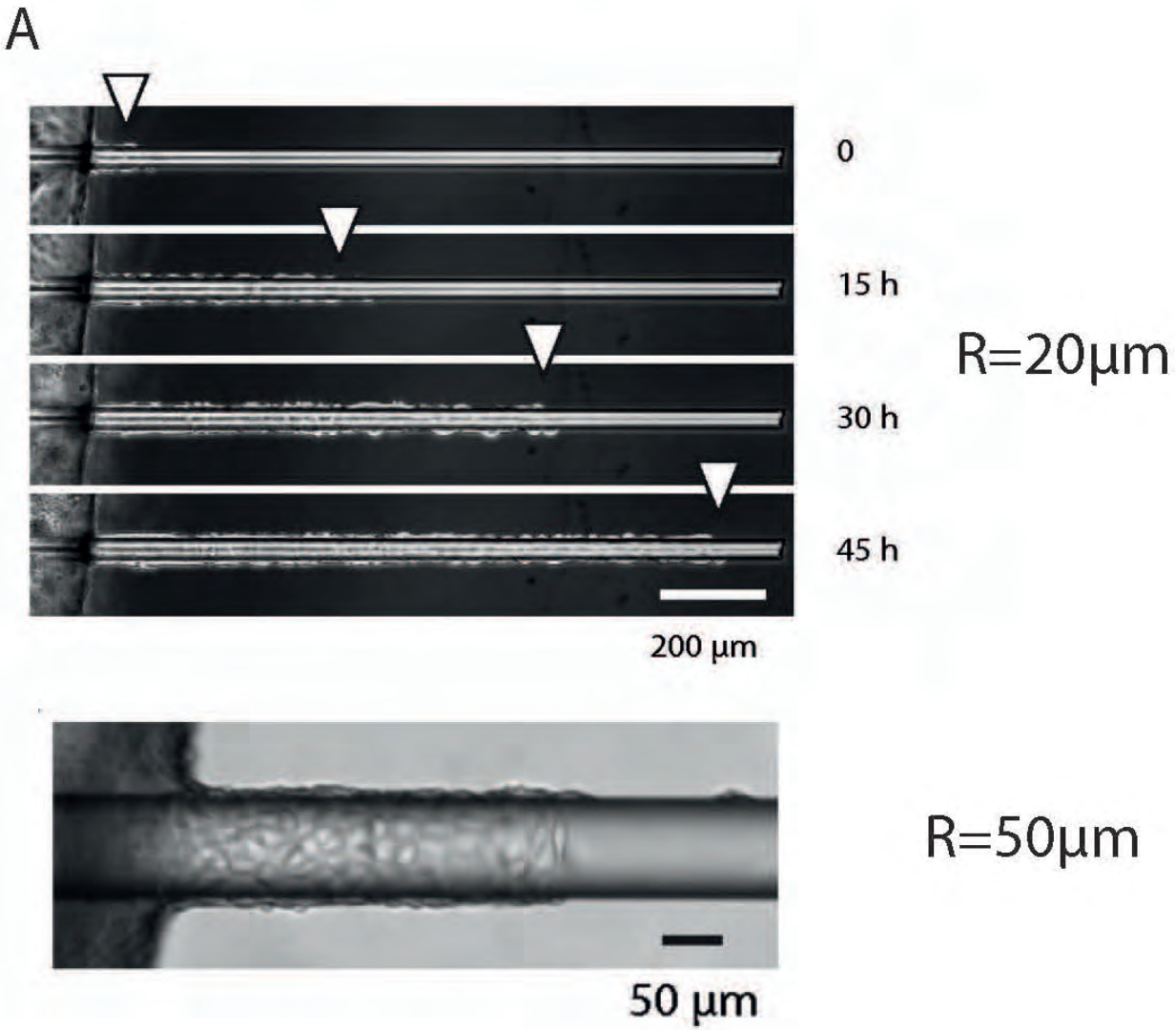

Figure 19